STUDIES OF COMBUSTION CHARACTERISTICS OF HEAVY HYDROCARBONS IN SIMPLE AND COMPLEX FLOWS

by

Runhua Zhao

A Dissertation Presented to the

FACULTY OF THE USC GRADUATE SCHOOL

UNIVERSITY OF SOUTERHN CALIFORNIA

In Partial Fulfillment of the

Requirements for the Degree

DOCTOR OF PHILOSOPHY

(MECHANICAL ENGINEERING)

May 2016

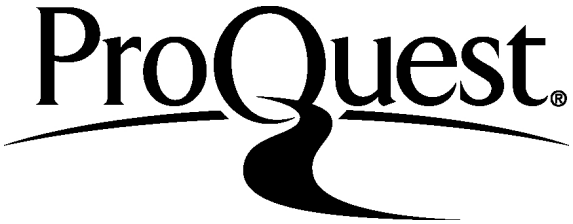

Dedication

To my parents, Guanhou Zhao and Qin Tang for their love and support.

Acknowledgments

The author wishes to thank Professor Fokion Egolfopoulos for his encouragement, support and guidance throughout this doctoral work.

Table of Contents

List of Tables

List of Figures

Abstract

The main focus of this dissertation was the experimental and numerical investigations of laminar flames of heavy liquid and solid hydrocarbons under simple (one-dimensional, steady state flow field using canonical configuration) and complex (two/three-dimensional, transient flow at high Karlovitz number) flow conditions.

A number of theories that have developed based on simplified assumptions and asymptotic analysis and more important for light fuels such as methane, were examined both experimentally and numerically in two steady state and canonical configuration, namely counter-flow configuration and Bunsen flame configuration. The counter-flow configuration was used to determine laminar flame speeds and extinction strain rates over a wide range of heavy hydrocarbons including normal alkanes (up to carbon number 16), practical gasolines and jet fuels and aromatics (cyclopentadiene). The analytical solution derived from asymptotic analysis provides good agreement for laminar flame speeds for fuel lean conditions. However notable discrepancies have been identified for fuel rich conditions due to lack of consideration of fuel-oxygen differential diffusion especially for heavy fuels for which the molecular weight disparity between oxygen and fuel is large.

For the Bunsen flame configuration, the area and angle methods were examined to measure laminar flame speeds of methane/air flames (representative of light fuel) and propane/air flames given that propane is the lightest hydrocarbon with distinctly higher

molecular weight than oxygen. The results indicated that apart from issues raised from inlet boundary condition, flame extinction induced complex flow distribution at burner edge and flame tip effect, such configuration can't produce quantitative results for fuels heavier than methane due to lack of consideration of flame speed variation to stretch for fuel/air mixtures with non-unity Lewis number.

Based on the understanding of the propagation of flames of heavy fuels, accurate measurements of laminar flame speeds were carried out using the counter-flow configuration at atmospheric pressure for a variety of complex fuel molecules for which data are non-existing and which are of direct relevance to practical fuels.

The interaction between a flame and turbulence is a fundamental aspect of combustion. To further illustrate the difference of flame behaviors between light and heavy fuels, the vortex laminar flame interaction was studied numerically in a canonical two-dimensional configuration for methane and *n*-dodecane flames. The *n*-dodecane exhibits early decomposition prior entering the flame due to the local temperature rise caused by the vortex, and such phenomenon is not observed in methane/air flames.

In summary, the main conclusion of this dissertation is that the fuel complexity that has been frequently ignored in flame research needs to be accounted for in simple and complex flows. It was shown that the fuel effects are both of physical and chemical nature.

Chapter 1: Introduction

1.1 Background

In desire of heat and light, our modern civilization depends to great extent on combustion of fuels. As such, its relevance as a field of study has never been of greater importance. The prosperity and progress of mankind relies on utilizing such energy source wisely. Developed countries, such as United States, accumulated wealth and power largely based on fossil fuel utilization. The conflict between emerging economies and the overwhelming evidence of global warming caused by greenhouse gases requires burning fuels in a more efficient and environmental friendly way.

Despite the recent booming growth in hybrid and electric automobile market, liquid fuel accounts for 97% of the energy consumption in the transportation sector. It indicates that conventional fossil fuel is and will continue being the largest transportation energy source in the foreseeable future. This is especially true in certain types of transport mode where high energy density fuel sources are required.

To better achieve the increasing demand for higher energy efficiency and lower emissions using liquid fuels, extensive research efforts have focused on the compilation of chemical kinetic models, which serve as a tool in better engine design. Chemical kinetic models have been investigated extensively for light hydrocarbons in the past and the implication is to project the knowledge gained from these gaseous fuels onto heavy

hydrocarbons that are relevant to practical fuels. The analytical derivation of combustion properties of gaseous fuels frequently requires approximations and assumptions that have been established for gaseous fuels and which may not necessary hold for large molecular weight hydrocarbons. In order to get quantitative results, the strong coupling between chemical reaction and molecular transport requires detailed numerical simulations to achieve the desired accuracy.

In light of these issues, the current work aims to quantify errors introduced when knowledge gained for light hydrocarbon flames is extrapolated to heavy ones, both in simple and complex canonical flows. The experiments reported in this dissertation were conducted in idealized flow conditions that can be well controlled and reproduced, allowing for the enhancement of the fundamental understanding of the chemical and transport phenomenon that take place during combustion.

1.2 Basic Concepts

1.2.1 Laminar Flame Speed

The laminar flame speed, S_u^o, defined as the propagation speed of a steady, laminar, one-dimensional, planar, adiabatic flame is a fundamental property of any combustible mixture. It is a measure of the mixture's reactivity, diffusivity, and exothermicity and depends primarily on ϕ, the temperature of the unburned mixture, and the pressure. The realization of flame stretch effects on flame propagation and its subsequent subtraction from the measurements, allowed for the accurate knowledge of S_u^o becomes

possible and essential towards validating kinetic models [1] and constraining uncertainties of rate constants [2].

1.2.2 Flame Stretch

Flame stretch, *K*, is a measure of the Lagrangian rate of flame surface "production" resulting from its motion and nonuniformities in the underlying flow field. It is defined at any point on the flame surface as the time derivative of the logarithm of the area, A, of an infinitesimal element of the surface [3-5]:

$$K = \frac{1}{A}\frac{dA}{dt}$$

K can be also expressed in terms of flow velocity [4]:

$$K = \nabla_t \cdot \mathrm{v}_\mathrm{t} + (\mathrm{V} \cdot n)(\nabla_t \cdot n)$$

Where ∇_t and $\mathrm{v_t}$ are the tangential components of ∇ and v evaluated at the surface, and n is the unit normal vector of the surface, pointed in the direction of the unburned gas. V is flame surface velocity, while the flow has a velocity v. The first term represents the rate of change of the tangential velocity along the flame surface. The second term represents the stretch by the movement of a curved flame.

For a flame established in the counterflow configuration, stabilization is via the tangential component of *K*. For such flames this then reduces to:

$$K = 2\frac{\partial \mathrm{v}_r}{\partial r}$$

where v_r is the radial velocity and r is the radial coordinate. Using the continuity equation this can then be related to the velocity gradient in the hydrodynamic zone i.e.:

$$K = -\frac{\partial v_x}{\partial x}$$

where V_x is the axial velocity and x is the axial coordinate, respectively.

1.2.3 Flame Extinction

Flame extinction occurs when the time available for chemical reaction becomes less than the time required to generate sufficient heat for the fresh mixture to reach its ignition temperature. Heat loss (convective, conductive, or radiative), radical quenching, and flame stretch are the mechanisms that can cause extinction and they can be synergistic. The value of *K* at which extinction occurs is defined as the extinction strain rate, K_{ext}.

For premixed flame extinction, if the mixture Lewis number is greater than unity, the flame temperature decreases as *K* increases. At certain point, the flame temperature is not sufficient enough to support the fresh mixture to reach ignition temperature, extinction occurs. On the other hand, for a mixture with Lewis number less than unity, flame temperature increases as *K* increases. The flame is not extinguished until pushed to the stagnation plane. As *K* increases even more, incomplete combustion and reactant leakage results in a drop in the flame temperature and extinction occurs eventually.

For non-premixed flame extinction, the heat release rate is governed by diffusion process, as stretch rate increases, the diffusion time scale decreases till the point

comparable to reaction time scale, and thus followed by incomplete combustion and reactant leakage which eventually leads to extinction.

1.2.4 Lewis Number

The current state of the art definition for (effective) Lewis number is a weighted average of the individual Lewis number, Le_{F} (fuel based Lewis number) and Le_{O} (oxidizer based Lewis number), defined as:

$$Le_{\mathrm{eff}} = \begin{cases} (Le_{\mathrm{O}} + (1+\bar{\phi})Le_{\mathrm{F}})/(2+\bar{\phi}), & \text{lean mixture} \\ (Le_{\mathrm{F}} + (1+\bar{\phi})Le_{\mathrm{O}})/(1+\bar{\phi}), & \text{rich mixture} \end{cases}$$

where $\bar{\phi}$ is always greater than zero, it is a measure of the mixture deviation from stoichiometry, defined as:

$$\bar{\phi} = \begin{cases} \beta(\phi^{-1}-1), & \text{lean mixture} \\ \beta(\phi-1), & \text{rich mixture} \end{cases}$$

For a stoichiometric mixture, the Le_{eff} is the average of Le_{F} and Le_{O}. For an off-stoichiometric mixture, the deficient component is more heavily weighted such that for very lean/rich mixtures the Le_{eff} is practically that of the fuel/oxidizer, respectively.

While *Le* effects have been studied extensively in past pertinent studies, this is not the case for reactant differential diffusion effect that can be rather important for large MW fuels as evident from Fig. 1.1 in which the ratio of oxygen to fuel diffusivities is shown to increase with the fuel carbon number for ϕ = 1.4 *n*-alkane/air mixtures, while the *Le* is nearly unity and barely changed. The differential diffusion effect is generally

overlooked and considered secondary when dealing with small MW fuels, the following chapter is to demonstrate its relative importance to fuels with large MW.

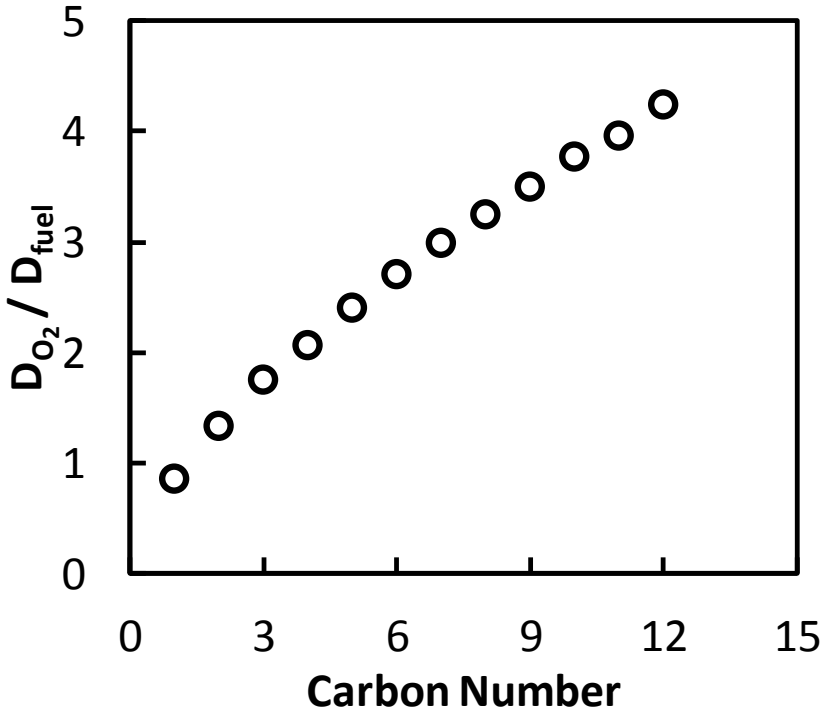

Figure 1.1 Variation of the ratio of oxygen diffusivity to fuel diffusivity with carbon number for ϕ = 1.4 *n*-alkane/air mixtures at p = 1 atm and T_u = 298 K.

1.2.5 Karlovitz Number

Stretch rate *K* can be often times deceiving when comparing flame speeds under similar stretch conditions. A more appropriate approach is to use Karlovitz number, *Ka*, which is a measure of the ratio of flame time scale, t_f, respect to aerodynamic time scale, defined as:

$$Ka = t_f K = \frac{l_f}{S_u^0} K \equiv \frac{D}{(S_u^0)^2} K$$

For a fixed burning intensity flame, large *Ka* indicates that flame experiencing stronger *K* and vice versa. Weakly burning flames exposed to the same *K* as strong flames, since weak flames exhibit lower S_u^o and thus higher *Ka*, are experiencing more profound hydrodynamic stretch effect than stronger flames.

1.2.6 Markstein Number

Markstein number, μ, (or Markstein Length, $\mathcal{L}$, which is the multiplication of Markstein number and flame thickness, $l_f = D_{th}/S_u^0$) is a measure of sensitivity of flame speed to stretch $S_f = S_u^0 - \mathcal{L}K$. It is defined as:

$$\mu = \frac{\sigma}{\sigma - 1}\int_1^{\sigma} \frac{\lambda(x)}{x}dx + \frac{\beta(Le - 1)}{2(\sigma - 1)}\int_1^{\sigma} \frac{\lambda(x)}{x}\ln\left(\frac{\sigma - 1}{x - 1}\right)dx$$

in which, $\sigma = \rho_u/\rho_b$ is thermal expansion coefficient, *Le* is effective Lewis number, $\beta = E(T_a - T_u)/R^o T_a^2$ is the Zeldovich number, $\lambda(x) = \frac{\tilde{\lambda}(x)}{\tilde{\lambda}_u}$ is scaled thermal conductivity at given temperature condition.

It determines to what extent the flame speed varies with stretch. For most of the hydrocarbons, μ is generally positive and decreases monotonically as the mixture varies from lean to rich conditions. The large variations among the various fuels at lean condition are due to the difference in their diffusive properties. For fuel rich conditions, the effective *Le* is basically that of oxygen and the difference in μ mainly attributes to different values of heat release rate for different mixtures.

It should be noted that the application of μ is only viable at sufficiently low *Ka* condition due to the limitation of asymptotic approach where l_f is considered order of magnitude smaller than hydrodynamic thickness. As will be discussed in the following chapters, when the flow field is at the condition with relatively large *Ka* i.e. close to extinction condition, the theoretical prediction is only in qualitatively agreement with the experimental observations.

1.3 Objectives

The primary objective of this dissertation is to study fuel effects on a variety of combustion phenomena in simple and complex flows. Among them are those associated to the global combustion responses of premixed and non-premixed flames as manifested by the laminar flame speed and extinction stretch rate. The effects of molecular transport of practical fuels and their surrogate compounds such as cyclopentadiene, *n*-dodedecane, *n*-tetradecane, and *n*-hexadecane on flame propagation and extinction was investigated in simple one- and two-dimensional flow configurations. Fuel effects were investigated also under realistic flow field conditions through direct numerical simulations of the interactions of a laminar premixed flame and a single vortex at the scale of the flame thickness during the course of this study.

1.4 References

[1] Law C. K., Sung, C. J., Wang, H., & Lu, T. F. *AIAA Journal* 41(9) (2003) 1629–1646.

[2] Sheen D. a., & Wang, H. Combustion and Flame 158 (2011) 2358–2374.

[3] Law C. K., Symposium (International) on Combustion (1989) 1381–1402.

[4] Matalon M., Combustion Science and Technology 31 (1983) 169-181.

[5] Williams F., *Combustion Theory* (2nd Editio) (1985).

Chapter 2: Experimental Approach

2.1 Experimental Setup

The experiments were carried out under atmospheric pressure in the counterflow configuration [1-4] as schematically shown in Fig. 2.1 along with the details of a typical burner. For flame propagation and premixed flame extinction measurements, the top burner is injected with N_2 and bottom burner injected with fuel and air mixture. For non-premixed flame extinction measurements, the top burner is injected with pure O_2 and the bottom burner is injected with fuel and N_2 mixture. The top burner is kept at ambient temperature, and the bottom burner is heated to the desired temperature for each specific experiment. The burner is designed to include a N_2 co-flow channel surrounding the nozzle to isolate the main jet. Two different types of burner, namely contour nozzle and screened straight nozzle are implemented to make sure uniform velocity profile coming out of the burner exit.

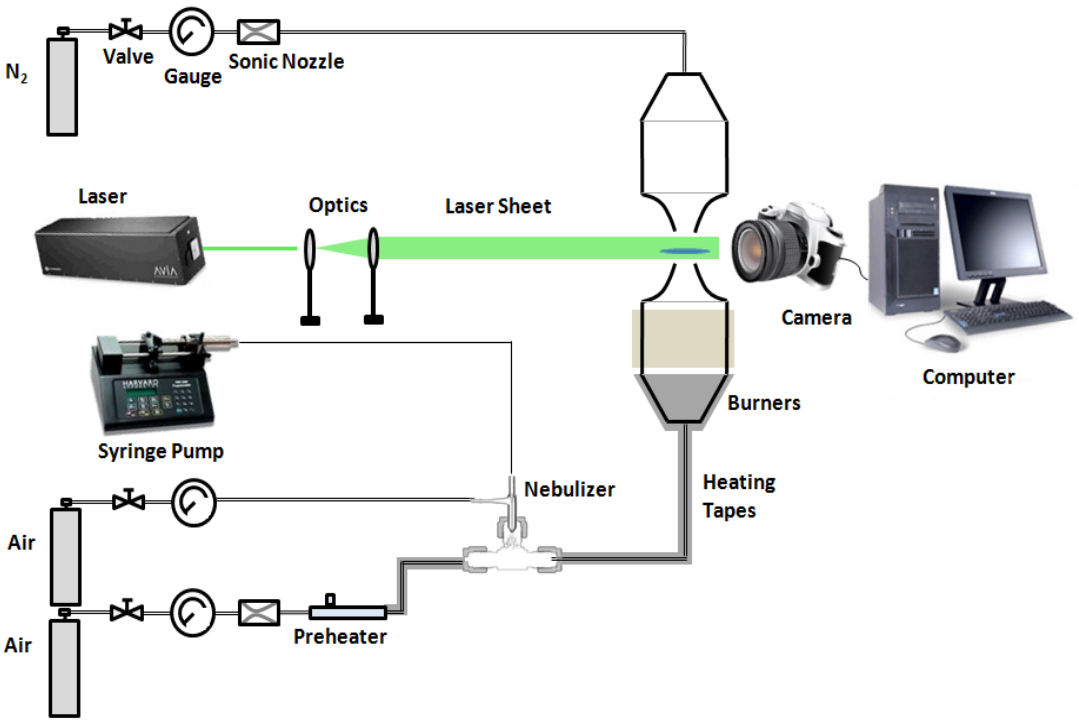

Figure 2.1 Representative example of the non-linear extrapolation technique.

The gaseous flow rates were metered using sonic nozzles, which were calibrated using a dry-test meter with a reported accuracy of ±0.21%. The upstream pressure of each sonic nozzle was monitored by a pressure gauge with ±0.25% precision. The vaporization system included a precision syringe pump of ±0.35% accuracy. All gas lines were heated to prevent fuel vapor condensation. The temperature of the gas lines was measured with K-type inline thermocouples. The temperature of the unburned fuel/N_2 stream, T_u, was measured at the center of the burner exit. The variation of this temperature is within ±5 K. Flow composition uncertainty has been determined to be less than 0.5%. Flow velocity measurements were made by seeding the flow with

submicron size silicon oil droplets and by using particle image velocimetry (PIV). The uncertainty associated with the PIV measurements is within 0.8 to 1.0%.

2.2 Liquid and Solid Fuel Preparation Procedure

The vaporization system included a high precision syringe pump (Harvard, PHD 22/2000) and a glass nebulizer (Meinhard, TR-50-A1) that injected fuel as fine droplets into a cross-flow of heated air and heated nitrogen for premixed flames and non-premixed flames respectively. It was determined that the cross-flow injection configuration minimizes the fluctuations stemming from vaporization, and allows very efficient mixing of the fuel with the heated gaseous stream. All tubes along the heating path were wrapped with heating elements and insulation to eliminate cold spots. To prevent fuel cracking, several inline K-type thermocouples were arranged along the heating path to ensure that the temperature of fuel/air mixture was maintained below 490 K, which ensured also that the partial pressure of the fuel was lower than its vapor pressure. The temperature of the unburned mixture, T_u, was measured at the center of the burner exit.

A major challenge with solid fuel experiments is that the fuel source is at solid state at room temperature. Accurate fuel injection becomes difficult with current technology. As a result, to better perform the experiments with solid fuel, modifications of the experimental configuration had to be made and are shown schematically in Fig. 2.2.

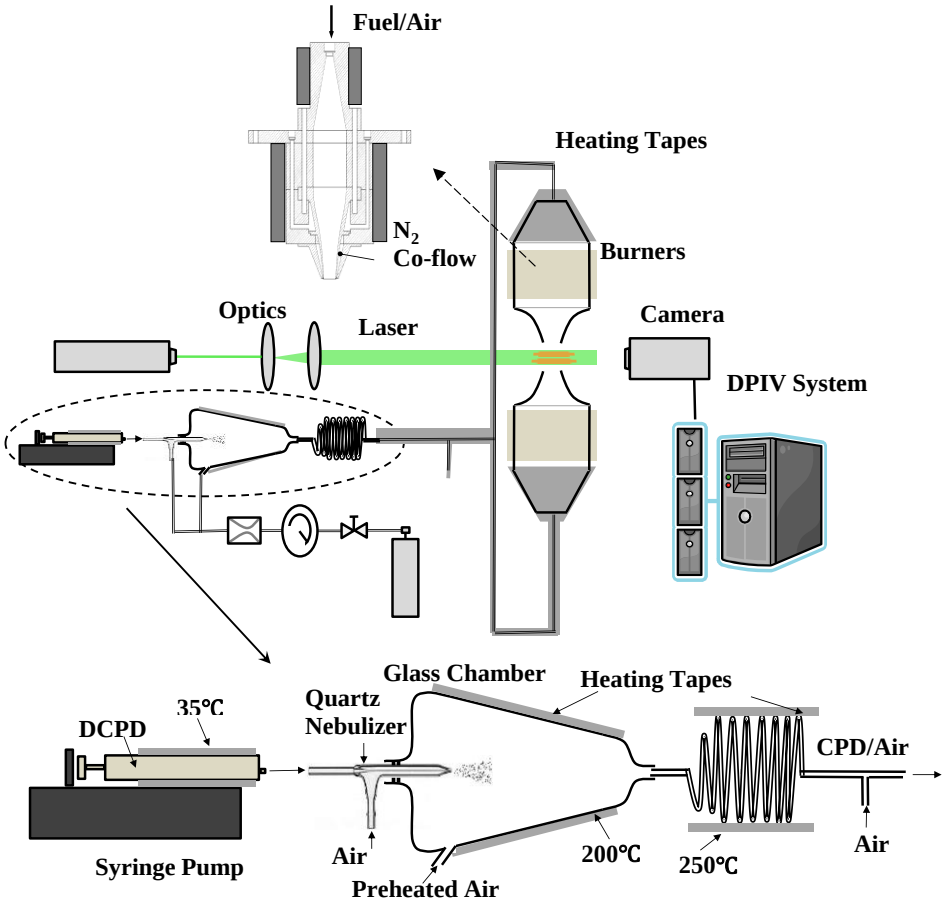

Figure 2.2 Schematic of the experiment configuration.

The solid fuel is first melted within a heated oil bath and then injected into a nebulizer by a high-precision syringe pump. The high-precision syringe pump was heated at temperatures slightly higher than melting temperature to keep the fuel in the liquid phase. Uniform size fuel droplets, ranging from 0.5 μm to 5 μm, were produced by a nebulizer that were mixed and vaporized instantly with portion of the test air instantly in a glass vaporization chamber heated at 490 K. The rest procedure is similar to those in liquid fuel experiments with the exception that apart from monitoring system heating temperature, liquefied fuel temperature lies within the syringe was recorded and the

density correction to the corresponding change in temperature was accounted for in the final mixture composition calculation.

2.3 Reference Flame Speed and Local Strain Rate

In the counterflow configuration, a reference flame speed, $S_{u,ref}$, is defined as the minimum velocity upstream of the flame along the stagnation streamline. The imposed $K$is defined upstream of $S_{u,ref}$ as the absolute value of the maximum gradient of the flow velocity. These points are indicated in Fig. 2.3.

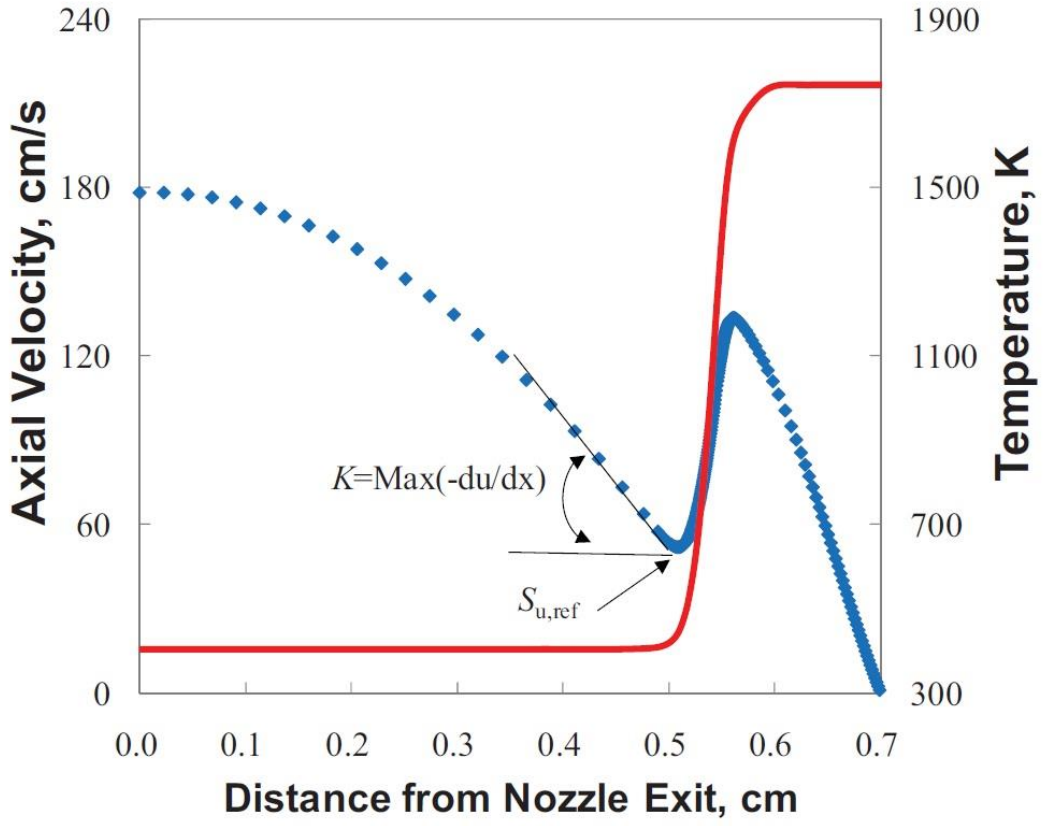

Figure. 2.3: Graphical definition of measurement points in counterflow.

There are two subtle and often times overlooked issues with this approach. First, $S_{u,ref}$ and K were obtained separately at adjacent locations close to the flame front. Second, the choice of these two points in the flow field as markers of a given stretched flame is mainly due to low level experimental complexity. A local velocity minimum point and local velocity maximum gradient point are relatively easy to measure as compared to other equally distinctive locations (i.e. maximum heat release rate point, maximum H radical concentration point, 1% temperature rise point etc.) and the applied stretch rate can be systematically extracted.

2.4 Determination of Laminar Flame Speed

S_u^o's could be determined, in principle, by plotting $S_{u,ref}$ vs K and extrapolating linearly the $S_{u,ref}$ data to K = 0 using Markstein formula [5]. However, Tien and Matalon [6] showed via asymptotic analysis that such relation is nonlinear due to the presence of thermal expansion. More recently, a non-linear extrapolation using a computationally assisted approach was developed by Egolfopoulos and coworkers [7-9] to determine S_u^o's as shown in Fig. 2.4.

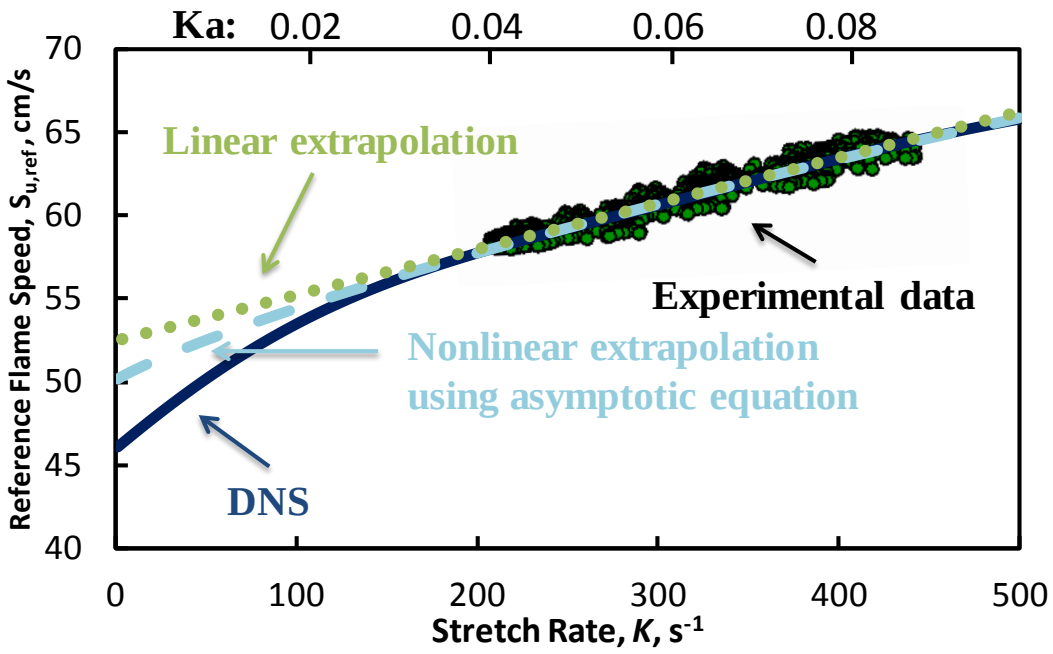

Figure. 2.4: Representative example of the non-linear extrapolation technique.

As will be discussed in later chapters, by introducing linear or nonlinear extrapolation to derive S_u^o will inherently increase the experimental uncertainty. The uncertainty will be further augmented as fuel molecular weight deviates from that of air or mixture equivalence ratio approaches richer condition. The reason for such phenomenon is due to the assumption limit in deriving analytical solutions [10]. This particular source of uncertainty could be avoided by comparing experimental data and detail numerical simulation results directly without further extrapolation [11].

2.5 Determination of Extinction Strain Rate

For the determination of K_{ext} of premixed and non-premixed flames, the single flame configuration instead of twin flame configuration is used due to simplicity in system

construction; lower fuel consumption rate which requires less heating elements and controllers; lower Reynolds number and thus minimizing intrinsic flow instabilities; and lower extinction strain rate for given equivalence ratio due to heat loss towards cold gas instead of burnt gas. The difference between single flame configuration and twin flame configuration can be modeled via 1D simulation, the results suggests that the extinction strain rate is, to the first order, not affected by downstream flow condition [9, 12].

The absolute value of maximum axial velocity gradient in the center line of the flow field just before flame extinguished is determined to be K_{ext}. However, experimental measurements and 2D simulation show that flow field non-uniformity can cause the maximum strain rate occur at off center location and local measurements in the center line are not the representative values of true extinction strain rates as shown in Fig 2.5. and Fig 2.6. The non-uniform flow field exhibits higher strain rate at the edge of the flame instead of at the center. This phenomenon is strengthened as the flow rate increases [13].

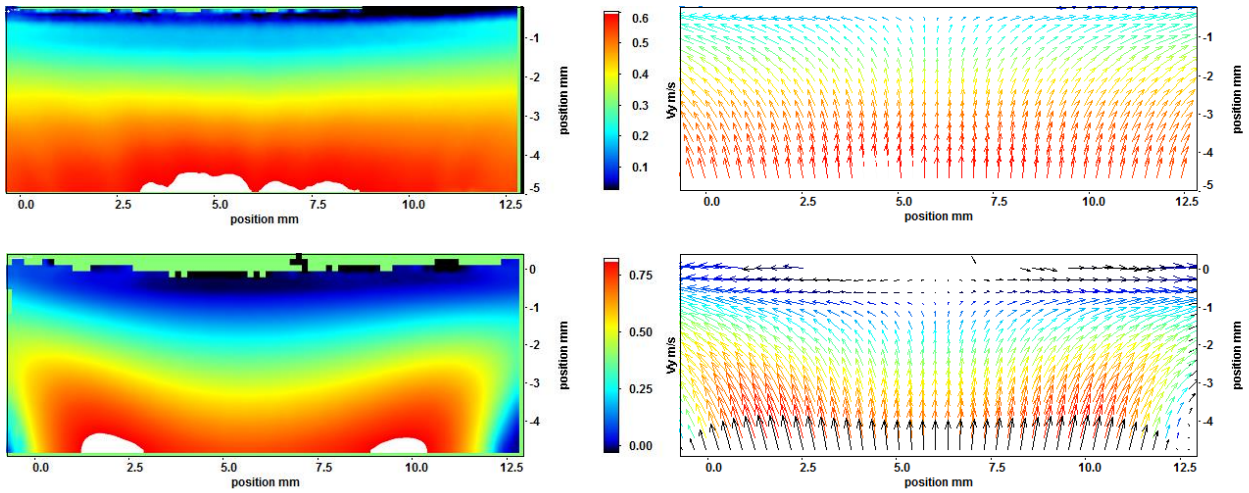

Figure 2.5: Experimental results comparison of uniform flow field using screened burner (top) and non-uniform flow field using open burners (bottom)[1].

[1] Open burner composites with screens ~5 Diameter upstream from the burner exit, burner with screens at the exit here referred as screened burner.

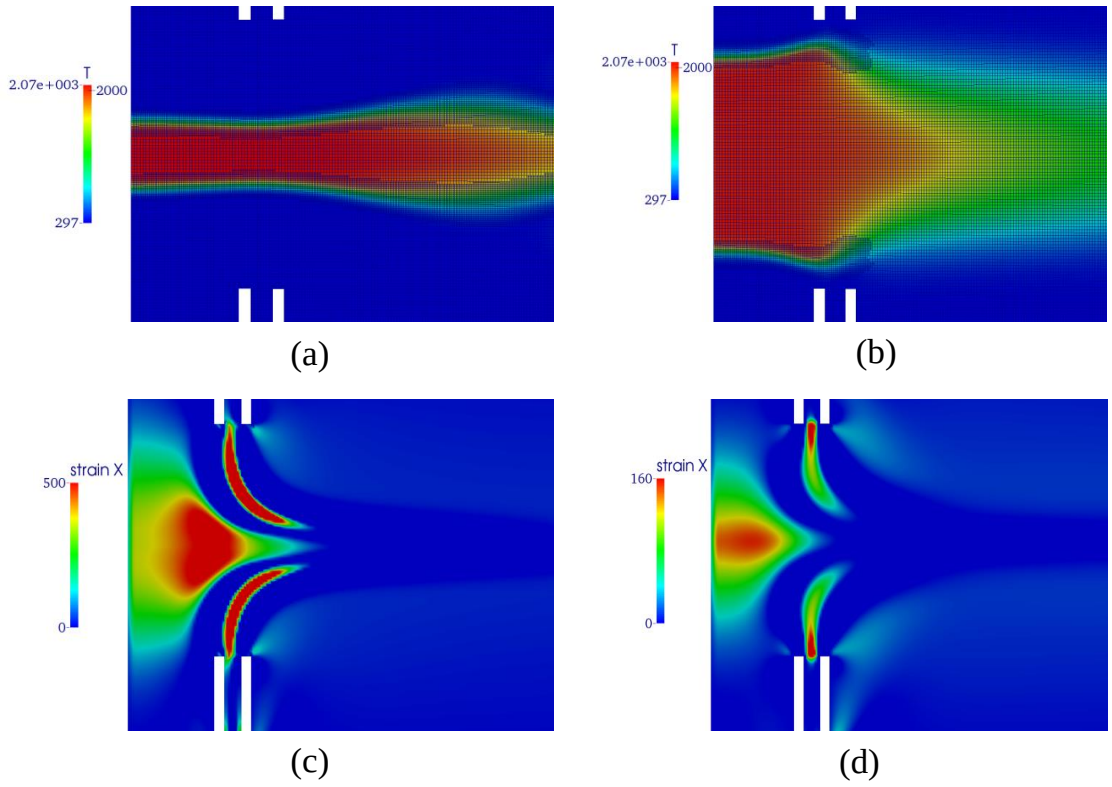

Figure 2.6: 2D axisymmetric simulation results of open burner opposing jet twin-flame configuration flame at high strain rate and low strain rate condition. (a) high flow rate flame and (b) low flow rate flame with adaptive grid resolution; (c) high flow rate flame and (d) low flow rate flame radial velocity gradient in the tangential direction.

The dynamic behavior of the extinction process can also be viewed with high-speed camera and images are shown in Fig 2.7. Time $t = 0$ ms corresponds to the moment the extinction process initiates. Extinction in open burner is found to initiate at a location away from the centerline, followed by transition to a propagating edge flame surrounding the still-burning flame core, and eventually resulting in global extinction at $t = 70$ ms; note that unavoidable minor asymmetry in the burner alignment caused the initiation of

extinction on the right edge of the images. For screened burners on the other hand, extinction initiates near the centerline before transitioning to an outwardly propagating edge flame followed by global extinction at $t = 30$ ms. It should be noted that both burners produced flat flame shapes, suggesting that a visual inspection of flame geometry is not sufficient to ensure flow field quality.

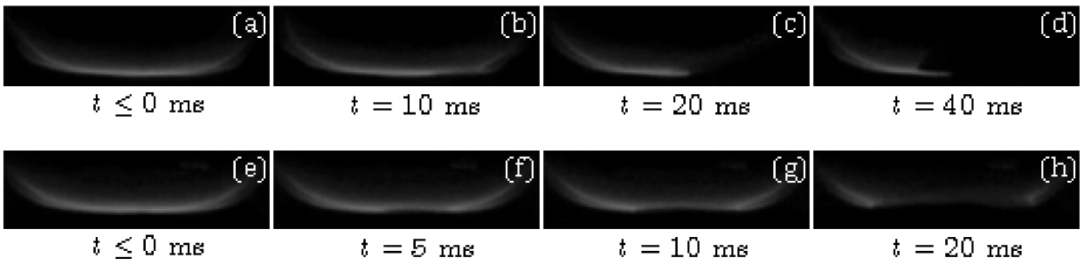

Figure 2.7: Evolution of the extinction process for lean CH_4/air flames produced by open burner (a-d) and screened (e-h) burners.

Furthermore, as extinction initiates on the centerline, the direction of edge flame propagation coincides with that of v_r while for off-center extinction the edge flame propagates opposite to v_r. This results in the different time scales from initiation to completion of the extinction process, e.g. 30 ms vs. 70 ms, of Fig. 2.7. The locally off-center extinction transitioning to global extinction in open burner produces Kext values that are systematically lower because the measured centerline velocity profiles are not representative of the extinction state. Additionally, the magnitude of flow non-uniformity has been shown [14] to scale with flow momentum and burner separation distance as $\rho v_x{}^2 \left(\frac{D}{L}\right)^2$. For a fixed L/D, extinction of stronger flames (higher

ϕ) necessitates greater v_x. As the stagnation pressure in counterflow is ellipsoidal in shape [15], the centerline velocity is preferentially decelerated compared to the edges, enhancing the exit velocity non-uniformity with increasing flow rate.

Based on these evidences, cautious must be taken to ensure uniform flow field coming out of the burner exit at various temperature, burner diameter, separation distance and pressure condition. On top of that, the burner exit axial velocity gradient can lead to discrepancy between experimentally measured strain rate and numerical simulation results. The reason for such difference is due to the implementation of plug flow boundary condition in the 1D code [7] and hence updated code packages have been applied to account for experimentally measured axial velocity gradient at the boundary.

2.6 References

[1] Davis S. G., & Law C. K. *Combustion Science and Technology*, 140 (1998) 427–449

[2] Law C. K. *Symposium (International) on Combustion*, (1989) 1381–1402.

[3] Vagelopoulos C. M., Egolfopoulos F. N., & Law C. K. *Symposium (International) on Combustion*, 25 (1994) 1341–1347.

[4] Wu C., & Law C. *Symposium (International) on Combustion*, (1985) 1941–1949.

[5] Bechtold J. K., & Matalon M. *Combustion and Flame*, 127 (2001) 1906–1913.

[6] Tien J., & Matalon M. *Combustion and Flame*, 84 (1991) 238-248.

[7] Ji C., Dames E., Wang Y. L., Wang H., & Egolfopoulos F. N. *Combustion and Flame*, 157 (2010) 277–287.

[8] Veloo P. S., Wang Y. L., Egolfopoulos F. N., & Westbrook C. K. *Combustion and Flame*, 157 (2010) 1989–2004.

[9] Wang Y. L., Holley A. T., Ji C., Egolfopoulos F. N., Tsotsis T. T., & Curran H. J. *Proc. Comb. Inst*, 32 (2009) 1035–1042.

[10] Jayachandran J., Zhao R., & Egolfopoulos F. N. *Combustion and Flame*, 161 (2014) 2305–2316.

[11] Jayachandran J., Lefebvre A., Zhao R., Halter F., Varea E., Renou B., & Egolfopoulos F. N. *Proc. Comb. Inst*, 35 (2015) 695–702.

[12] Wang Y. L., Feng Q., Egolfopoulos F. N., & Tsotsis T. T. *Combustion and Flame*, 158 (2011) 1507–1519.

[13] Burrel R., Zhao R., Lee D.J., Burbano H., & Egolfopoulos F.N. *Proc. Comb. Inst*, (2016) under review.

[14] Niemann U., Seshadri K., & Williams F.A. *Combustion and Flame*, 162 (2015) 1540-1549.

[15] Sarnacki B. G., Esposito G., Krauss R. H., & Chelliah H. K. *Combustion and Flame*, 159 (2012) 1026–1043.

Chapter 3: Numerical Approach

3.1 One Dimensional Modeling

3.1.1 Codes Description

S_u^o's and K_{ext}'s were computed using the PREMIX code [1,2] and an opposed-jet code [3,4] respectively. Both are modified to account for thermal radiation of CH_4, CO, CO_2, and H_2O in the optically thin limit and are coupled with the Sandia CHEMKIN [5] and Transport [6] subroutine libraries. The H and H_2 diffusion coefficients of several key pairs are based on the recently updated set of Lennard–Jones parameters [7,8].

For K_{ext} computations, a vigorously burning flame was established first, and then K was increased to achieve extinction. At the extinction state, a two-point continuation approach solves for K at the state of extinction [9,10]. The experimental values of the axial velocity gradients at the burner exits, $(du/dx)_{exit}$, burner separation distance, L, and burner exit temperature, T_u, were considered as the respective boundary conditions in the simulation [11].

3.1.2 Mixture-Averaged and Multicomponent Transport Formulations

Both the PREMIX and the opposed-jet codes allow for the use of either mixture-averaged or multicomponent formulations of transport coefficients. For the mixture-averaged formulation, the diffusion velocity is assumed to be sum of the ordinary diffusion velocity, thermal diffusion velocity (for low molecular weight species

H, H_2 and He), and a correction velocity. The ordinary diffusion velocity is determined in the Curtiss-Hirschfelder approximation [12] by given the mixture-averaged diffusion coefficient. The correction velocity is recommended by Coffee and Heimerl [13] to insure the mass fraction sum to unity. For the multicomponent option, the transport property evaluation follows the method described by Dixon-Lewis [14]. Multicomponent diffusion coefficients, thermal conductivities and thermal diffusion coefficient are computed through the solution of a system of equations involving the binary diffusion coefficients, the species mole fraction, and the thermodynamic and molecular properties of the species [15]. The correction velocity is not required in the multicomponent formulation.

As will be described in later chapters, a recent developed theory for binary diffusion coefficient of long chain alkanes has been used to compare with experimental measurements along with original theory which is based on Chapman-Enskog (CE) expansion employing the Lennard-Jones (LJ) 12-6 potential function. In this new theory, the drag force due to relative motion of a small cylinder in a dilute gas and in the free molecule regime was obtained analytically from a rigorous gas-kinetic theory analysis. The expression for the diffusion binary diffusion coefficient may be derived from the Einstein relation (or the Einstein-Smoluchowski relation) via the drag coefficient, that is, the diffusion coefficient is equal to the drag force divided by the drift velocity [16].

It should also be noted that the mixture-averaged transport formulation of the original Sandia PREMIX and OPPDIF codes does not consider the Soret effect of large/heavy molecules even if the thermal diffusion is considered. To account for thermal diffusion of heavy fuel molecules, the approximation of Rosner et al. [17] for the thermal diffusion factor α_T was implemented into the mixture-averaged formulation. The thermal diffusion factor of species B in A takes the form of

$$\alpha_T = [0.454 \cdot d(\Lambda + 0.261) + 0.116(\Lambda - 1)][1 - C/T],$$

where Λ is related to molecular size disparity, which may be evaluated by $\Lambda \cong 1.31\ \mathrm{Sc}\ (1 + \mathrm{d})^{-1/2}$, Sc is the Schmidt number, $d = (M_B\text{-}M_A)/(M_B\text{+}M_A)$ is the normalized molecular mass disparity, and $C = 1.45[\varepsilon_{BA}/k_B - 85]$

For the cases considered here, C/T $\ll 1$ and thus the temperature correction is unimportant.

3.1.3 Sensitivity Analysis Methodology

A logarithmic sensitivity function is defined as:

$$\frac{d(\log A)}{d(\log B)}$$

where A is the dependent variable and B is the perturbing variable. The advantage of this approach is to allow comparisons between parameters i.e. B_i and B_j in a dimensionless form and isolate the effect of one source from another. It also indicates the relative "strength" of the influence of perturbing variable. The value greater than

unity is considered influential while value less than a fraction of unity is considered not very important.

In combustion research, to assess the effects of chemical kinetics and molecular diffusion on S_u^o and K_{ext}. Sensitivity analysis is used to provide insight and help to interpret the results from simulation, i.e.

$$\frac{d(\log S_u^o)}{d(\log A_i)} = \frac{A_i}{S_u^o}\frac{\partial S_u^o}{\partial A_i}$$

It calculates the logarithmic sensitivity coefficient of laminar flame speed with respect to each individual reaction rate. Similar procedure can be done to analyze chemical and transport effect with respect to K_{ext}, which is originated by Dong and Holley [7, 18] where the dependent variable is the maximum axial velocity gradient close to extinction condition and the perturbing variable can be either chemical reaction rate or molecular diffusivity of certain species.

As will be discussed in later chapters, a "brute force" approach is implemented to determine the sensitivity of extinction strain rate with respect to thermal diffusion coefficient in order to study the soret effect of heavy hydrocarbon in non-premixed flames. It takes the form:

$$\frac{d(\log K_{ext})}{d(\log D_k^T)} = \frac{D_k^T}{K_{ext}}\frac{\partial K_{ext}}{\partial D_k^T}$$

where D_k^T is the thermal diffusion coefficient of K_{th} species.

3.2 Three Dimensional Modeling

3.2.1 Codes Description

The reduction of partial differential equations into algebraic equations still leaves their method of solution an open question. Traditional 1-D and 0-D combustion codes have employed non-linear techniques to great effect [19]. These principally involve defining a residue for each algebraic equation and finding its roots via a modified Newton method, retaining the coupling between all primitive variables during each iteration. This approach cannot be easily extended to notably more complex geometries as the size and number of operations of the matrices when using implicit methods very quickly becomes prohibitive. An alternative is to linearize the algebraic equations such that each is assumed to contain only one unknown while all others are substituted with available guesses and iterated over until all the equations are satisfied [20]. This linearized "predictor-corrector" approach is a widely used template in most finite volume based solvers. Cuoci et al have released 'laminarSMOKE' [21] (A Cuoci et al. 2011), a finite-volume based code built using the OpenFOAM [22] suite of CFD tools and the OpenSMOKE library [23] of functions that handles detailed chemistry and transport while offering an interface to various ODE solvers.

The stiff chemistry is handled by laminarSMOKE's operator splitting algorithm, first introduced by Strang [24]. The problem's reaction step is thus a spatial array of homogeneous reactors with appropriate initial conditions whose time integration is

handled by standard ODE solvers [25]. The momentum equation is solved via the PISO algorithm (Pressure Implicit with Splitting of Operators) [26] - used for the pressure-velocity coupling - to complete the algorithm for solving the discretized conservation equations. Thermodynamic, transport and kinetic quantities were evaluated using the OpenSMOKE library.

3.2.2 Mesh Generation Methodology

An example of grid generation is shown in Fig. 3.1, with axisymmetric grid layout and a radius of 6 cm and height of 20 cm is used in the numerical simulations. The approximate flame height and thickness are estimated using the 1-D calculations. The initial grid is constructed to be uniform in the area where the flame is expected to reside. The grid spacing in this region is set to be about 3 cells per flame thickness.

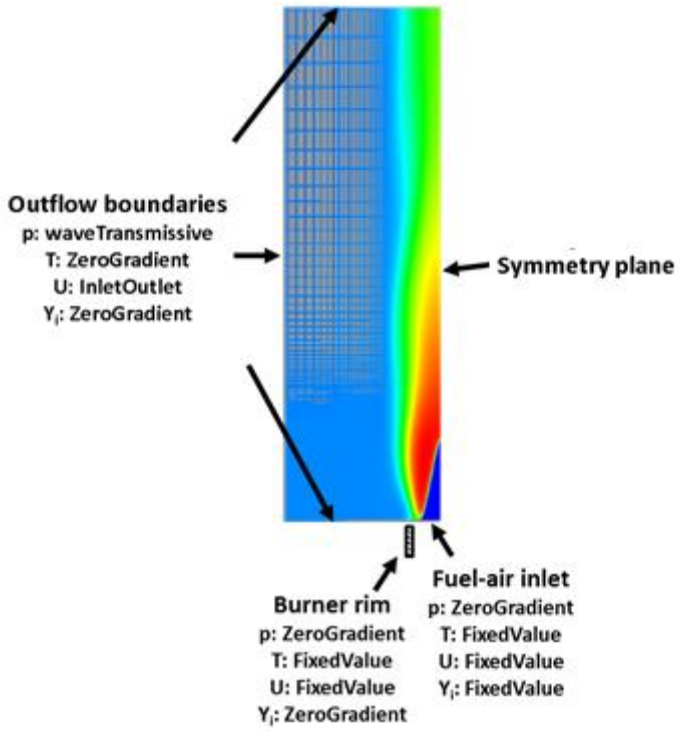

Figure 3.1. Computational grid used in the numerical simulations overlaid with boundary conditions applied for pressure, temperature, velocity, and chemical species.

A stretched non-uniform grid is utilized outside of this refined area. An initial non-reacting flow-field is established following which the mixture is ignited and the simulation is carried on until a steady-state solution for the flame is reached. Steady-state is established by ensuring that residuals for pressure, temperature, and velocity have reached a constant value. Further, the flame position and height are observed to be constant. At this point, an adaptive mesh refinement is performed at the flame front to increase the grid resolution in that location. The location of the flame

front is determined by computing the gradient and curvature of the temperature field. The simulation results from steady state are mapped on to the refined grid and computations are performed till a new steady state is achieved. This sequence of steps is carried out repeatedly till a highly refined flame region is established with an average of 70-80 cells through the flame thickness for each condition investigated. This level of refinement is considered adequate for the laminar conditions investigated in this work. Figure 3.2 shows a plot of temperature as a function of distance along a 1-D cut through the flame for a CH4-air mixture with ϕ=0.80 at the high Re condition. The data points in Fig. 3.2 correspond to individual grid points illustrating the refinement achieved in the solution through the flame thickness.

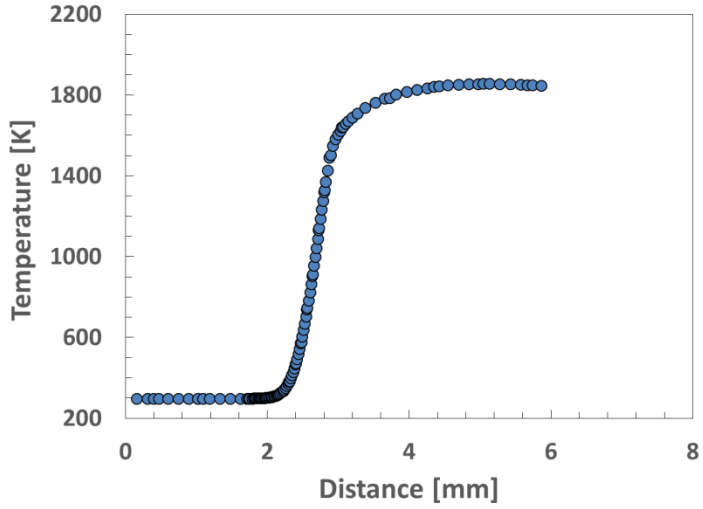

Figure 3.2. Temperature as a function of distance along a 1-D cut through the flame front for a CH4/air mixture with ϕ=0.80 at the high Re condition.

3.3 Kinetic Models

3.3.1 Models Used in Current Study

In order to address the liquid and solid fuel molecule oxidation and pyrolysis procedure, detail mechanism has been adopted in the current dissertation. The majority of the simulation is conducted using USC Mech II consisting 111 species and 784 reactions [27] and JetSurF 1.0 kinetic model consisting of 348 species and 163 reactions [28]. GRI 3.0 is used for natural gas related combustion simulation which consists 53 species and 325 reactions [29]. A skeletal mechanism based on a detailed C8-C16 n-alkane high-temperature kinetic model developed by Westbrook et al. [30] for *n*-alkanes up to *n*-$C_{16}H_{34}$ is used, consisting of 157 species and 1161 reactions. For gasoline and its surrogates simulation, a reduced 679 species and 3479 reaction mechanism by Westbrook et al.[31] is used and followed by a further reduced 323 species version mechanism for the Oppose-Jet simulation due to computation limitation. For solid fuel simulation, a detailed kinetic model for jet fuel surrogates that include oxidation kinetics of toluene is adopted [32] and compared with results from USC Mech II. A recent developed lump model for jet fuel is used to validate against experiments regarding the assumption of separation between pyrolysis process and combustion reaction in the vigorous burning system.

3.3.2 Kinetic Model Reduction Using Directed Relation Graph Method

Detailed kinetic models for large hydrocarbons involve typically hundreds of species and thousands of reactions to describe fuel oxidation and pyrolysis. However, as the computational time scales with the square of number of species, it is desirable to produce skeletal reduction with the elimination of unrelated species and reactions to the given system. The method employed here to reduce chemical models is the Directed Relation Graph (DRG) [33] which include solution sets from freely propagating flames, stretched flames and close to extinction flames.

DRG seeks to resolve the coupling between major and minor species. Major species are identified a priori and can be, for example, the fuel. The extent of the coupling is quantified by:

$$r_{\mathrm{AB}} \equiv \frac{\sum_{\mathrm{i}=1,\mathrm{II}} \left|\nu_{\mathrm{A,i}}\omega_i\delta_{\mathrm{B,i}}\right|}{\sum_{\mathrm{i}=1,\mathrm{II}} \left|\nu_{\mathrm{A,i}}\omega_{\mathrm{i}}\right|}$$

$$\delta_{\mathrm{B,i}} = \begin{cases} 1, & \text{if the ith reaction involves species B} \\ 0, & \text{otherwise} \end{cases}$$

where ν_{A} is the net stoiciometric coefficient of species *A* and ω is the net reaction rate. Thus, r_{AB} represents the relative error induced to *A* upon the elimination of *B*. The user specifies an error tolerance, ε, defined such that B is considered important to A for $r_{\mathrm{AB}} > \varepsilon$. All species for which this relationship is not true are removed from the model, generating a skeletal mechanism.

Recent modification includes the solution from both stretched flames and flames at close to extinction condition [34]. The reason for such modification is due to the findings of molecular differential diffusion phenomena in combustion process that the local concentration of fuel to oxygen ratio may vary at close to the flame front location and stretched flames may take drastically different reaction path than stretch-less flames.

3.4 References

[1] Grcar J. F., Kee R. J., Smooke M. D., & Miller J. A. *Symposium (International) on Combustion*, 21 (1988) 1773–1782.

[2] Kee R.J., Grcar J.F., Smooke M.D., & Miller J.A. Sandia Report SAND85-8240, Sandia Natioanl Laboratories. (1985).

[3] Egolfopoulos F., & Campbell C. *Combustion and Flame*, 117 (1999) 206–226.

[4] Kee R.J., Rupley F.M., and Miller J.A. Sandia Report SAND89-8009, Sandia National Laboratories. (1989).

[5] Kee R.J., & Miller J.A. Sandia Report SAND86-8841, Sandia National Laboratories. (1986).

[6] Kee R.J., Warnatz J., & Miller J.A. Sandia Report SAND83-8209, Sandia National Laboratories. (1983).

[7] Dong Y., Holley A. T., Andac M. G., Egolfopoulos F. N., Davis S. G., Middha P., & Wang H. *Combustion and Flame*, 142 (2005) 374–387.

[8] Middha P., & Wang H. *Combustion Theory and Modelling*, 9 (2005) 353–363.

[9] Egolfopoulos F. N., & Dimotakis P. E. *Symposium (International) on Combustion*, 27 (1998) 641–648.

[10] Nishioka M., Law C. K., & Takeno T. *Combustion and Flame*, 104 (1996) 328–342.

[11] Ji C., Dames, E., Wang Y. L., Wang H., & Egolfopoulos F. N. *Combustion and Flame*, 157 (2010) 277–287.

[12] Curtiss C. F., & Hirschfelder J. O. *The Journal of Chemical Physics*, 17 (1949) 550.

[13] Coffee T., & Heimerl J. *Combustion and Flame*, 43 (1981) 273–289.

[14] Dixon-Lewis G. *Proceedings of the Royal Society of London A: Mathematical, Physical and Engineering Sciences*, 307 (1968) 111–135.

[15] Glarborg P., Miller J. A., & Kee R. J. *Combustion and Flame*, 65 (1986) 177–202.

[16] Einstein A. Annalen der Physik 17 (1905) 549-560.

[17] Rosner D., Israel R., & La Mantia B. *Combustion and Flame*, 123 (2000) 547–560.

[18] Holley A. T., You X. Q., Dames E., Wang H., & Egolfopoulos F. N. *Proc. Comb. Inst*, 32 (2009) 1157–1163.

[19] Kee, R. J., Coltrin, M. E., & Glarborg, P. (2005). *Chemically reacting flow: theory and practice*. John Wiley & Sons.

[20] Peric, M. (1996). Computational methods for fluid dynamics. *Heidelberg: Springer—Verlag*.

[21] A. Cuoci, A. Frassoldati, T. Faravelli, E. Ranzi, Combust. Flame 160 (2013) 870-886

[22] OpenFOAM, www.openfoam.org, 2014

[23] A. Cuoci et al., OpenSMOKE: numerical modeling of reacting systems with detailed kinetic mechanisms, in: XXXIV Meeting of the Italian Section of the Combustion Institute, Rome, Italy, 2011.

[24] G. Strang, SIAM Journal on Numerical Analysis 5 (1968), 506-517

[25] P. N Brown, G. D. Byrne, A. C. Hindmarsh, SIAM journal on scientific and statistical computing 10(5) (1989), 1038-1051

[26] R.I Issa, Journal of Computational Physics, 62 (1986) 40-65

[27] Wang H., You X., Joshi A.V., Davis S.G., Laskin A., Egolfopoulos F.N., and Law C.K.(2007) (http://ignis.usc.edu/USC_Mech_II.htm)

[28] Wang H., Dames E., Sirjean B., Sheen D.A., Tangko R., Violi A., Lai J.Y.W., Egolfopoulos F.N., Davidson D.F., Hanson R.K., Bowman C.T., Law C.K., Tsang W., Cernansky N.P., Miller D.L., and Lindstedt R.P. (2010) (http://melchior.usc.edu/JetSurF/JetSurF2.0)

[29] Smith G. P., Golden D. M., Frenklach M., Moriarty, N. W., Eiteneer, B., Goldenberg M., Gardiner Jr, W. C. (1999). GRI-Mech 3.0.

[30] Westbrook, C. K., Pitz, W. J., Herbinet, O., Curran, H. J., & Silke, E. J. *Combustion and Flame*, 156 (2009) 181–199.

[31] Mehl M., Pitz W. J., Westbrook C. K., & Curran H. J. *Proc. Comb. Inst*, 33 (2011) 193–200.

[32] Dooley S., Won S. H., Chaos M., Heyne, J., Ju Y., Dryer F. L., Oehlschlaeger M. A. *Combustion and Flame*, 157 (2010) 2333–2339.

[33] Lu T., & Law C. K. *Combustion and Flame*, 144 (2006) 24–36.

[34] Jayachandran J., Lefebvre A., Zhao R., Halter F., Varea E., Renou B., & Egolfopoulos F. N. *Proc. Comb. Inst*, 35 (2015) 695–702.

Chapter 4: Determination of Laminar Flame Speeds: Molecular Transport Effects

4.1 Introduction

As discussed in Chapter 1, S_u^o is a fundamental property of any combustible mixture and it serves to constrain and validate kinetic models [1,2].Furthermore, S_u^o along with the Markstein length, L, which characterizes the response of laminar flame propagation to stretch, are inputs in turbulent flame models under conditions that the flamelet concept is applicable [3-5].

Measurement of S_u^o began as early as in the 1920's when Stevens [6,7] studied flame propagation at constant pressure by tracking spherically expanding flames, SEF, in a soap bubble filled with a flammable mixture. Since then, significant progress has been made both in the experimental and numerical determination of S_u^o. However, notable scatter by as much as 25 cm/s was persistent in published S_u^o's of methane flames [8] until the 1980's when the effect of flame stretch [9] on flame propagation was accounted for and subtracted from the measurements reducing thus the experimental uncertainty notably [10-13]. Despite this progress, due to the relatively low sensitivity of S_u^o to chemical kinetics [14], there is need for experimental data with even lower uncertainty compared to what is reported currently so that they can be used for kinetic model validation.

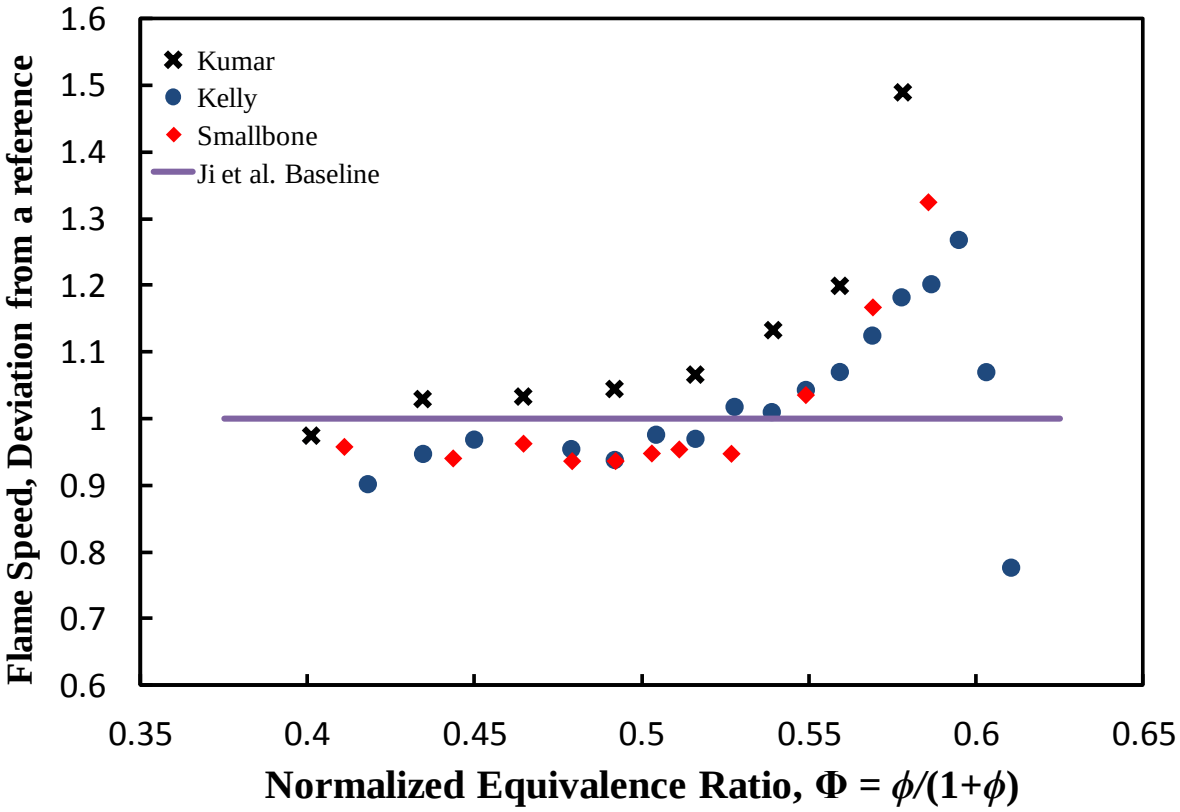

Figure 4.1. Deviation of experimental S_u^o's of *n*-heptane/air mixtures at p = 1 atm from that of Ji et al. [16] (T_u = 353 K) represented by the solid line. Data represented by symbols include: (●) Kelley et al. [17] (T_u = 353 K), (♦) Smallbone et al. [18] (T_u = 350 K) and (**x**) Kumar et al. [19] (T_u = 360 K).

Despite the fact that considerable effort has been devoted to understanding the intricacies and physics behind the measurements, significant discrepancies persist in reported data, even when using the same method. Figure 4.1 depicts the relative deviation of experimental S_u^o with a normalized equivalence ratio $\Phi \equiv \phi/(1+\phi)$ [15], where ϕ is the equivalence ratio, of *n*-heptane/air mixtures reported in different studies from the data of Ji et al. [16] that are used as the reference value. One can observe the

increasing discrepancy between data obtained using the SEF [17] and counter flow flames, CFF, [18,19] configurations for off-stoichiometric $\phi > 1$ mixtures; corrections of the data reported in Refs. 18 and 19 to account for the different unburned mixture temperatures, T_u, were made using the recommendation of Wu et al. [20]. It is evident that the disparity between the S_u^o data sets increases with ϕ and this trend persists for flames of several high molecular weight, MW, fuels [16]. For $\phi > 1$ hydrocarbon/air mixtures, air is abundant on both mass and molar basis compared to the fuel. Thus, the thermal diffusivity of the mixture is nearly that of nitrogen, and hence a Lewis number, *Le*, calculated based on oxygen, being the deficient reactant for $\phi > 1$ mixtures, will be close to unity as shown in Fig. 4.2a regardless of the fuel MW.

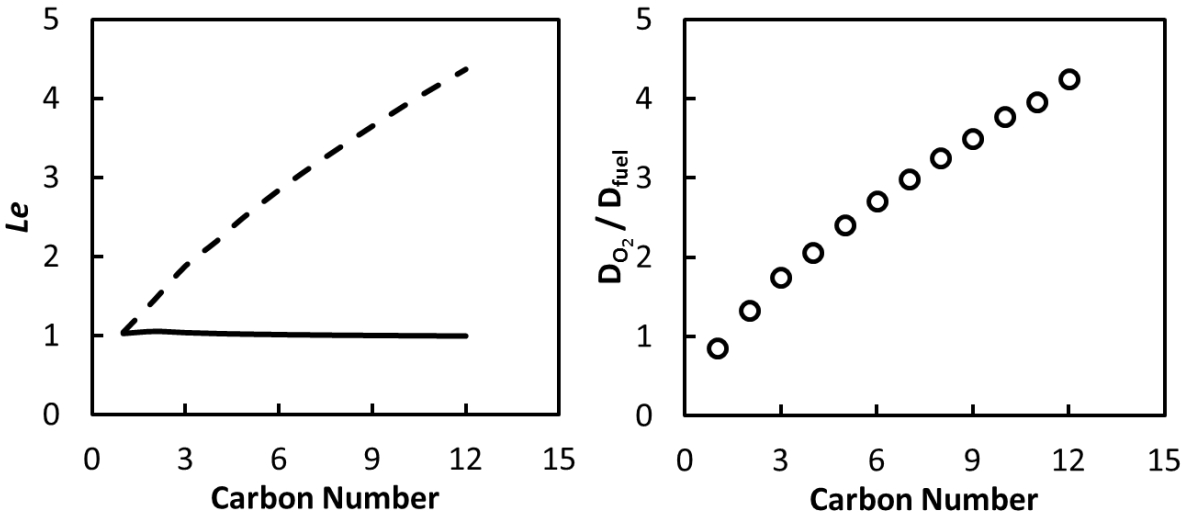

(a) (b)

Figure 4.2. (a) Variation of *Le* with carbon number for *n*-alkane/air mixtures at p = 1 atm and T_u = 298 K, for ϕ = 0.7 (dashed line) and ϕ = 1.4 (solid line). (b) Variation of the ratio of oxygen diffusivity to fuel diffusivity with carbon number for ϕ = 1.4 *n*-alkane/air mixtures at p = 1 atm and T_u = 298 K.

These inconsistencies point to possible uncertainties in the experimental determination of S_u^o, and could be associated with the reactant flow rates, i.e. ϕ, diagnostic equipment, the flow velocity measuring approach, data analysis, and finally data interpretation. In order to tackle uncertainties associated with each experimental approach, detailed understanding of the physics controlling the flame behavior and response to fluid mechanics and loss mechanisms is required.

At pressures less than 10 atm, S_u^o can be measured using the CFF approach in which steady, laminar, and planar flames (e.g. [5,13]) are established. Under such conditions,

the only parameter that can be varied for a given set of thermodynamic conditions is the flame stretch, and this effect can be characterized readily using available quasi-one dimensional codes (e.g. [22]).

Law and co-workers introduced the CFF approach to determine S_u^o [5,13,23]. The method involves the determination of the axial velocity profile along the system centerline and subsequently the identification of two distinct observables. A reference flame speed, Su,ref, which is the minimum velocity just upstream of the flame, and a characteristic stretch, K, which is the maximum absolute value of the axial velocity gradient in the hydrodynamic zone. Thus, by varying Su,ref with K in the experiments, it was proposed [5,13,23] that S_u^o can be determined by performing a linear extrapolation of the experimental data to zero stretch given that as $K \rightarrow 0$, Su,ref should degenerate to S_u^o. This approach was used in several studies (e.g., [24-26]) for H2 and C1-C2 hydrocarbon flames.

Subsequently, Tien and Matalon [27] demonstrated through asymptotic analysis that the $S_{u,ref}$ vs. K response is non-linear as $K \rightarrow 0$, and that linear extrapolation of $S_{u,ref}$ to K = 0 results in the over-estimation of S_u^o; it should be noted that $S_{u,ref}$ is not the stretched flame speed, Su, as it is affected by thermal dilatation and flow divergence effect [13,27,28]. Tien and Matalon [27] produced also a non-linear expression describing the variation $S_{u,ref}$ with K, which subsequently was expressed by Davis and Law [29] in a more compact way as:

$$S_{u,ref} = S_u^o \{1 - (\mu - 1) Ka + Ka \ln[(\sigma - 1)/Ka]\}. \quad (1)$$

In Eq. 1, μ is the Markstein number, $Ka \equiv \alpha K / (S_u^o)^2$ the Karlovitz number, α the thermal diffusivity of the mixture, and $\sigma \equiv (\rho_u / \rho_b)$ with ρ_u and ρ_b being the densities of the unburned and burned states at equilibrium respectively.

Chao et al. [30] used asymptotic analysis to show that the error introduced by linear extrapolations can be reduced for small *Ka* and large burner separation distance relative to the flame thickness. Vagelopoulos et al. [31] further showed computationally and experimentally that in order for the linear extrapolation to be accurate, *Ka* must be of the order of 0.1 for CH_4/air, C_3H_8/air, and lean H_2/air flames.

Recently, Egolfopoulos and co-workers [16,32,33] introduced a computationally assisted approach in quantifying the non-linear variation of $S_{u,ref}$ with *K*. Specifically, direct numerical simulations (DNS) of the experiments are carried out with detailed description of molecular transport and chemical kinetics to avoid simplifying assumptions used in asymptotic analysis. Thus, the variation of $S_{u,ref}$ with *K* is computed and can be used to perform the non-linear extrapolations of the experimental data; indeed the DNS approach reproduces the non-linear behavior of $S_{u,ref}$ with *K* as predicted by Tien and Matalon [27]. Given that the computed $S_{u,ref}$ vs. *K* curve may lie over or below the data due to transport and kinetic model uncertainties, it was shown that as long as the discrepancies between data and predictions are not large, say within 30-40%, the shape of the $S_{u,ref}$ vs. *K* curve is minimally affected and could be translated

to best fit the data and derive S_u^o at $K = 0$. This was confirmed through DNS in which the rates of main H+O2 $\rightarrow$ OH+O branching or CO+OH $\rightarrow$ CO2+H oxidation reactions as well as the diffusion coefficients of the reactants were modified intentionally by as much as 30-40%. It was shown that even under such notable but not excessive modifications of the overall reaction rate, the shape of the computed $S_{u,ref}$ vs. K curves are nearly indistinguishable [32].

Ji et al. [16] showed that for the same sets of experimental data of C5-C12 n-alkanes, linear extrapolation yield higher S_u^o's for fuel rich mixtures, as compared to nonlinear extrapolation using the computationally assisted approach. Considering also the results shown in Fig. 4.1, it is reasonable to assume that the discrepancies between reported S_u^o's for $\phi > 1$ mixtures could be attributed partially to the extrapolations.

4.2 Numerical Approach

In order to assess the validity of current practices in determining S_u^o, detail numerical simulation were performed using a variety of codes and detailed description of chemical kinetics and molecular transport. The DNS results were treated as "data" for the range of K's that are typically used in both types of experiments, and subsequently Eqs. 1 was used to perform extrapolations. The advantage of this approach is that both the response of flame propagation to K from high to near-zero values and S_u^o are known so that the merits and shortcomings of Eqs. 1 can be assessed.

Furthermore, the DNS approach allows for the rigorous assessment of reactant differential diffusion effects. A parametric study was performed on the effect of the fuel diffusivity on the response of CH_4/air flames to K given the relatively small size of the kinetic model and the fact that diffusivities of CH_4 and O_2 do not differ substantially. The variation of the CH_4 diffusivity was implemented through modification of its Lennard-Jones (L-J) parameters. The unperturbed case is referred to as OD (original diffusivity). ID (increased diffusivity) and DD (decreased diffusivity) refer to the cases in which the L-J parameters of CH_4 were replaced with those of H_2 and n-$C_{12}H_{26}$ respectively. This approach ensures that the chemistry is consistent in all computations, and also circumvents the complexities associated with fuel cracking which high MW fuels are susceptible to. The values of Le and ratio of fuel to oxygen diffusivities in the mixture are shown in Table 4.1 for ϕ = 0.7, 1.0, and 1.4. DNS were performed also for steady n-$C_{12}H_{26}$/air flames in order to verify the results obtained from CH_4/air flames.

Table 4.1. Lewis number, *Le* and ratio of fuel to O_2 diffusivities for the mixtures used in the present study.

ϕ	*Le*	D_{fuel}/D_{O2}
Original L-J Parameters (OD)		
0.7	1.0	1.14
1.0	N/A	1.16
1.4	1.1	1.17
n-$C_{12}H_{26}$ L-J Parameters (DD)		
0.7	2.3	0.45
1.0	N/A	0.48
1.4	1.0	0.51
H_2 L-J Parameters (ID)		
0.7	0.7	1.67
1.0	N/A	1.67
1.4	1.2	1.68

S_u^o's and variation of $S_{u,ref}$ with K were computed respectively, using the PREMIX code [55,56] and an opposed-jet flow code [57] that was originally developed by Kee and co-workers [22]. Both codes were integrated with the CHEMKIN [58] and the Sandia transport [59,60] subroutine libraries. The H and H_2 diffusion coefficients of several

key pairs are based on the recently updated set [61]. Both codes have been modified to account for thermal radiation (OTL) of CH_4, CO, CO_2, and H_2O [57,62].

S_u^o's and the variation of $S_{u,ref}$ with K were computed using the USC-Mech II [63] and JetSurF 1.0 [64] kinetic models for CH_4/air and n-$C_{12}H_{26}$/air flames respectively. The simulations were performed for the twin flame configuration and for a large burner separation distance (10 cm) to avoid conductive heat loss to the burner at very low K's.

4.3 Results and Discussion

Figure 4.3 depicts the variation of S_u^o with ϕ for CH_4/air mixtures for various CH_4 diffusivities, D_{CH4}, while in Fig. 4.4 the logarithmic sensitivity coefficients of S_u^o to the CH_4-N_2 and O_2-N_2 binary diffusion coefficients are shown. Results indicate that the modification of D_{CH4} has an opposite effect on S_u^o for $\phi < 1.0$ and $\phi \geqslant 1.0$.

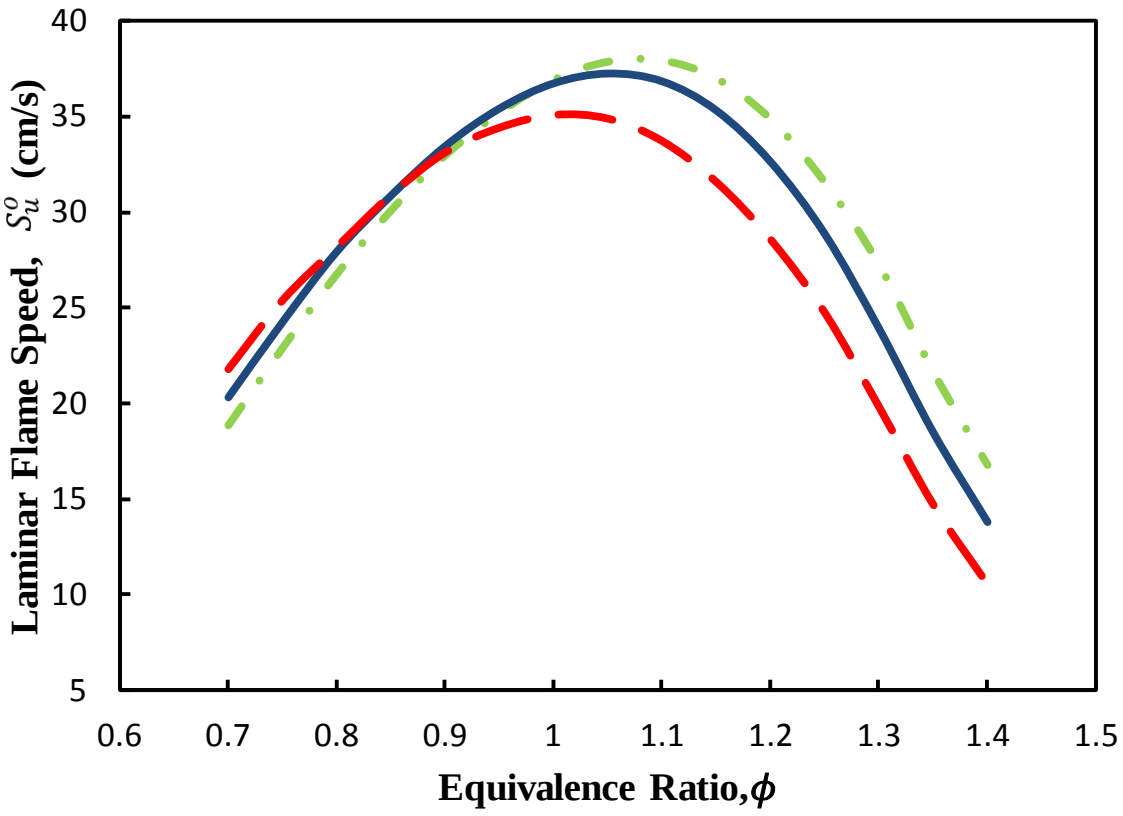

Figure 4.3. Computed S_u^o's of CH_4/air flames at p = 1 atm and T_u = 298 K using USC-Mech II. (—) OD; (---) DD; (–· –) ID.

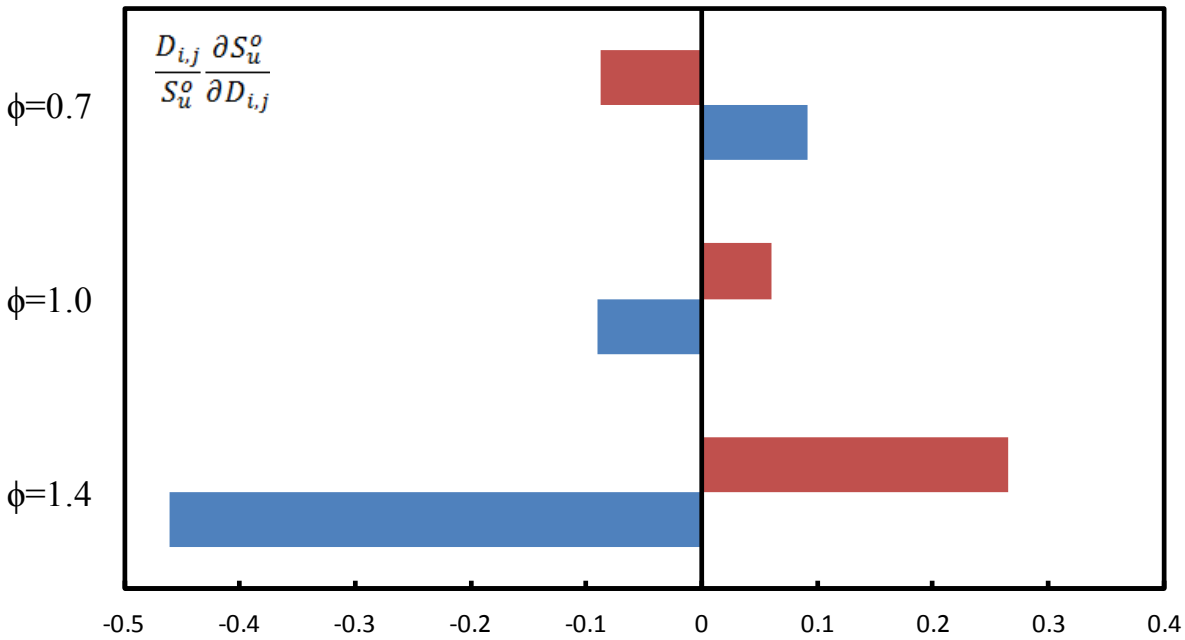

Figure 4.4. Logarithmic sensitivity coefficients of S_u^o to the CH_4-N_2 (red) and O_2-N_2 (blue) binary diffusion coefficients for CH_4/air flames at p = 1 atm, T_u = 298 K, and various ϕ's.

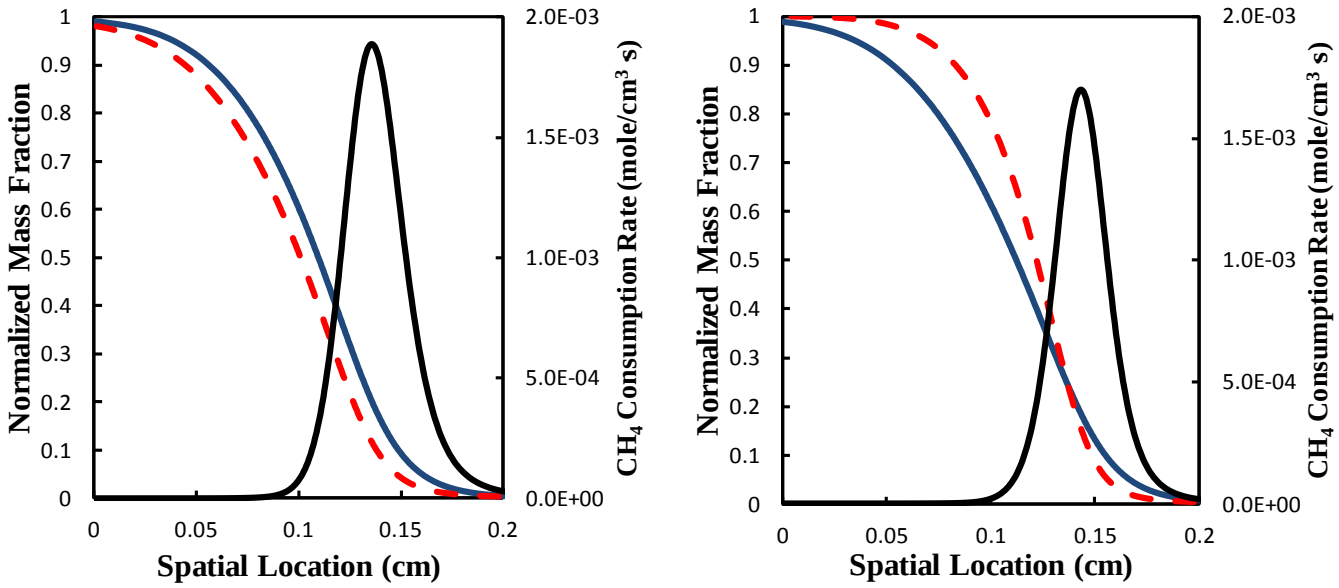

(a) (b)

Figure 4.5. (a) Normalized mass fraction profiles of CH_4 (---) and O_2 (—), and CH_4 consumption rate profile (—) for a $\phi = 1.4$ freely propagating CH_4/air flame at $T_u = 298$ K and $p = 1$ atm, computed using USC-Mech II and OD. (b) Normalized mass fraction profiles of CH_4 (---) and O_2 (—), and CH_4 consumption rate profile (—) for a freely propagating flame at $T_u = 298$ K, $p = 1$ atm, and $\phi = 1.4$, computed using USC-Mech II and DD.

Details of the flame structure are shown in Fig. 4.5, and it can be seen that a change in D_{CH4} results in a corresponding change in its diffusion length relative to O_2. The diffusion length of CH_4 for a $\phi = 1.4$ CH_4/air flame computed with DD (Fig. 4.5b) is reduced compared to the OD case (Fig. 4.5a). Thus, Y_{CH_4} and the local equivalence ratio,

ϕ_{local}, increase at the location at which the CH_4 consumption initiates as shown in Fig. 4.6, which results in the reduction of reactivity, shown also in Fig. 4.6.

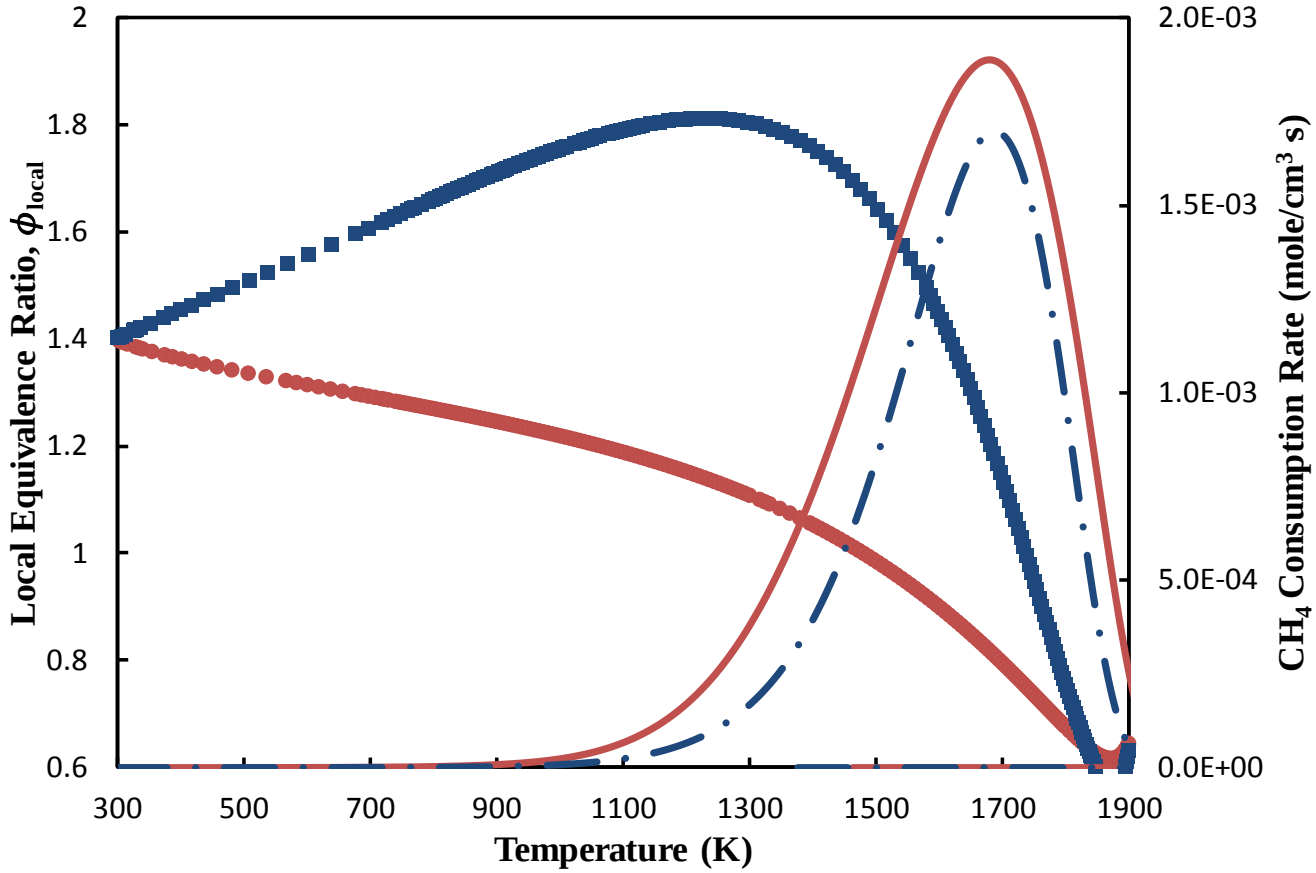

Figure 4.6. Variation of ϕ_{local} with temperature in a ϕ = 1.4 freely propagating CH_4/air flame at p = 1 atm, and T_u = 298 K computed using USC-Mech II with OD (●) and DD (■), and variation of CH_4 consumption rate with temperature with OD (—) and DD (– · –).

Similar analysis can be used to explain the dependence of S_u^o on D_{CH4} for all mixtures shown in Table 4.1. Furthermore, it is of interest to note that the dependence

of S_u^o on D_{CH4} is not captured by the following equation that is based on *Le* considerations [76]:

$$S_u^o(Le \neq 1) = S_u^o(Le = 1)\ \sqrt{Le} \qquad (3)$$

The effect of reactant differential diffusion on the propagation of stretched flames was assessed in the CFF configuration. Figures 4.7-4.9 depict the variation of $S_{u,ref}/S_u^o$ with *Ka* for ϕ = 0.7, 1.0, and 1.4 mixtures respectively. These figures include also the extrapolation curves using Eq. 1 that fit the DNS results for a range of *Ka* that are representative of those used in experiments (e.g. [27, 29]). Using OD, Eq. 1 predicts closely the DNS results. As D_{CH4} starts deviating from the oxygen diffusivity, D_{O2}, for the ID and DD cases, a discrepancy is observed between the extrapolated S_u^o from its known value by as much as 5% for ϕ = 0.7 with ID and 30% for ϕ = 1.4 with DD.

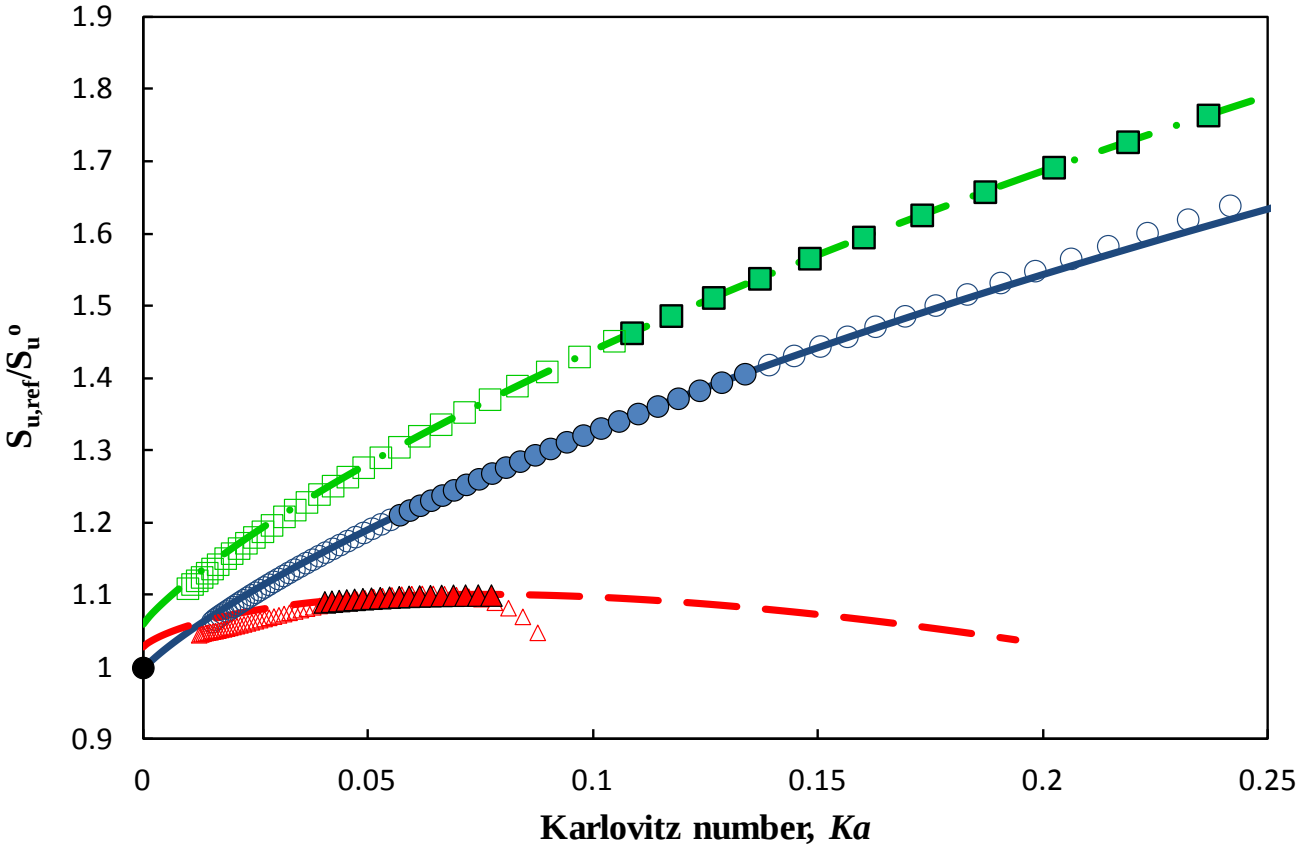

Figure 4.7. Variation of $S_{u,ref}/S_u^o$ with Ka of a ϕ = 0.7 CH_4/air CFF at p = 1 atm and T_u = 298 K computed using USC-Mech II with ID (■), OD (●), and DD (▲). ID (–· –), OD (—), and DD (---) correspond to fitting using Eq. 1. The full range DNS results are shown in hollow symbols, while the DNS results used for fitting Eq. 1 are shown in solid symbols.

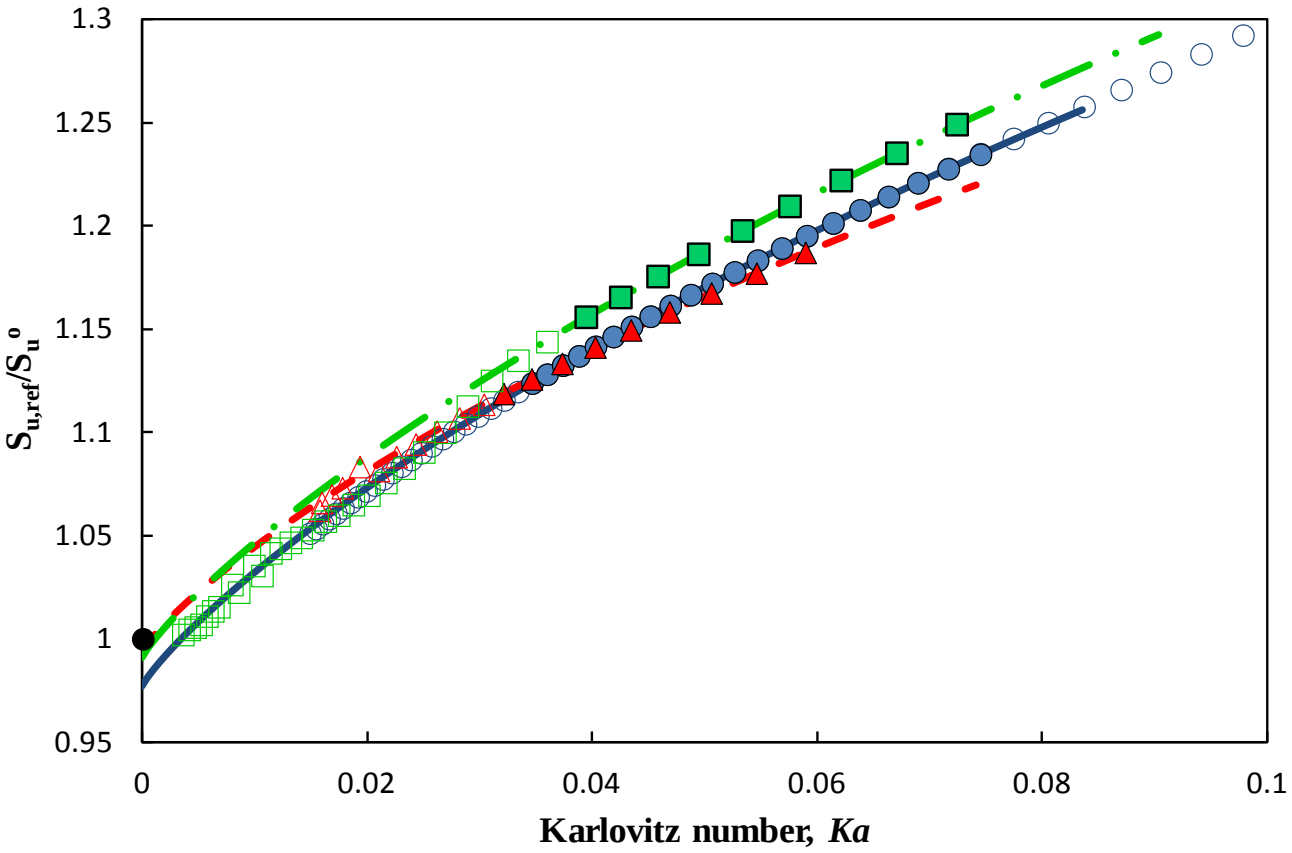

Figure 4.8. Variation of $S_{u,ref}/S_u^o$ with Ka of a ϕ = 1.0 CH_4/air CFF at p = 1 atm and T_u = 298 K computed using USC-Mech II with ID (■), OD (●), and DD (▲). ID (–· –), OD (—), and DD (---) correspond to fitting using Eq. 1. The full range DNS results are shown in hollow symbols, while the DNS results used for fitting Eq. 1 are shown in solid symbols.

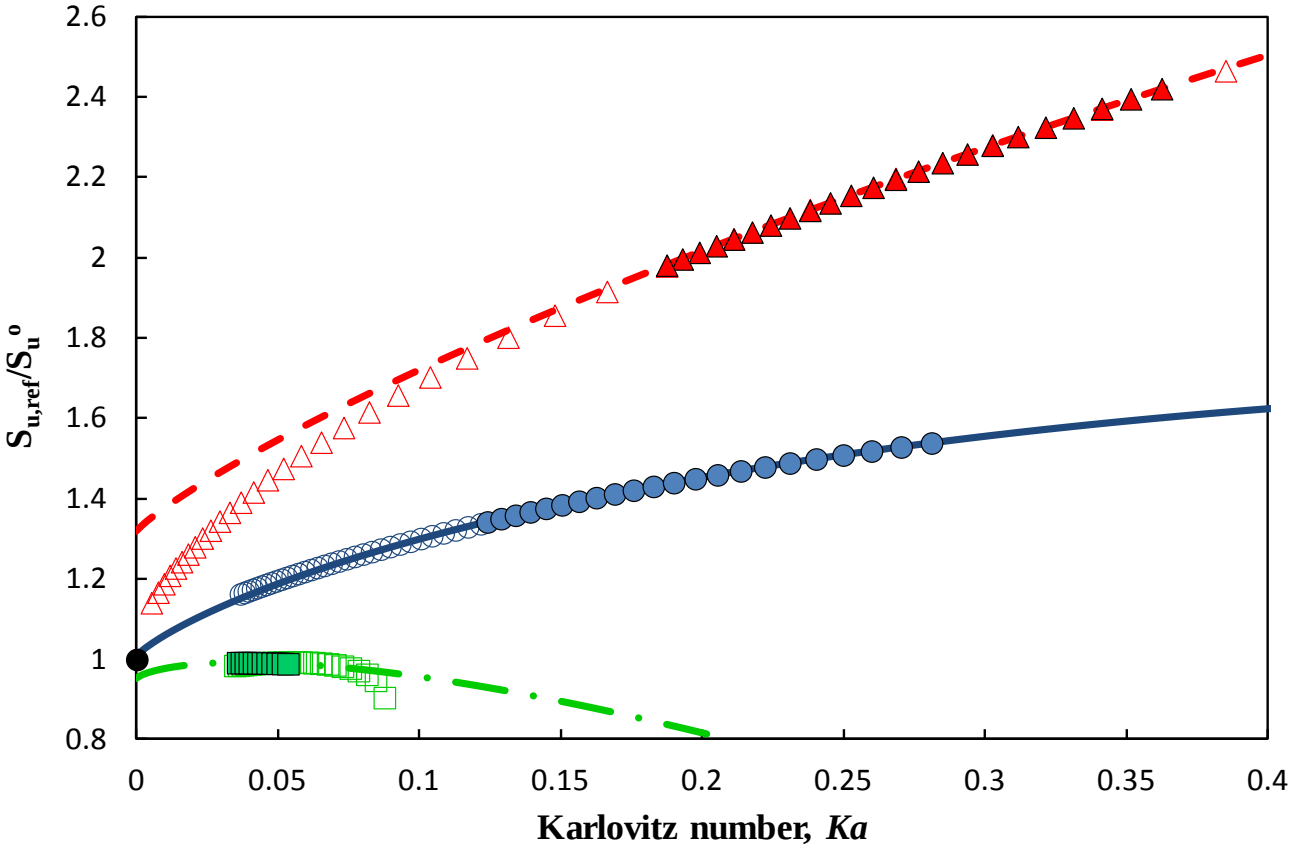

Figure 4.9. Variation of $S_{u,ref}/S_u^o$ with *Ka* of a ϕ = 1.4 CH_4/air CFF at p = 1 atm and T_u = 298 K computed using USC-Mech II with ID (■), OD (●), and DD (▲). ID (–· –), OD (—), and DD (---) correspond to fitting using Eq. 1. The full range DNS results are shown in hollow symbols, while the DNS results used for fitting Eq. 1 are shown in solid symbols.

From Figs. 4.7-4.9 it is apparent also that there is a significant change in slope of the $S_{u,ref}/S_u^o$ vs. *Ka* curve when D_{CH_4} is modified for the ϕ = 0.7 and 1.4 mixtures. In CFF's, it is not possible to monitor the modification of the burning intensity with *K* by simply tracking the variation of $S_{u,ref}$ with *K*, as $S_{u,ref}$ is affected also by thermal dilatation and

flow divergence [13,28,29]. On the other hand, the burning intensity is best described by the total heat release rate per unit area, HRR_{tot}, obtained by integrating the heat release rate over the entire flame. Figures 4.10-4.12 depict the variation of HRR_{tot} with Ka for ϕ = 0.7, 1.0, and 1.4 mixtures respectively. The results for the ϕ = 0.7 mixture shown in Fig. 10 can be explained based on $Le \neq 1.0$ effects caused by the imbalance of energy loss from and energy gain by the reaction zone [76]. For the ϕ = 1.4 mixture however, even though $Le \approx 1.0$ for all hydrocarbons, a substantial increase in HRR_{tot} with Ka is seen for the DD case for which there is a notable difference between D_{CH_4} and D_{O_2}. Thus, the diffusion rate of O_2 towards the reaction zone increases compared to CH_4 with increasing K, making thus the mixture more stoichiometric and increasing the overall reactivity [76]. For the ϕ = 1.0 mixture the slope of HRR_{tot} with Ka does not change for the different D_{CH_4} values. This is due to the fact that for near-stoichiometric mixtures there is a minor sensitivity of the overall reactivity to modifications in ϕ as it reaches a maximum value.

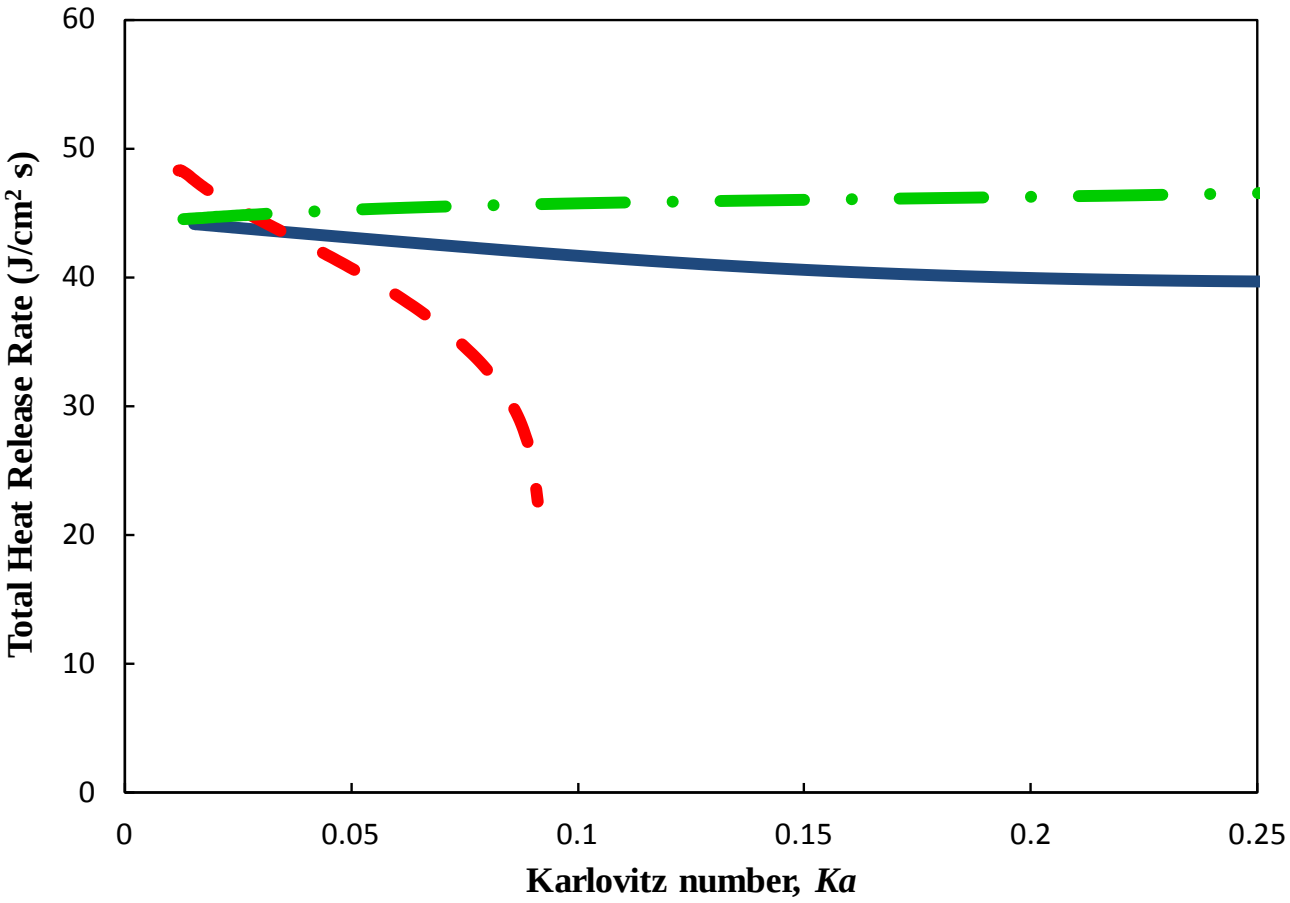

Figure 4.10. Variation of HRR_{tot} with Ka of a ϕ = 0.7 CH_4/air CFF at p = 1 atm and T_u = 298 K computed using USC-Mech II with ID (–· –), OD (—), and DD (---).

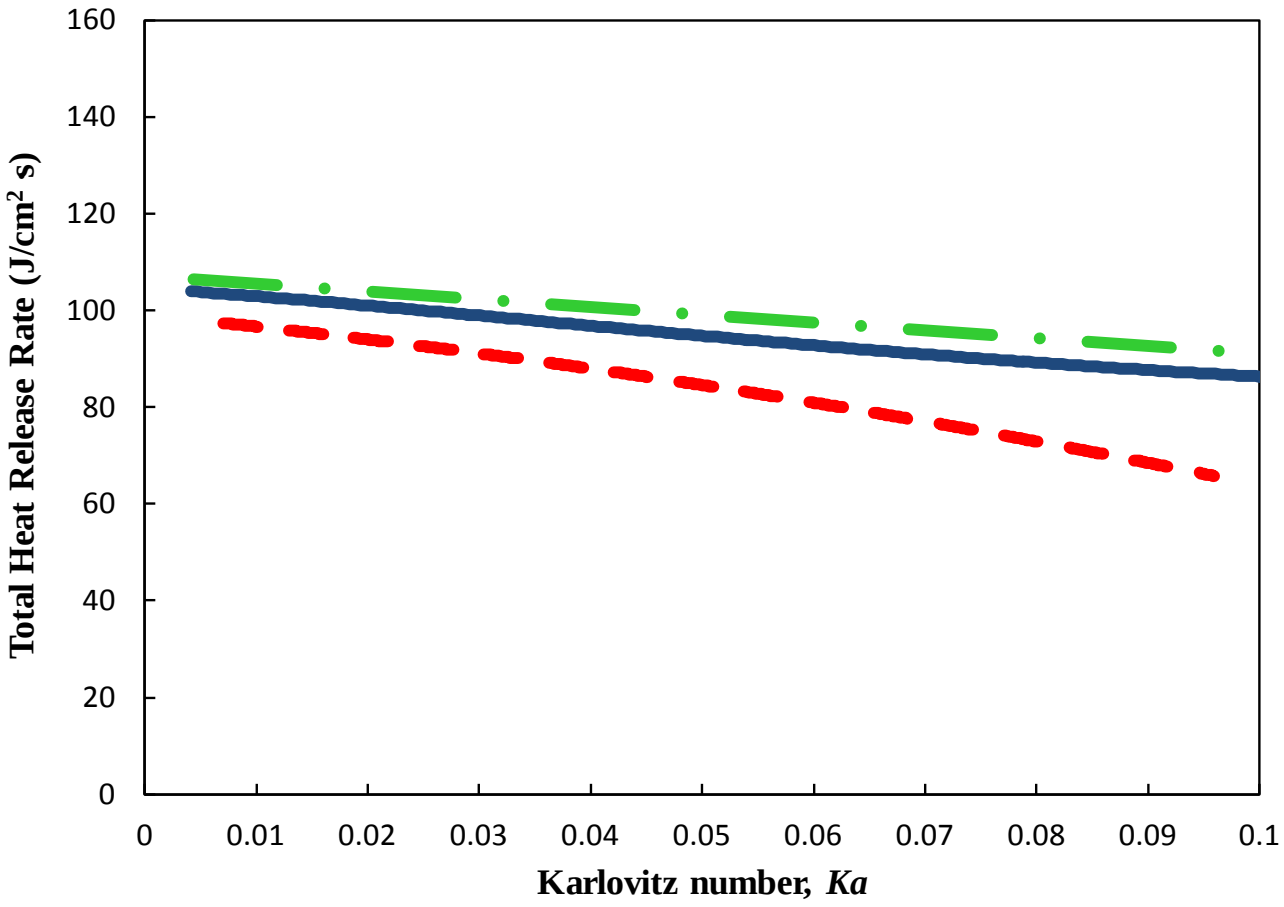

Figure 4.11. Variation of HRR_{tot} with Ka of a ϕ = 1.0 CH_4/air CFF at p = 1 atm and T_u = 298 K computed using USC-Mech II with ID (–· –), OD (—), and DD (---).

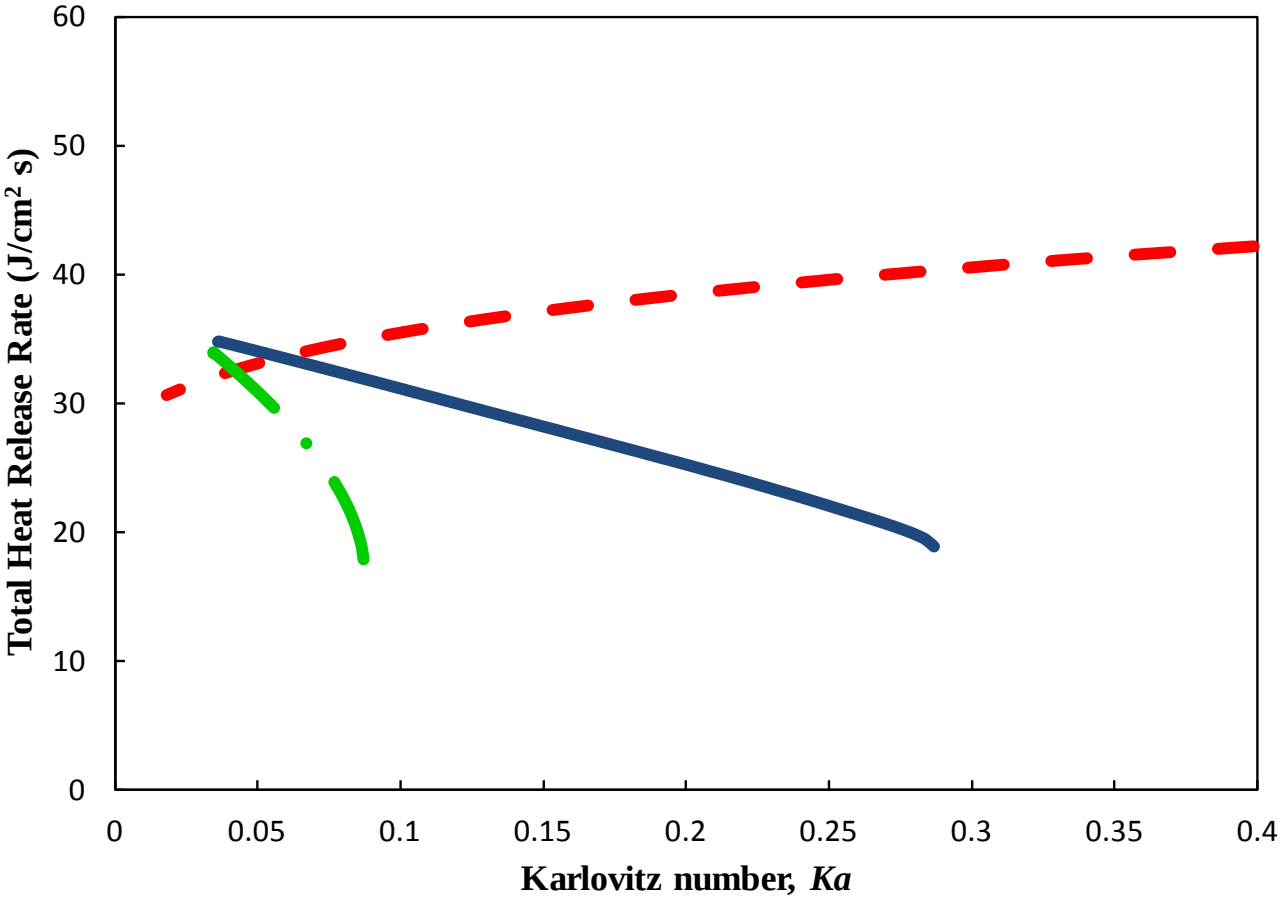

Figure 4.12. Variation of HRR_{tot} with Ka of a ϕ = 1.4 CH_4/air CFF at p = 1 atm and T_u = 298 K computed using USC-Mech II with ID (–· –), OD (—), and DD (---).

Figures 4.13 and 4.14 depict the variations of ϕ_{local} and the consumption rate of CH_4 for a ϕ = 1.4 flame at K = 30 and 200 s^{-1} respectively and computed with OD and DD. The results confirm that as K increases, ϕ_{local} decreases at the locations at which the CH_4 consumption begins. As a result, there is a notable increase of the CH_4 consumption rate as K increases for the DD case compared to OD. More specifically, the maximum CH_4 consumption rate is about 40% higher for the DD case for K = 30 $s,^{-1}$ and by a factor

of 3.5 for K = 200 s.$^{-1}$ These results reveal the basis physics that control the dependence of the overall flame reactivity with stretch for rich mixtures of high MW fuels and which need to be accounted for when raw experimental data are interpreted to determine non-directly measured properties such as S_u^o.

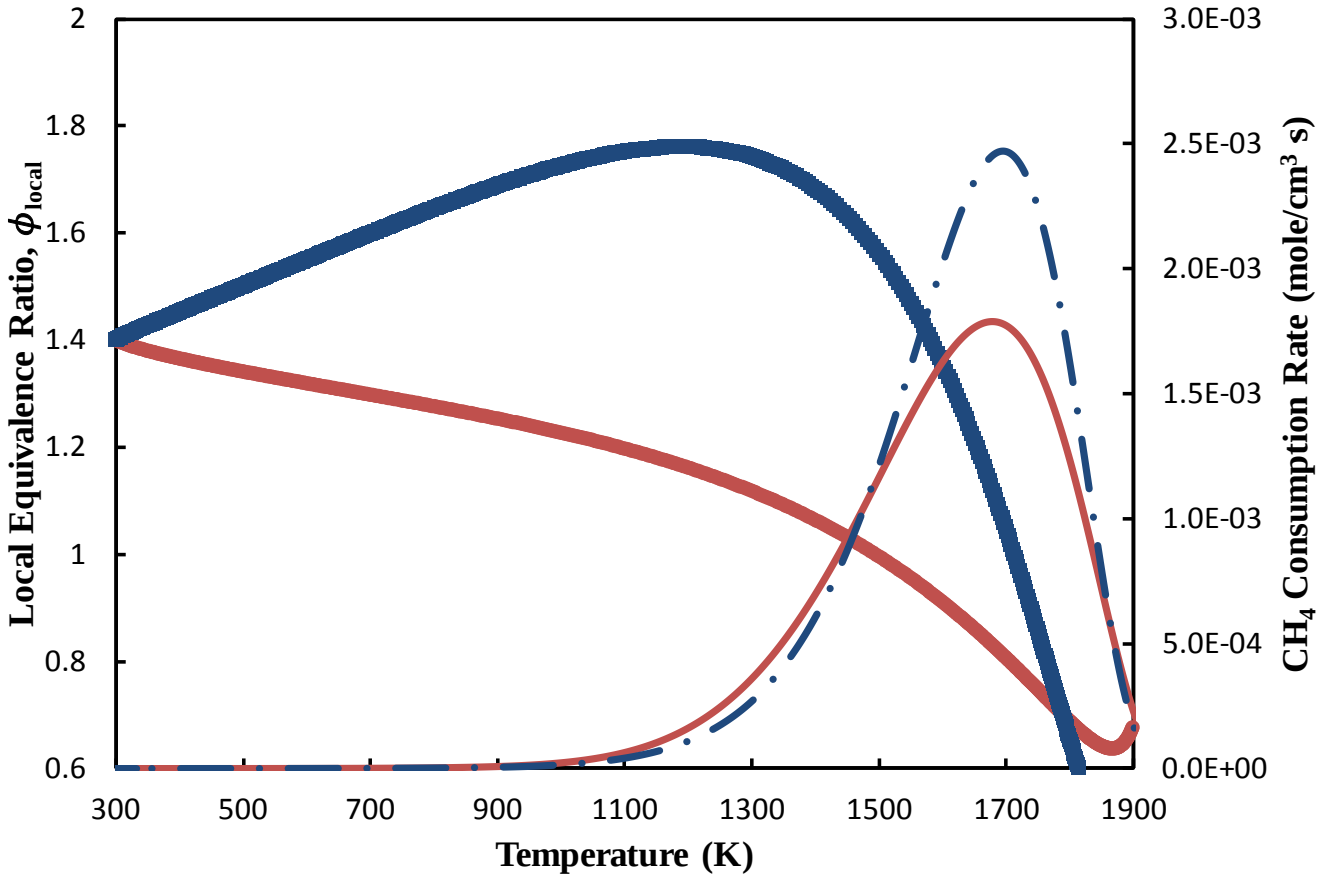

Figure 4.13. Variation of ϕ_{local} with temperature in a ϕ = 1.4 CH_4/air CFF at p = 1 atm, T_u = 298 K, and K = 30 s^{-1} computed using USC-Mech II with OD (●) and DD (■), and variation of CH_4 consumption rate with temperature with OD (—) and DD (–· –).

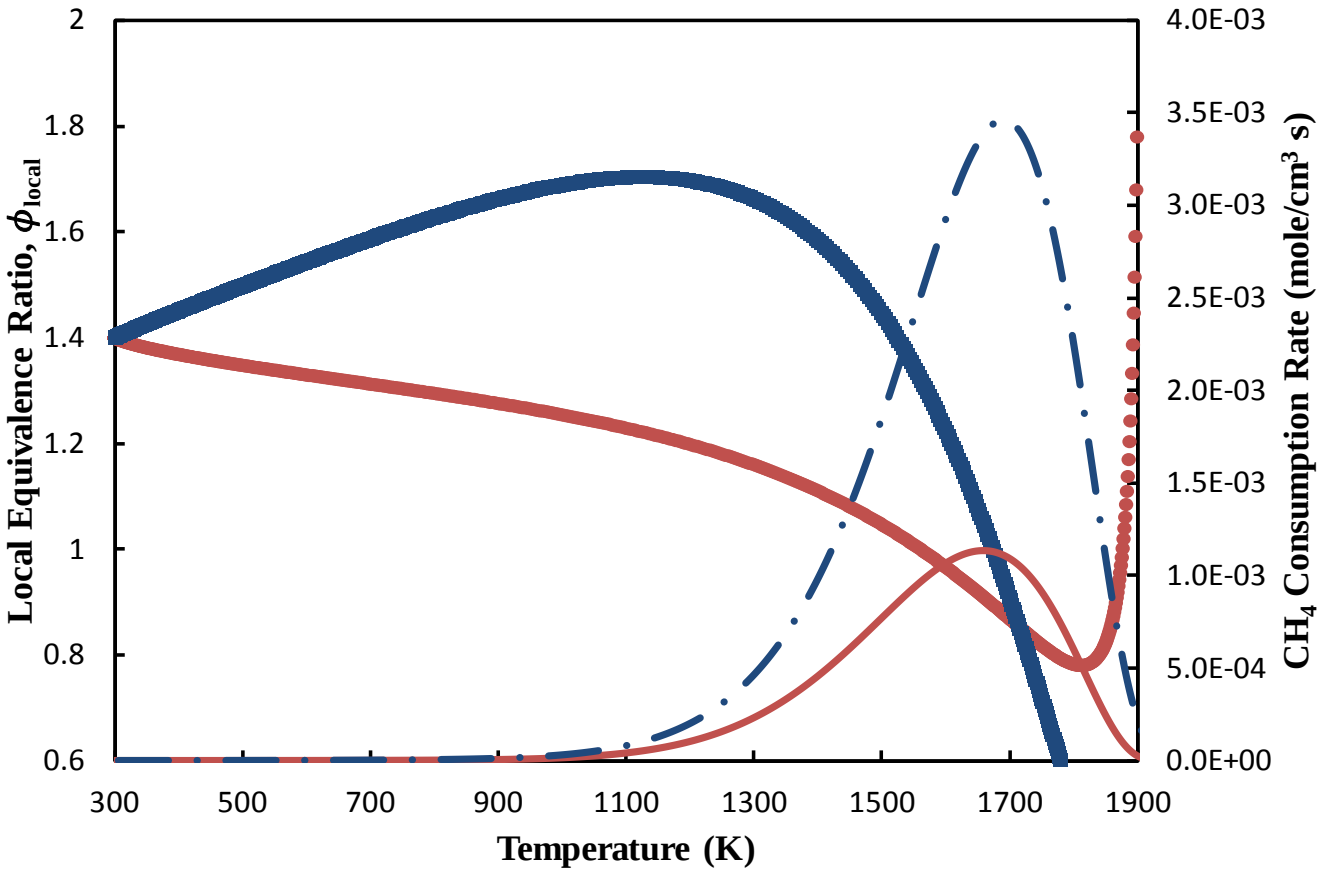

Figure 4.14. Variation of ϕ_{local} with temperature in a ϕ = 1.4 CH_4/air CFF at p = 1 atm, T_u = 298 K, and K = 200 s^{-1} computed using USC-Mech II with OD (●) and DD (■), and variation of CH_4 consumption rate with temperature with OD (—) and DD (–· –).

n-$C_{12}H_{26}$/air CFF's were computed also in order to verify the findings for CH_4/air flames. The diffusivity of n-$C_{12}H_{26}$/air was modified also by using the L-J parameters of CH_4 and this case is referred to as ID given that n-$C_{12}H_{26}$ becomes more diffusive. Figures 4.15 and 4.16 depict the variation of $S_{u,ref}/S_u^o$ with Ka for ϕ = 0.7 and 1.4 respectively and the behavior is consistent with that observed for CH_4/air flames. The ϕ = 0.7 flame computed with OD mixture exhibits lower $S_{u,ref}$ values and the flame

extinguishes at lower K compared to the ID case as shown in Fig. 4.15. Furthermore, the use of Eq. 1 in both OD and ID cases results in S_u^o's that are close to its known value. On the other hand, for the ϕ = 1.4 flame, using Eq. 1 results in the over-prediction of the known S_u^o value by 9% and 4% for the OD and ID cases respectively. The variations of the peak local equivalence ratio, of $(\phi_{local})_{peak}$ and HRR_{tot} are shown in Fig. 4.17 for a ϕ = 1.4 n-$C_{12}H_{26}$/air flame computed with OD. Similarly to CH_4/air flames computed with DD, $(\phi_{local})_{peak}$ decreases and HRR_{tot} increases as Ka increases given that the flame becomes more stoichiometric.

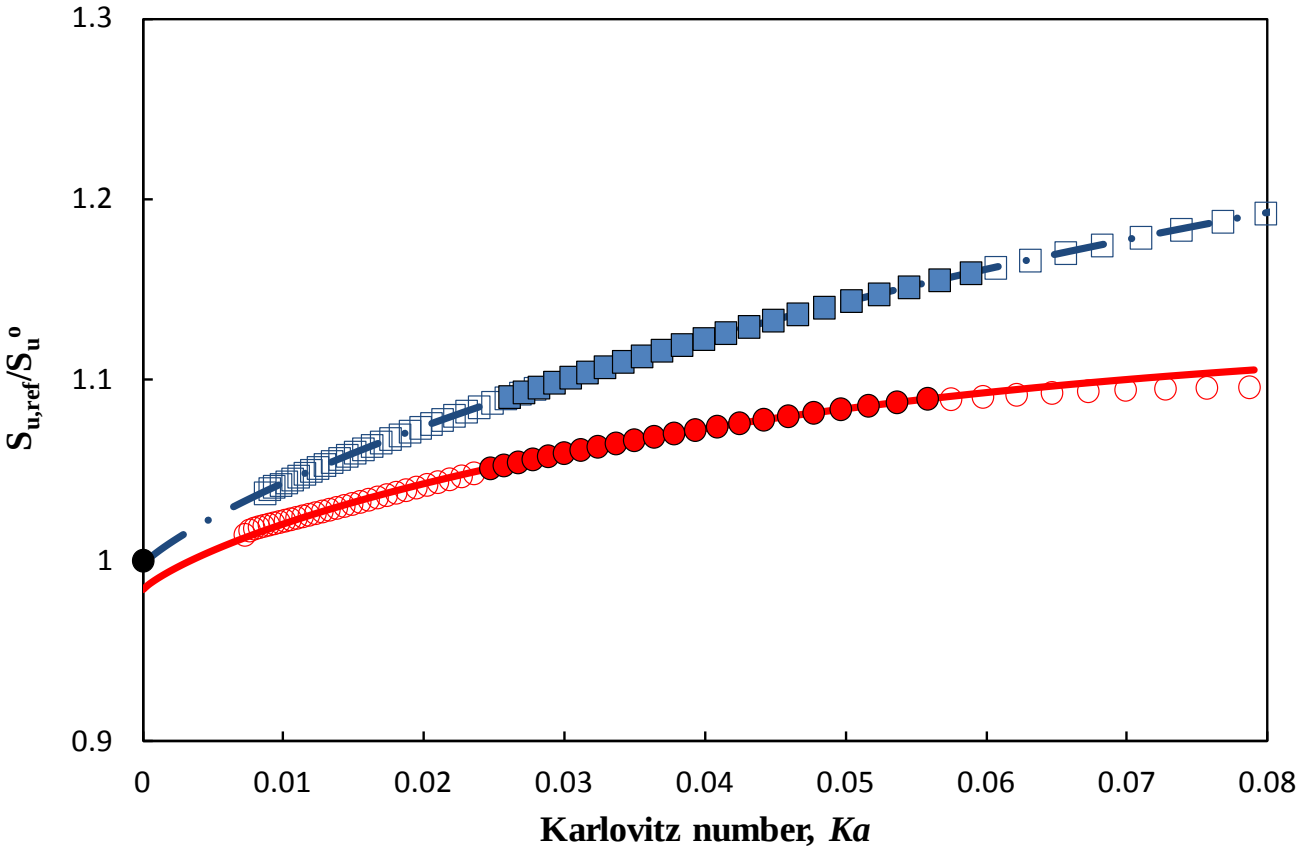

Figure 4.15. Variation of $S_{u,ref}/S_u^o$ with *Ka* of a ϕ = 0.7 *n*-$C_{12}H_{26}$/air CFF at p = 1 atm and T_u = 443 K computed using JetSurF 1.0 with ID (■) and OD (●). ID (–· –) and OD (—) correspond to fitting using Eq. 1. The full range DNS results are shown in hollow symbols, while the DNS results used for fitting Eq. 1 are shown in solid symbols.

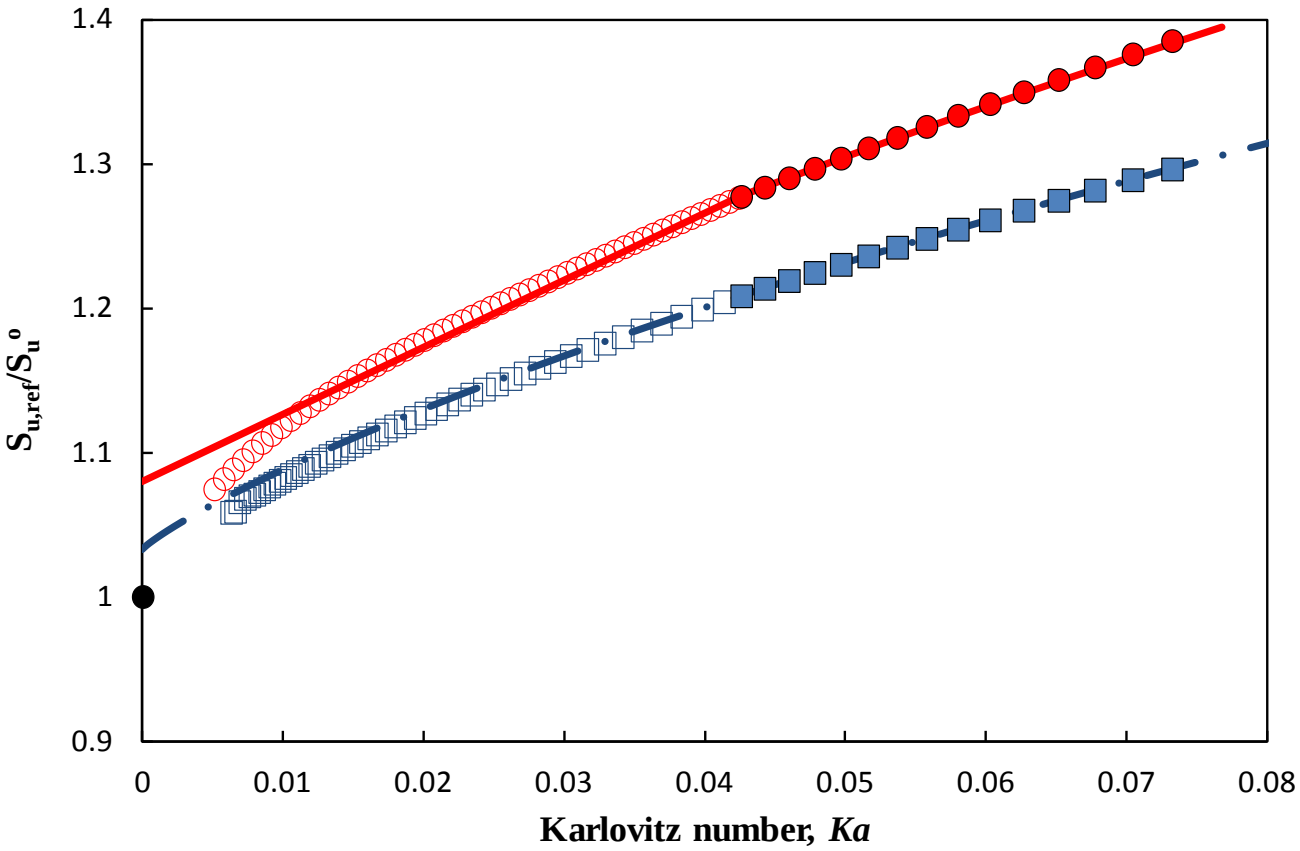

Figure 4.16. Variation of $S_{u,ref}/S_u^o$ with *Ka* of a ϕ = 1.4 *n*-$C_{12}H_{26}$/air CFF at p = 1 atm and T_u = 443 K computed using JetSurF 1.0 with ID (■) and OD (●). ID (–· –) and OD (—) correspond to fitting using Eq. 1. The full range DNS results are shown in hollow symbols, while the DNS results used for fitting Eq. 1 are shown in solid symbols.

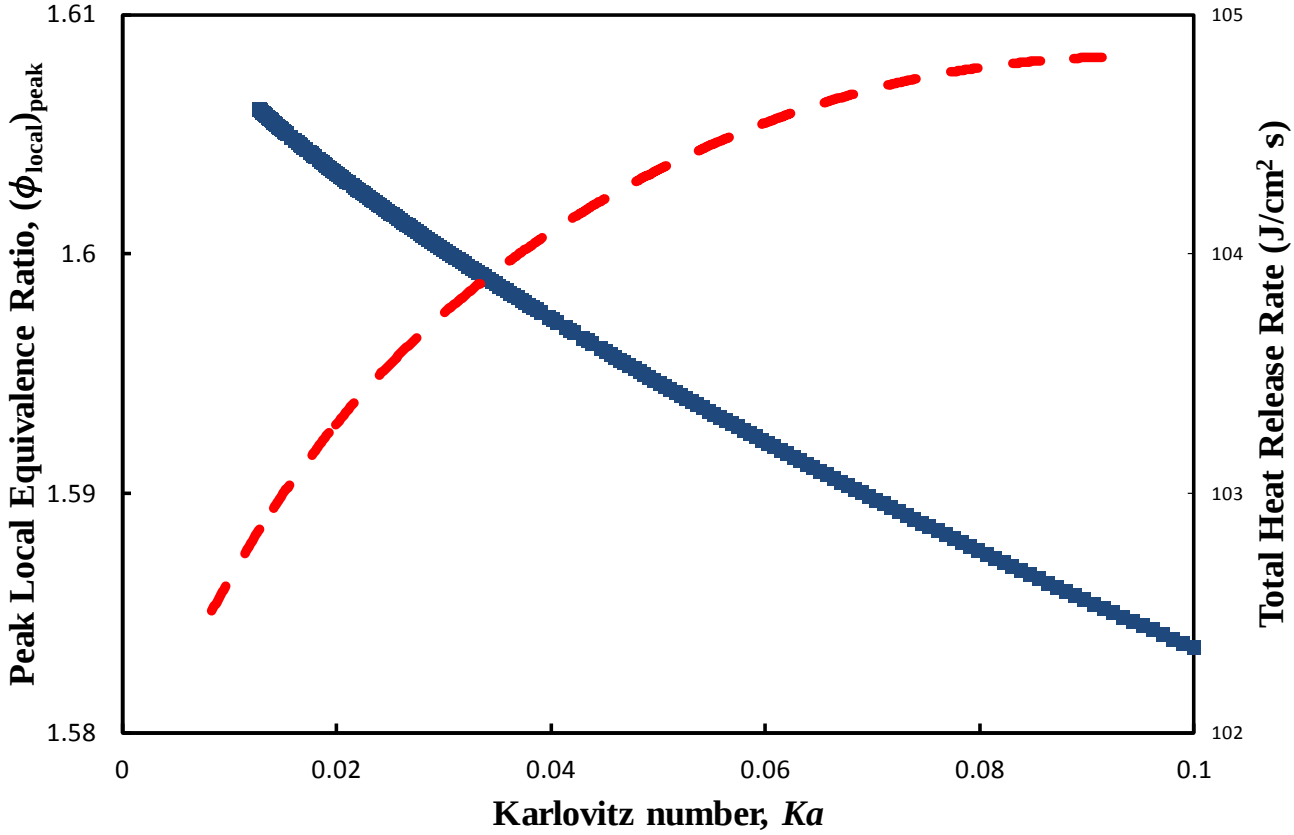

Figure 4.17. Variation of $(\phi_{local})_{peak}$ (—) and HRR_{tot} (--) with Ka of a ϕ = 1.4 n-$C_{12}H_{26}$/air CFF at p = 1 atm and T_u = 443 K computed using JetSurF 1.0 with OD.

Clearly, in steady state experiments like those of CFF's the directly measured $S_{u,ref}$'s can be optimized so that the uncertainties are minimized. In carefully performed CFF experiments, the uncertainty based on 2σ, where σ is the standard deviation, can be as low as 5% [16]. However, the uncertainty of CFF experiments can be 10% or higher if issues related to the quality of the flow, reactant concentrations especially for $\phi > 1.0$ flames of liquid fuels, flow tracer seeding density, the implementation of particle image velocimetry (PIV) or laser Doppler velocimetry (LDV) to measure flow velocities, and

interpretation of the raw data are not addressed carefully and rigorously. It should be noted that uncertainties in the reported S_u^o of the order of 10% or higher are not desirable as such data cannot be used effectively for the validation of kinetic models given the relatively low sensitivity of S_u^o to kinetics. An alternative viable approach in validating kinetic models is to compare the raw experimental data from experiments against corresponding DNS results, so that the uncertainties associated with extrapolations are removed.

4.4 Concluding Remarks

Direct numerical simulations of counterflow flames were carried out in order to assess uncertainties stemming from current practices that are used to interpret experimental data and derive the laminar flame speed. The results of the simulations were treated as data in the range of stretch rates that are encountered in experiments, and were used to perform extrapolations to zero stretch using formulas that have been derived from asymptotic analyses. The validity of these practices was tested upon comparing the results against the known answers of the direct numerical simulations.

The effect of molecular transport was studied by varying the fuel diffusivity. It was concluded that for fuel lean hydrocarbon/air mixtures, the preferential diffusion of heat or mass as manifested by the Lewis number dominates the flame response to stretch. For fuel rich mixtures, the controlling factor was determined to be the differential diffusion of the reactants into the reaction zone for heavy hydrocarbons. It was found also that using

extrapolation equations derived based on asymptotics analysis and simplifying assumptions to obtain the laminar flame speeds, could result in significant errors for rich flames of heavy hydrocarbons.

4.5 References

[1] C.K. Law, C.J. Sung, H. Wang, T.F. Lu, AIAA J. v41 (2003) 1629-1646.

[2] D.A. Sheen, H. Wang, Combust. Flame 158 (2011) 2358-2374.

[3] P.A. Libby, F.A. Williams, Combust. Flame 44 (1982) 287-303.

[4] N. Peters, Twenty-First Symposium (International) on Combustion (1986) 1231-1250.

[5] C.K. Law, D.L. Zhu, G. Yu, Proc. Combust. Inst. 21 (1986) 1419–1426.

[6] F.W. Stevens, J. Am. Chem. Soc. 48 (1926) 1896-1906.

[7] F.W. Stevens, J. Am. Chem. Soc. 50 (1928) 3244-3258.

[8] G.E. Andrews, D. Bradley, Combust. Flame 18 (1972) 133-153.

[9] F.A. Williams, Combustion Theory, Benjamin Cummins, Palo Alto, CA, 1985.

[10] J.D. Buckmaster, Acta Astronaut. 6 (1979) 741-769.

[11] M. Matalon, Combust. Sci. Technol. 31 (1983) 169-181.

[12] S.H. Chung, C.K. Law, Combust. Flame 55 (1984) 123-125.

[13] C.K. Wu, C.K. Law, Proc. Combust. Inst. 20 (1985) 1941–1949.

[14] A.T. Holley, X.Q. You, E. Dames, H. Wang, F.N. Egolfopoulos, Proc. Combust. Inst. 32 (2009) 1157-1163.

[15] C.K. Law, F. Wu, F.N. Egolfopoulos, and H. Wang, "A Note on Rational Interpretation of Data on Laminar Flame Speeds," submitted to Combustion and Flame

[16] C. Ji, E. Dames, Y.L. Wang, H. Wang, F.N. Egolfopoulos, Combust. Flame 157 (2010) 277-287.

[17] A.P. Kelley, A.J. Smallbone, D.L. Zhu, C.K. Law, Proc. Combust. Inst. 33 (2011) 963-970.

[18] A.J. Smallbone, W. Liu, C. Law, X. You, H. Wang, Proc. Combust. Inst. 32 (2009) 1245-1252.

[19] K. Kumar, J.E. Freeh, C.J. Sung, Y. Huang, J. Propuls. Power 23 (2007) 428-436.

[20] F. Wu, A.P. Kelley, C.K. Law, Combust. Flame 159 (2012) 1417-1425.

[21] A.P. Kelley, C.K. Law, Combust. Flame 156 (2009) 1844-1851.

[22] R.J. Kee, J.A. Miller, G.H. Evans, G. Dixon-Lewis, Proc. Combust. Inst. 22 (1988) 1479–1494.

[23] D.L. Zhu, F.N. Egolfopoulos, C.K. Law, Proc.Combust. Inst. 22 (1988) 1537–1545.

[24] F.N. Egolfopoulos, P. Cho, C.K. Law, Combust. Flame 76 (1989) 375-391.

[25] F.N. Egolfopoulos, D.L. Zhu, C.K. Law, Proc. Combust. Inst. 23 (1991) 471-478.

[26] C.M. Vagelopoulos, F.N. Egolfopoulos, Combust. Inst. 25 (1994) 1317-1323.

[27] J.H. Tien, M. Matalon, Combust. Flame 84 (1991) 238-248.

[28] G. Dixon-Lewis, S.M. Islam, Proc. Combust. Inst. 19 (1982) 283–291.

[29] S.G. Davis, C.K. Law, Combust. Sci. Technol. 140 (1998) 427-449.

[30] B.H. Chao, F.N. Egolfopoulos, C.K. Law, Combust. Flame 109 (1997) 620-638.

[31] C.M. Vagelopoulos, F.N. Egolfopoulos, C.K. Law, Combust. Inst. 25 (1994) 1341-1347.

[32] Y.L. Wang, A.T. Holley, C. Ji, F.N. Egolfopoulos, T.T. Tsotsis, H. Curran, Proc. Combust. Inst. 32 (2009) 1035–1042.

[33] P.S. Veloo, Y.L. Wang, F.N. Egolfopoulos, C.K. Westbrook, Combust. Flame 157 (2010) 1989-2004.

[34] G.E. Andrews, D. Bradley, Combust. Flame 19 (1972) 275-288.

[35] M. Metghalchi, J.C. Keck, Combust. Flame 38 (1980) 143-154.

[36] S.C. Taylor, Burning Velocity and Influence of Flame Stretch, Ph.D. Thesis, University of Leeds, 1991.

[37] L.K. Tseng, M.A. Ismail, G.M. Faeth, Combust. Flame 95 (1993) 410-426.

[38] D. Bradley, P.H. Gaskell, X.J. Gu, Combust. Flame 104 (1996) 176-198.

[39] S.D. Tse, D.L. Zhu, C.K. Law, Proc. Combust. Inst. 28 (2000) 1793-1800.

[40] X. Qin, Y. Ju, Proc. Combust. Inst. 30 (2005) 233-240.

[41] P.D. Ronney, G.I. Sivashinksy, SIAM J. Appl. Math. 49 (1989) 1029-1046.

[42] A.P. Kelley, J.K. Bechtold, C.K. Law, J. Fluid Mech. 691 (2012) 26-51.

[43] Z. Chen, Combust. Flame 158 (2011) 291-300.

[44] Z. Chen, M.P. Burke, Y. Ju, Proc. Combust. Inst. 32 (2009) 1253-1260.

[45] M.P. Burke, Z. Chen, Y. Ju, F.L. Dryer, Combust. Flame 156 (2009) 771-779.

[46] I.C. Mclean, D.B. Smith, S.C. Taylor, Proc. Combust. Inst. 25 (1994) 749-757.

[47] C.K. Law, F.N. Egolfopoulos, Proc. Combust. Inst. 24 (1992) 137-144.

[48] Z. Chen, Combust. Flame 157 (2010) 2267-2276.

[49] J. Santer, F.M. Haas, Y. Ju, F.L. Dryer, Combust. Flame 161 (2014) 147-153.

[50] Z. Chen, X. Qin, B. Xu, Y. Ju, F. Liu, Proc. Combust. Inst. 31 (2007) 2693-2700.

[51] J. Ruan, H. Kobayashi, T. Niioka, Y. Ju, Combust. Flame (2001) 225-230.

[52] B. Lecordier. Etude de l'interaction de la propagation d'une flamme de prémélange avec le champ aérodynamique par association de la tomographie laser et de la PIV. PhD Thesis Report, Université de Rouen, France, 1997.

[53] S. Balusamy, A. Cessou, B. Lecordier, Exp. Fluids 50 (2011) 1109-1121.

[54] E. Varea, V. Modica, A. Vandel, B. Renou, Combust. Flame 159 (2012) 577-590.

[55] R.J. Kee, J.F. Grcar, M.D. Smooke, J.A. Miller, Premix: A FORTRAN Program for Modeling Steady Laminar One-dimensional Premixed Flames, Sandia Report, SAND85- 8240, Sandia National Laboratories, 1985.

[56] J.F. Grcar, R.J. Kee, M.D. Smooke, J.A. Miller, Proc. Combust. Inst. 21 (1986) 1773–1782.

[57] F.N. Egolfopoulos, Proc. Combust. Inst. 25 (1994) 1375–1381.

[58] R.J. Kee, F.M. Rupley, J.A. Miller, Chemkin-II: A Fortran Chemical Kinetics Package for the Analysis of Gas-Phase Chemical Kinetics, Sandia Report, SAND89-8009, Sandia National Laboratories, 1989.

[59] R. J. Kee, F. M. Rupley, J. A. Miller, M. E. Coltrin, J. F. Grcar, E. Meeks, H. K. Moffat, A. E. Lutz, G. DixonLewis, M. D. Smooke, J. Warnatz, G. H. Evans, R. S. Larson, R. E. Mitchell, L. R. Petzold, W. C. Reynolds, M. Caracotsios, W. E. Stewart, P. Glarborg, C. Wang, O. Adigun, CHEMKIN Collection, Release 3.6, Reaction Design, Inc., San Diego, CA (2000).

[60] R.J. Kee, J. Warnatz, J.A. Miller, A FORTRAN Computer Code Package for the Evaluation of Gas-phase Viscosities, Conductivities, and Diffusion Coefficients, Sandia Report, SAND83-8209, Sandia National Laboratories, 1983.

[61] Y. Dong, A.T. Holley, M.G. Andac, F.N. Egolfopoulos, S.G. Davis, P. Middha, H. Wang, Combust. Flame 142 (2005) 374–387.

[62] G.L. Hubbard, C.L. Tien, ASME J. Heat Transfer 100 (1978) 235-239.

[63] H. Wang, X. You, A. V. Joshi, Scott G. Davis, A. Laskin, F.N. Egolfopoulos C. K. Law, USC-Mech Version II. High-Temperature Combustion Reaction Model of H2/CO/C1-C4 Compounds. http://ignis.usc.edu/USC_Mech_II.htm.

[64] B. Sirjean, E. Dames, D. A. Sheen, X. You, C. Sung, A. T. Holley, F. N. Egolfopoulos, H. Wang, S. S. Vasu, D. F. Davidson, R. K. Hanson, H. Pitsch, C. T. Bowman, A. Kelley, C. K. Law, W. Tsang, N. P. Cernansky, D. L. Miller, A. Violi, R. P. Lindstedt, "A High-Temperature Chemical Kinetic Model of *n*-Alkane Oxidation, JetSurF Version 1.0," http://melchior.usc.edu/JetSurF/JetSurF1.0/ Index.html.

[65] T. Lu, C.K. Law, Proc. Combust. Inst. 30 (2005) 1333–1341.

[66] C.K. Law, Combustion Physics, Cambridge University Press, 2008.

Chapter 5: An Experimental and Modeling Study of the Propagation and Extinction of Neat Hydrocarbons, Practical Fuels and Jet Fuels

5.1 Introduction

Conventional and practical fuels and their surrogates are complex mixtures of hundreds or even thousands of chemical components, and as a result it is not possible to model and understand their combustion characteristics. On the other hand, the formulation of reliable fuel surrogates is a viable solution towards providing the much-needed fundamental understanding, as they can be modeled from first principle. Along with studies in homogeneous systems, flame studies are essential towards the formulation of fuel surrogates given that the kinetics can be evaluated over wide ranges of temperature and species concentrations.

For neat liquid hydrocarbons, flame studies have focused on C_5-C_{12} hydrocarbons (e.g., [1-11]). For example, the experimental and computational studies of Ji et al. [3,8] for *n*-$C_{10}H_{22}$ and *n*-$C_{12}H_{26}$ premixed and non-premixed flames showed that the *n*-$C_{10}H_{22}$ flames exhibit lower extinction propensity than *n*-$C_{12}H_{26}$ flames. Kumar et al. [5] investigated the extinction limits of premixed *n*-$C_{10}H_{22}/O_2/N_2$ and *n*-$C_{12}H_{26}/O_2/N_2$ flames, and computed results obtained using two kinetic models were found to over-predict the data.

Flame studies for fuels with carbon numbers higher than 12, e.g. *n*-$C_{14}H_{30}$ and *n*-$C_{16}H_{34}$, are scarce or non-existing. At the same time it should be realized that such

heavier compounds dominate the composition of a range of practical fuels including those used in naval aviation and diesel engines. The reason behind the lack of systematically derived flame data for those heavy fuels is that in order to be sustained in the gaseous phase in concentrations that are sufficiently large to support a flame, they must be heated to temperatures that are high enough to cause cracking. In the recent review, of Pitz and Mueller [12] emphasized that for the development of surrogates of diesel fuels there is a profound need for experimental data for hydrocarbon oxidation in the C_{15}-C_{20} carbon range.

Recently, detailed kinetic models for *n*-alkanes up to C_{16} have been developed [13-15]. Shen et al. [16] studied the ignition of *n*-$C_{14}H_{30}$ in a shock tube at elevated pressures. Holley et al. [17] investigated the extinction of non-premixed C_5-C_{14} *n*-alkane flames and it was found that the single-component hydrocarbon fuels with lower carbon number exhibit greater resistance to extinction. Jet stirred reactor studies of the oxidation of *n*-$C_{16}H_{34}$ [14] and *n*-$C_{16}H_{34}$/*n*-$C_{10}H_{22}$ blends [15] have been carried out at atmospheric pressure. Ristori et al. [14] found that *n*-$C_{16}H_{34}$ follows the general oxidation paths already delineated for lighter alkanes. Biet et al. [18] found that C_{16} compounds exhibit a slightly larger reactivity than *n*-$C_{10}H_{22}$, but the formation of the lighter intermediates are similar for *n*-$C_{10}H_{22}$ and *n*-$C_{16}H_{34}$. Seshadri and coworkers [19,20] have studied the extinction and autoignition of *n*-$C_{16}H_{34}$ in non-premixed flames. It was found that the critical conditions of autoignition for the straight-chain hydrocarbons depend on the

relative importance of low- and high-temperature kinetic pathways as well as of molecular transport. It was shown also, that the *n*-$C_{16}H_{34}$ flames exhibit a higher extinction propensity compared to lighter hydrocarbons due to the lower fuel diffusivity. Haylett et al. [21] measured ignition delay times of *n*-$C_{16}H_{34}$ in a shock tube and the experimental results were compared against predictions using different kinetic models.

As for practical fuels, there are notably fewer flame studies compared to neat heavy liquid fuels. The oxidation of diesel fuels has been studied in jet-stirred reactors [22,23]. The ignition of Jet-A and JP-8 has been studied in shock tubes [24] and counterflow flames [25]. Laminar flame speeds, S_u^o, and extinction limits of conventional and alternative fuels have been studied at different preheat temperatures [26] also in the counterflow configuration. The jet-wall stagnation flame configuration was used for measuring S_u^o's of jet and diesel fuels [27]. Ji et al. [8] investigated the extinction of premixed and non-premixed flames of conventional and alternative jet fuels, and the results revealed that flames of conventional jet fuels exhibit greater extinction propensity compared to *n*-$C_{10}H_{22}$ and *n*-$C_{12}H_{26}$.

Studies of surrogate fuels have appeared recently also (e.g., [28-30]). In terms of flames studies, Ji and Egolfopoulos [28] measured S_u^o's of mixtures of air with [80% *n*-$C_{12}H_{26}$ + 20% methylcyclohexane] and [80% *n*-$C_{12}H_{26}$ + 20% toluene] in the counterflow configuration, and a mixing rule was established to estimate S_u^o's for fuel blends. Furthermore, Honnet et al. [29] investigated the ignition and extinction

characteristics [80% *n*-$C_{10}H_{22}$ + 20% 1,2,4-trimethyl-benzene] non-premixed flames.

Finally, Holley et al. [31] determined numerically that flame extinction is, in addition to kinetics, very sensitive to the fuel diffusivity especially for large molecular weight fuels under non-premixed conditions, and this finding was confirmed also by the subsequent studies of Ji et al. [8] and Wang et al. [32].

Based on the aforementioned literature search, it is apparent that studies of *n*-$C_{14}H_{30}$ and *n*-$C_{16}H_{34}$ have been carried out largely in homogeneous reactors, while flame studies are scarce and thus no extensive database is available that could be used towards the validation of kinetic models.

Thus, the first part of this study focuses on providing archival data of laminar flame speed and extinction strain rate for gasoline ethanol blends. The second half of this study was to validate a recently developed lump kinetic model for aviation fuels, and to gain further insight into the controlling physical and chemical mechanisms that control flame propagation.

5.2 Experimental Approach

The experiments were carried out under atmospheric pressure in the counterflow configuration [e.g., (3,4,6-9,32-38)] as schematically shown in Fig 2.2. The vaporization system included a high precision syringe pump and a glass nebulizer that injected fuel as fine droplets into a cross-flow of heated air and heated nitrogen for

premixed flames and non-premixed flames respectively. It was determined that the cross-flow injection configuration minimizes the fluctuations stemming from vaporization, and allows very efficient mixing of the fuel with the heated gaseous stream. All tubes along the heating path were wrapped with heating elements and insulation to eliminate cold spots. To prevent fuel cracking, six K-type thermocouples were arranged along the heating path to ensure that the temperature of fuel/air mixture was maintained below 490 K, which ensured also that the partial pressure of the fuel was lower than its vapor pressure. The temperature of the unburned mixture, T_u, was measured in the center of the burner exit. All the measurements were taken at T_u = 443 K in this study.

The single-flame configuration was chosen for the premixed flame experiments as compared to twin-flames, it results in lower extinction strain rates, K_{ext}, and thus in lower Reynolds numbers to minimize the intrinsic flow instabilities [37,38] and establish stable flames. Single premixed flames were established by counterflowing an ambient temperature N_2 jet against a preheated fuel/air jet. The extinction measurements for premixed flames were similar to previous studies (e.g., [3,8,37]). A near-extinction flame was established first, the prevailing strain rate K, defined as the maximum absolute value of the axial velocity gradient in the hydrodynamic zone, was measured then by using particle image velocimetry (PIV), and finally extinction was achieved by slightly varying the fuel flow rate. The modification to K due to the small variations in the fuel flow rate has been determined to be insignificant, and thus the measured K for the

near-extinction flame is reported as K_{ext}. Burner nozzle diameters of $D = 14$ mm and burner separation distance of $L = 14$ mm were used for all measurements

For premixed flames, measurements were performed for the equivalence ratio range $0.8 < \phi < 1.5$ for all mixtures. A RD387 gasoline (LLNL surogate) was used as the target gasoline candidate for the gasoline-ethanol blends study. Total of five cases were studied where gasoline volume fraction varied from 0 to 100 %. Case 1 (E100) represents 100% pure ethanol with less than 0.1% water content; Case 2 (E85) represents 15% gasoline and 85% ethanol in volume basis; Case 3 (E50) represents 50% of both gasoline and ethanol; Case 4 (E15) represents 85% gasoline and 15% ethanol in volume basis and Case 5 (E0) represents gasoline and no ethanol. The Air Force Research Laboratory (AFRL) has provided three jet fuels with attendant "POSF" identification numbers, and their compositions are summarized in Table 5.1. Jet-A, JP8 and JP5 were selected as the representative aviation fuel.

Table 5.1. Fuel specific properties.

	Jet A[a] (POSF 10325)	JP- 8[b] (POSF 10264)	JP-5[c] (POSF 10289)	RD387 [d]
iso-paraffin	29.45%	39.69%	18.14%	73%
n-paraffins	20.03%	26.82%	13.89%	
Aromatics	18.66%	13.41%	20.59%	>23%
Cycle-paraffin	24.87%	17.01%	31.33%	4.2%
Dicyclo-paraffin	6.78%	2.95%	15.97%	
Trycyclo-paraffin	0.21%	0.12%	0.08%	

[a] Average carbon number ~ $C_{11.37}$ [b] Average carbon number ~ $C_{10.83}$ [c] Average carbon number ~ $C_{11.98}$

[d] Average carbon number ~ $C_{14.8}$

5.3 Numerical Approach

S_u^o's and K_{ext}'s were computed with PREMIX and opposed-jet flow code [39], which was developed originally by Kee and coworkers [40]. This code has been modified to allow for any type of boundary conditions and to account for thermal radiation of CH_4, H_2O, CO and CO_2 at the optically thin limit [41]. Additionally, the code was integrated with the CHEMKIN [42] and Sandia Transport [43] subroutine libraries. The H and H_2 diffusion coefficients of several key pairs are based on an updated set of Lennard-Jones (L-J) parameters [44].

For the K_{ext} computations, a two-point continuation approach was used to solve for K at the state of extinction [45,46]. In the simulations, a vigorously burning flame was established first, and then K was increased to achieve extinction. At the extinction state, the opposed-jet code solves around the turning-point behavior by introducing a two-point continuation approach [45,46]. The experimental values of the axial velocity gradients at the burners exits, $(du/dx)_{exit}$, L, and T_u were accounted for in the simulations; in all experiments it was determined that $(du/dx)_{exit} \approx 0$.

The effects of chemical kinetics and molecular diffusion on K_{ext} were evaluated by performing rigorous sensitivity analysis with respect to rate constants and binary diffusion coefficients [31]. Molecular transport was treated using mixture-averaged formulation for premixed flames, while for the non-premixed extinction simulations the Rosner formulation was chosen as shown in Chapter 5, the computed K_{ext} can differ significantly from the mixture-average formulation without considering soret effect [8].

As mentioned in Chapter 3, a detailed C_8-C_{16} *n*-alkane high-temperature kinetic model is used in the simulation. A skeletal mechanism based on a detailed C_8-C_{16} *n*-alkane high-temperature kinetic model for *n*-alkanes up to *n*-$C_{16}H_{34}$ is used, consisting of 157 species and 1161 reactions. For gasoline and its surrogates simulation, a reduced 679 species and 3479 reaction mechanism is used and followed by a reduced 323 species version mechanism. A gasoline surrogate compositions suggested is used to represent the RD387 fuel in the simulation; the compositions are listed in Table 5.2. A

recent developed lump model built based on USC-Mech II for jet fuel simulation is used, consisting 115 species and 805 reactions.

Table 5.2. RD 387 Surrogate Molar Compositions.

RD387	
C_5H_{10}-2	0.053
$C_6H_5CH_3$	0.306
i-C_6H_{18}	0.488
n-C_7H_{16}	0.153

5.4 Results and Discussion

5.4.1 Propagation and extinction of n-$C_{14}H_{30}$/air and n-$C_{16}H_{34}$/air flames

Figure 5.1 illustrates the results for experimental and computed S_u^o's for flames of *n*-$C_{14}H_{30}$/air mixture and *n*-$C_{16}H_{34}$/air mixtures at p = 1 atm with T_u = 443 K. The dashed line represents a skeletal version of the recent developed high temperature kinetic model by Westbrook et al. [44] for *n*-alkanes up to *n*-$C_{16}H_{34}$, consisting of 157 species and 1161 reactions, here referred as Model I. The *n*-$C_{14}H_{30}$ and *n*-$C_{16}H_{34}$ sub-models of Model I were superimposed on to JetSurF 2.0 that describes the hydrocarbon kinetics up to C12, and which has been tested successfully against flame propagation data for n- and

cyclo-alkanes. This combined model, hereafter referred to as Model II, consists of 241 species and 1841 reactions.

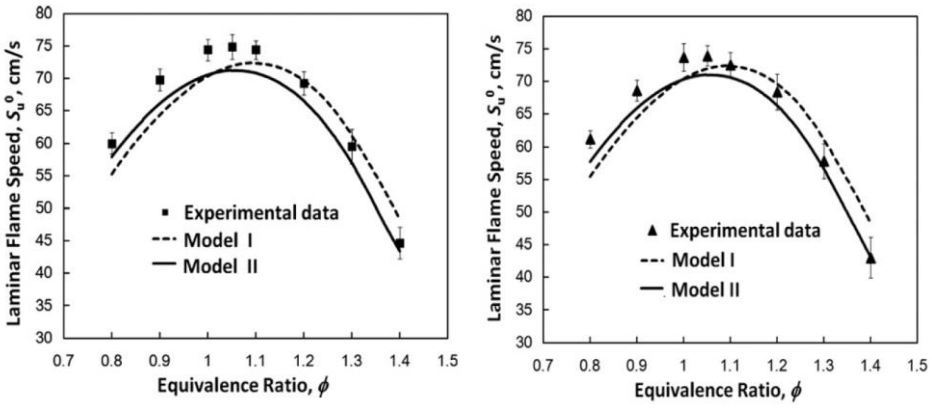

Figure 5.1. (a) Experimental and computed laminar flame speeds of (a) *n*-$C_{14}H_{30}$/air mixture, (b) *n*-$C_{16}H_{34}$/air mixtures at p = 1 atm and T_u = 443 K.

For *n*-$C_{14}H_{30}$/air mixture, the experimental peak value, $(S_u^o)_{peak}$, is 75 cm/s at ϕ = 1.05. The computed S_u^o's using Model I are slightly higher than the data for ϕ > 1.0 and notably lower for ϕ < 1.0, with a maximum discrepancy of 6.0 cm/s at ϕ = 0.9. Furthermore, using Model I $(\phi)_{peak}$ = 1.1. The predicted S_u^o's using Model II are in better agreement with data, with a maximum discrepancy of 3.8 cm/s around ϕ = 1.0, and $(\phi)_{peak}$ = 1.05 in agreement with the experimental $(\phi)_{peak}$.

For *n*-$C_{16}H_{34}$/air mixture, the experimental peak value, $(S_u^o)_{peak}$, is 74 cm/s at ϕ = 1.05. Similarly to *n*-$C_{14}H_{30}$/air flames, the predicted S_u^o's using Model I under-predict the data for ϕ > 1.0, with a maximum discrepancy of 2.5 cm/s around ϕ = 1.0. On the other hand, the predicted S_u^o's using Model II are more consistent with the data and result in $(\phi)_{peak}$ = 1.05. Note that both the experimental and computed S_u^o's for *n*-$C_{14}H_{30}$/air mixture and *n*-$C_{16}H_{34}$/air flames are very close to each other for the same T_u. This is reasonable, as flame propagation is sensitive to small hydrocarbon kinetics [15].

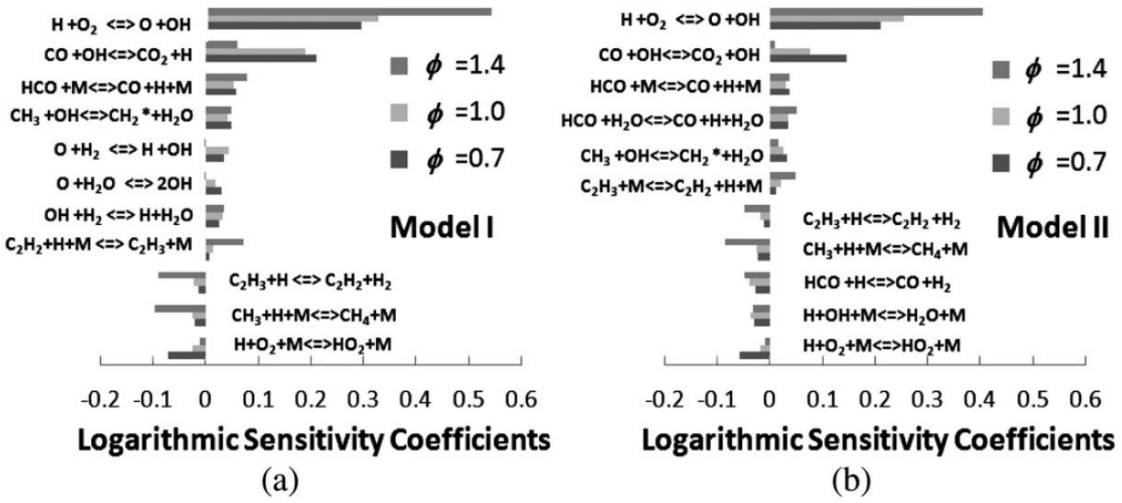

Figure 5.2. Ranked logarithmic sensitivity coefficients of laminar flame speed with respect to kinetics computed using (a) Model I and (b) Model II, for ϕ = 0.7, 1.0, and 1.4 *n*-$C_{14}H_{30}$/air mixture at T_u = 443 K.

In order to obtain further insight into the effects of kinetics and molecular transport, sensitivity analyses are performed using Models I and II. Figure 5.2 depicts the

logarithmic sensitivity respect to S_u^o for n-$C_{14}H_{30}$/air flames at ϕ = 0.7, 1.0 and 1.4, respectively. Results show that the high-temperature oxidation of n-$C_{14}H_{30}$ is dominated by H_2, CO, and small hydrocarbon kinetics only. This is as expected as fuel rapidly decomposes into intermediates through β-session.

Extinction phenomenon is more sensitive to chemical kinetics and molecular transport than flame speed measurements. Thus it is worthwhile to conduct extinction measurement to validate against kinetic models. Figure 5.3 depicts the experimental and computed extinction strain rates of n-$C_{14}H_{30}$/air mixture and n-$C_{16}H_{34}$/air mixtures at p = 1 atm with T_u = 443 K.

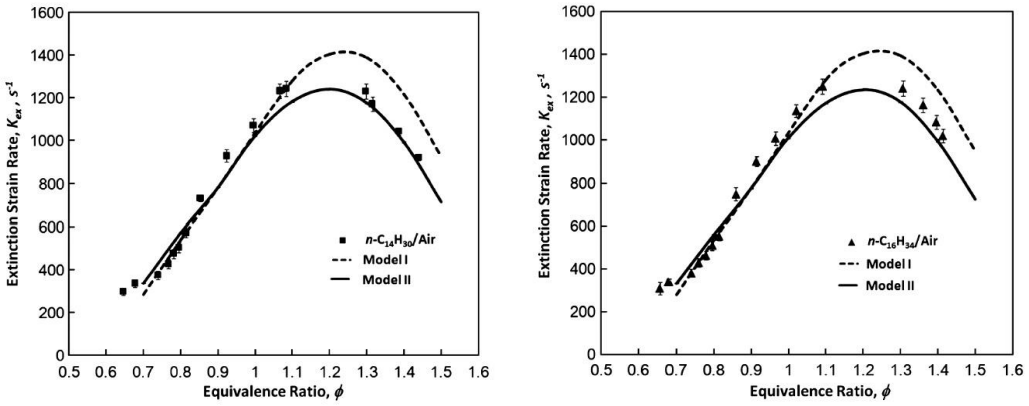

(a) (b)

Figure 5.3. (a) Experimental and computed extinction strain rate of (a) n-$C_{14}H_{30}$/air mixture, (b) n-$C_{16}H_{34}$/air mixtures at p = 1 atm and T_u = 443 K.

Figure 5.3.a depicts the experimental and computed K_{ext} of n-$C_{14}H_{30}$/air mixture at p = 1 atm with T_u = 443 K. Experimental peak value $(K_{ext})_{peak} \approx 1220\ s^{-1}$ at $(\phi)_{peak}$ = 1.2,

which is higher compared with that of S_u^o. This can be attributed to stretch and preferential diffusion effects. For ϕ > 1.0, the *Le* is less than unity, and thus positive stretch increases the flame temperature for conditions far from extinction, increasing the extinction resistance. The computed K_{ext} using Model I are in satisfactory agreement with the data for ϕ < 1.0, whereas for ϕ > 1.0, Model I overpredicted the data notably, with the maximum discrepancy being 240 s^{-1}. Model II provides in general closer agreements with the data, with the maximum discrepancy being 59 s^{-1} at ϕ = 1.13. Considering both the experimental and numerical uncertainties, the agreements obtained using Model II are considered as satisfactory. Figure 5.3.b depicts the experimental and computed K_{ext} of *n*-$C_{16}H_{34}$/air mixtures at T_u = 443 K. Experimentally, $(K_{ext})_{peak} \approx$ 1250 s^{-1} and $(\phi)_{peak}$ = 1.2. The simulation results are similar to *n*-$C_{14}H_{30}$/air flames, with Model II providing closer agreement with the data compared with Model I. Additionally, it is determined that the experimental and computed K_{ext} for *n*-$C_{14}H_{30}$/air and *n*-$C_{16}H_{34}$/air flames are close to each other as expected.

5.4.2 Propagation and extinction of Gasoline Ethanol Blends

Figure 5.4 depicts the experimentally determined S_u^o's of E100/air, E85/air, E50/air, E15/air and E0/air flames at T_u = 393 K for $0.7 \leq \phi \leq 1.5$ in the present study. ϕ is calculated based on the surrogate molar compositions listed in Table 5.2. S_u^o's of E100/air flames are the highest among all fuels while E0/air flames exhibits the lowest. The experimental peak value, $(S_u^o)_{peak}$, is at $\phi \approx$ 1.1. E100/air and E85/air flames exhibit

similar S_u^o's across all ϕ's. E15 and E0 flames also show similar S_u^o at stoichiometric and rich condition, while deviated from each other at lean condition. The computed S_u^o's are slightly lower than the data at ϕ < 1.0 for ethanol and ethanol/gasoline blends while notably higher at ϕ > 1.0 for all three cases, as shown in Fig. 5.5. The general trend is consistent with the combustion theory as ethanol has higher flame speed then normal alkanes due to the replacement of C-H bond in the n-alkane molecule by an OH functional group and thus has a large effect in enhancing the rate of flame propagation. For gasoline/air flames, the S_u^o's are lower than normal alkanes due to the presence of branched alkanes and aromatics in the mixture.

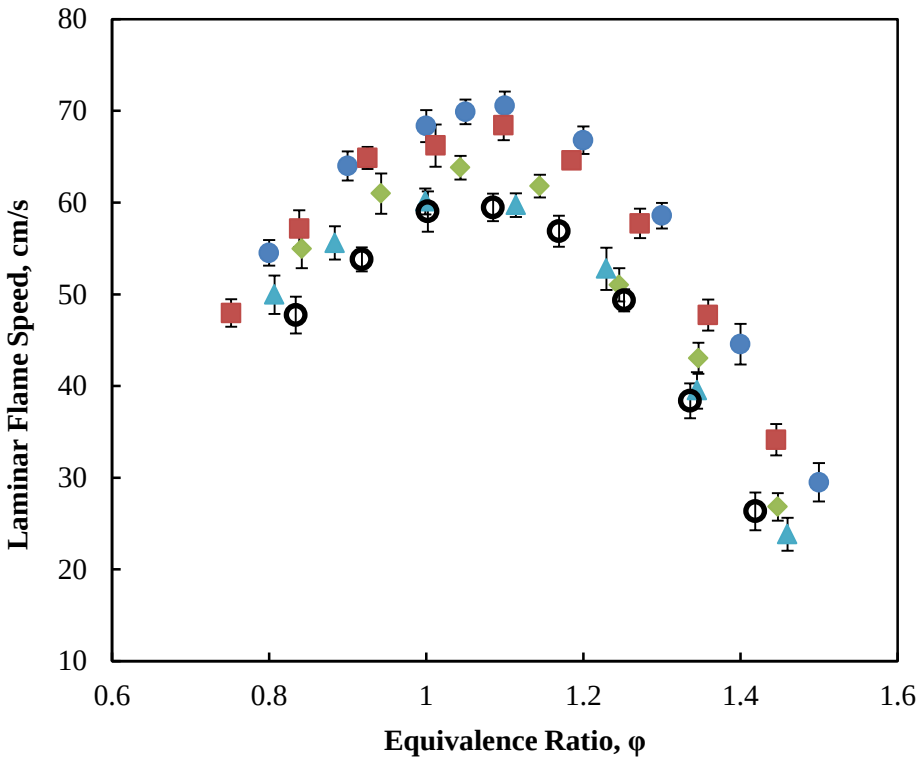

Figure 5.4. Experimentally determined S_u^o's at T_u = 393 K of E100/air (●), E85/air (■), E50/air (♦), E15/air (▲), and E0/air (○). The error bars shown in the present experimental data are based on the 2-σ standard deviations.

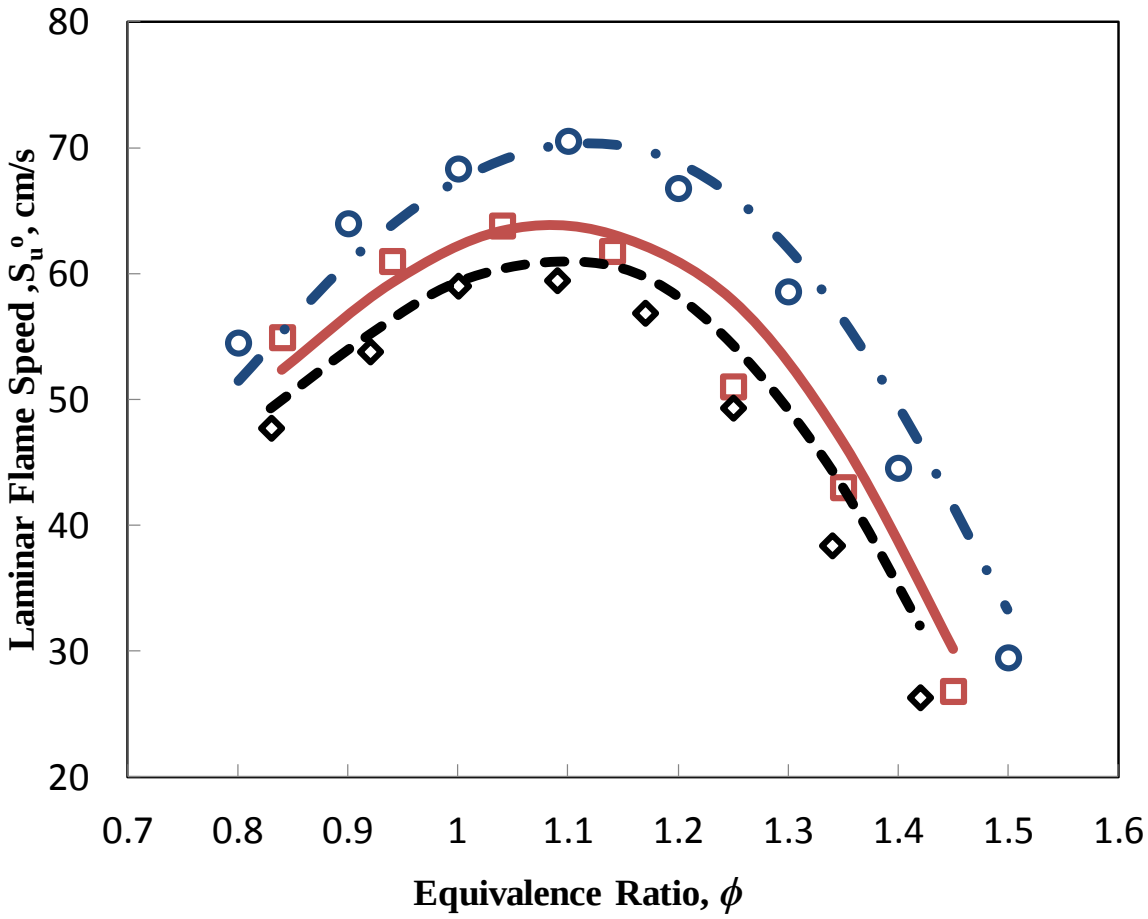

Figure 5.5. Experimental and computed laminar flame speeds of (○) E100/air mixture, (□) E50/air mixtures, and (◇) E0/air mixtures at p = 1 atm and T_u = 393 K.

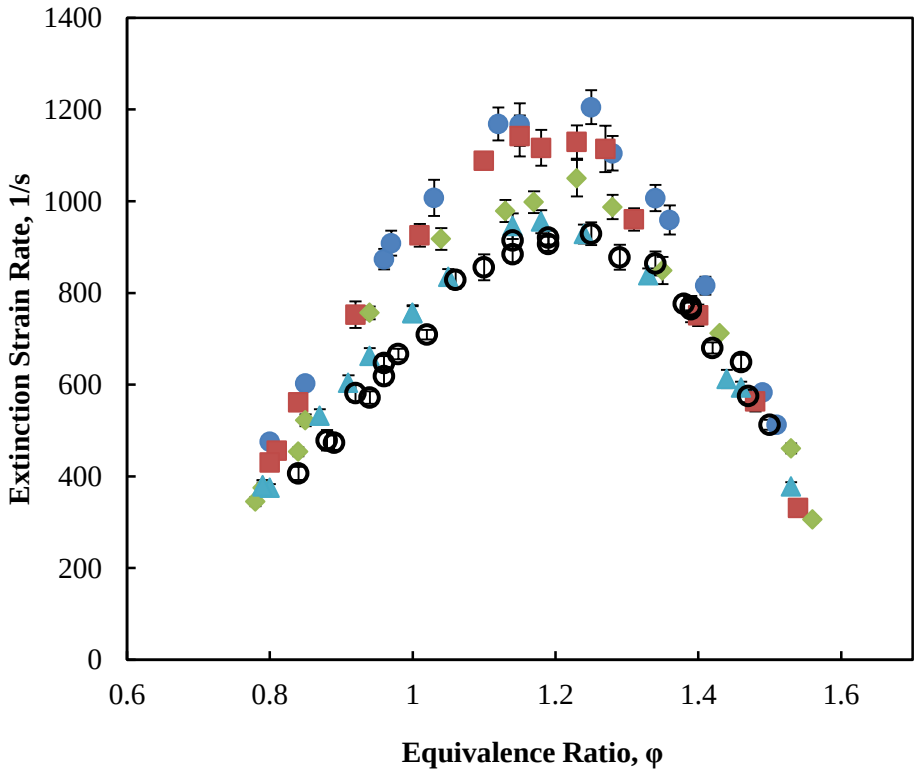

Figure 5.6. Experimentally determined K_{ext}'s at T_u = 393 K of E100/air (●), E85/air (■), E50/air (♦), E15/air (▲), and E0/air (○). The error bars shown in the present experimental data are based on the 2-σ standard deviations.

Figure 5.6 depicts the experimentally determined K_{ext}'s of E100/air, E85/air, E50/air, E15/air and E0/air flames at T_u = 393 K for $0.8 \leq \phi \leq 1.5$. Similar to S_u^o, E100/air flames flames exhibits stronger resistance to extinction than E0/air flames. The maximum extinction strain rate happens at close to $\phi = 1.2$ for all mixtures. The K_{ext}'s of E100/air and E85/air flames showed similar extinction propensity, similar phenomenon can be observed for E0/air and E15/air flames as well. Interestingly, as the equivalence ratio moves towards $\phi > 1.4$ condition, the K_{ext}'s for all five cases merge.

5.4.3 Propagation and extinction of jet fuel flames

Figure 5.7 depicts the experimental and computed S_u^o's of Jet-A/air, JP8/air and JP5/air flames at T_u= 403 K for $0.7 \leq \phi \leq 1.4$. S_u^o's of JP8/air flames are the highest among all three fuels. The maximum values of S_u^o's are 57.9 cm/s, 59.4 cm/s and 55.65 cm/s for Jet-A/air, JP8/air and JP5/air flames respectively and all occur at $\phi = 1.05$ condition. While S_u^o's of JP5/air flame at $\phi = 1.4$ is highest among all three fuels, raw data of reference flame speed of JP5/air flames exhibits steeper dependence to stretch rate which is not captured by simulation indicating this may be an artifact due to improper transport parameter assigned in the chemical model.

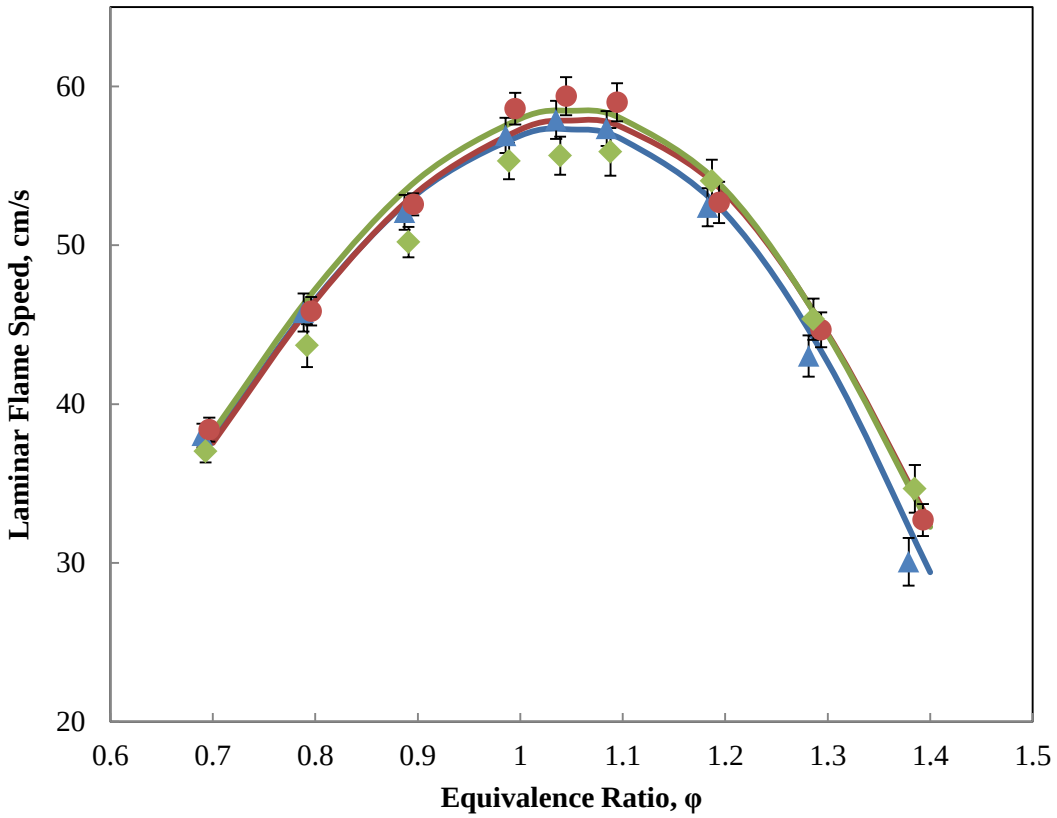

Figure 5.7. Experimental and computed S_u^o's at T_u = 403 K of Jet A/air (▲), JP-8/air (●), and JP-5/air (♦). The error bars shown in the present experimental data are based on the 2-σ standard deviations.

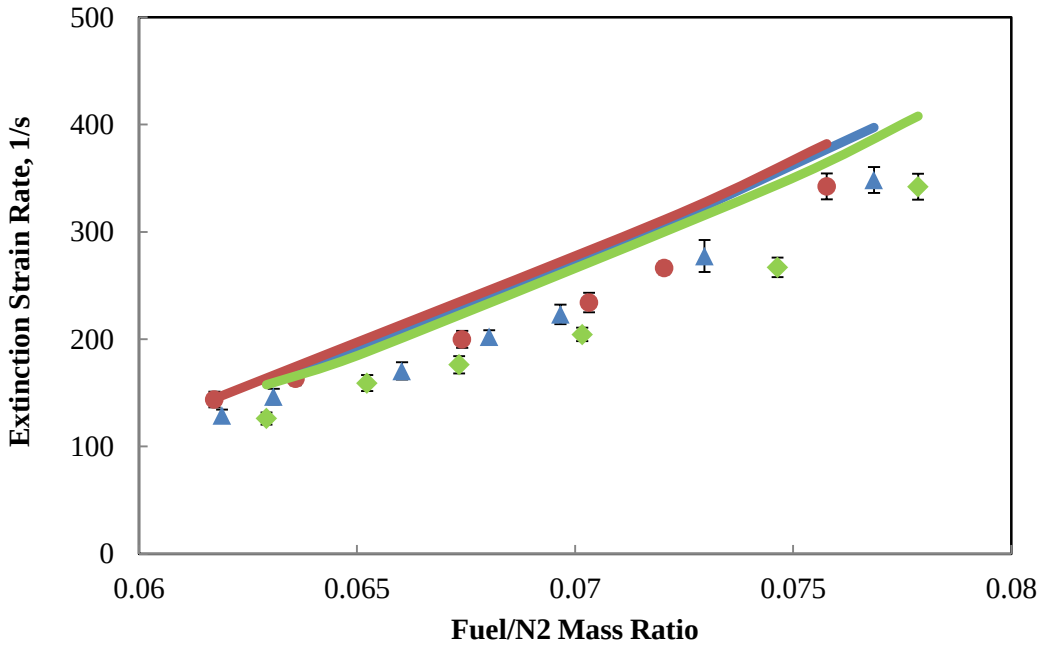

Figure 5.8. Experimental and computed K_{ext}'s at T_u = 473 K of Jet A/air (▲), JP-8/air (●), and JP-5/air (♦). The error bars shown in the present experimental data are based on the 2-σ standard deviations.

Figure 5.8 depicts the experimental and computed K_{ext}'s as function of fuel/N_2 mass ratio, $(F/N_2)_{mass}$, for non-premixed flames of Jet-A, JP8 and JP5; in all experiments the oxidizer was O_2. The simulation is conducted with updated thermal diffusion ratio by Rosner formula as mentioned earlier. It should be noted that the L-J parameters for all aviation fuels considered here are considered as *n*-alkanes' with similar molecular weight i.e. Jet-A and JP8 are treated as *n*-decane and JP-5 is treated as *n*-dodecane, respectively. The JP-8 exhibits strongest resistance to extinction for a given fuel/N_2 mass ratio and JP-5 shows the weakest resistance. The numerical results show a similar trend as the data,

and reaches good agreement at low fuel/N_2 mass ratio. Compared to the data, the simulation is over-predicted by roughly 10% at high fuel/N_2 mass ratio which could be attributed to the use of transport parameter from normal alkanes.

5.5 Concluding Remarks

Laminar flame speeds of mixtures of air with *n*-$C_{14}H_{30}$, *n*-$C_{16}H_{34}$, Jet-A, JP8 and JP5 were determined in the counterflow configuration at atmospheric pressure and elevated reactant temperatures. Measurements for such heavy fuels became possible after upgrading the liquid fuel injection and heating path so that vaporization unsteadiness as well as fuel decomposition and condensation are eliminated. The flow velocities were measured using digital particle image velocimetry. The experiments were modeled using several recently developed kinetic models that describe the pyrolysis and oxidation kinetics of H_2, CO, C_1-C_{16} hydrocarbons and practical fuel surrogates. Insight into the controlling mechanisms was obtained through sensitivity analysis on both the kinetics and molecular transport.

The results showed that the laminar flame speeds of *n*-$C_{14}H_{30}$/air and *n*-$C_{16}H_{34}$/air mixtures are indistinguishable, stemming from the fact that for both flames fuel-related kinetics are not rate-controlling and that flame propagation is sensitive largely to H_2, CO, and small hydrocarbon chemistry. The simulations reproduced the experimental data for both *n*-$C_{14}H_{30}$/air and *n*-$C_{16}H_{34}$/air mixtures satisfactorily. Compared to *n*-$C_{14}H_{30}$/air and *n*-$C_{16}H_{34}$/air mixtures, the laminar flame speeds for the petroleum-derived fuels are

lower due to the presence of aromatic compounds. On the other hand, the compositions of the bio-derived fuels are dominated by *n*- and *iso*-alkanes and as a result they exhibit laminar speeds that are higher that the petroleum-derived fuels but lower compared to *n*-alkanes.

The close assembly of laminar flame speed and extinction strain rate for gasoline-ethanol blends E0 and E15 suggests that ethanol could be a good additive candidate to gasoline. Laminar flame speed and non-premixed extinction strain rate of JP8 shows greatest performance, while JP5 shows the worst.

It is emphasized in closing, that the measured laminar flame speeds for those higher molecular weight fuels in this study are the first ones to be reported, and are expected to be of notable importance towards the fundamental understanding of the combustion of low vapor pressure practical fuels.

5.6 References

[1] Holley A.T., Dong Y., Andac M.G., Egolfopoulos F.N., Combust. Flame 144 (2006) 448–460.

[2] Huang Y., Sung C.J., Eng J.A., Combust. Flame 139 (2004) 239–251.

[3] Ji C., Dames E., Wang Y.L., Wang H., Egolfopoulos F.N., Combust. Flame 157 (2010) 277–287.

[4] Liu N., Ji C., Egolfopoulos F.N., Combust. Flame 159 (2012) 465–475.

[5] Kumar K., Sung C.J., Combust. Flame 151 (2007) 209–224.

[6] Ji C., Dames E., Wang H., F.N. Egolfopoulos, Combust. Flame 159 (2012) 1070-1081.

[7] Ji C., Sarathy S.M., Veloo P.S., Westbrook C.K., Egolfopoulos F.N., Combust. Flame 159 (2012) 1426-1436.

[8] Ji C., Wang Y.L., Egolfopoulos F.N., J. Propul. Power 27 (2011) 856–863.

[9] Kumar K., Mittal G., Sung C.J., Combust. Flame 156 (2009) 1278-1288.

[10] Dagaut P., Reuillon M., Cathonnet M., Combust. Sci. Technol. 103 (1994) 349-359.

[11] Won S.H., Sun W., Ju Y., Combust. Flame 157 (2010) 411-420.

[12] Pitz W.J., Mueller C.J., Prog. Energy Combust. Sci. 37 (2011) 330-350.

[13] Westbrook C.K., Pitz W.J., Herbinet O., Curran H.J., Sillke E.J., Combust. Flame 156 (2009) 181–199.

[14] Ristori A., Dagaut P., Cathonnet M., Combust. Flame 125 (2001) 1128-1137.

[15] Ranzi E., Frassoldati A., Granata S., Faravelli T., Ind. Eng, Chem, Res, 44(2005) 5170-5183.

[16] H.S. Shen, J. Steinberg, J. Vanderover, Oehlschlaeger M.A., Energy Fuels, 23(2009) 2482-2489.

[17] Holley A.T., Dong Y., Andac M.G., Egolfopoulos F.N., Edwards T., Proc. Combust. Inst. 31 (2007) 1205–1213

[18] Biet J., Hakka M.H., Warth V., Glaude P., Battin-Leclerc F., Energy Fuels, 22(2008), 2258-2269

[19] Grana R., Seshadri K., Cuoci A., Niemann U., Faravelli T., Ranzi E., Combust. Flame 159 (2012) 130–141.

[20] Seshadri K., Humer S., Seiser R., Combust. Theory Model. 12(2008) 831-855.

[21] Haylett D.R., Davidson D.F., Hanson R.K., Combust. Flame 159 (2012) 552–561.

[22] Mati K., Ristori A., Gail S., Pengloan G., Dagaut P., Proc. Combust. Inst. 31 (2007) 2939–2946

[23] Ramirez L H.P.R., Hadj-Ali K., Dievart P., Moreac G., Dagaut P., Energy Fuels, 24(2010), 1668-1676

[24] Vasu S.S., Davidson D. F., Hanson R.K., Combust. Flame 152 (2008) 125–143

[25] Humer S., Frassoldati A., Granata S., Faravelli T., Ranzi E., Seiser R., Seshadri K., Proc. Combust. Inst. 31 (2007) 393–400.

[26] Kumar K., Sung C.J., Combust. Flame 151 (2007) 209–224.

[27] Chong C.T., Hochgreb S., Proc. Combust. Inst. 33 (2011) 979–986.

[28] Ji C., Egolfopoulos F.N., Proc. Combust. Inst. 33 (2011) 955-961.

[29] Honnet S., Seshadri K., Niemann U., Peters N., Proc. Combust. Inst. 32 (2009) 485-492.

[30] Natelson R.H., Kurman M.S, Cernansky N.P., Miller D.L., Fuel, 87(2008) 2339-2342.

[31] Holley A.T., You X.Q., Dames E., Wang H., Egolfopoulos F.N., Proc. Combust. Inst. 32 (2009) 1157-1163.

[32] Wang Y.L., Veloo P.S., Egolfopoulos F.N., Tsotsis T.T., Proc. Combust. Inst. 33 (2011) 1003-1010.

[33] Zhang H., Egolfopoulos F.N., Proc. Combust. Inst. 28 (2000) 1875-1882.

[34] Wu C.K., Law C.K., Proc. Combust. Inst. 20 (1984) 1941–1949.

[35] Law C.K., Zhu D.L., Yu G., Proc. Combust. Inst. 21 (1986) 1419–1426.

[36] Zhu D.L., Egolfopoulos F.N., Law C.K., Proc. Combust. Inst. 22 (1988) 1537–1545.

[37] Wang Y.L., Feng Q.Y., Egolfopoulos F.N., Tsotsis T.T., Combust. Flame 158 (2011) 1507–

1519.

[38] Wang Y.L., Holley A.T.,Ji C., Egolfopoulos F.N., Proc. Combust. Inst. 32 (2009) 1035–1042.

[39] Egolfopoulos F.N., Campbell C.S., J. Fluid Mech. 318 (1996) 1-29.

[40] Kee R.J., Miller J.A., Evans G.H., Lewis G.D., Proc. Combust. Inst. 22 (1988) 1479–1494.

[41] Egolfopoulos F.N., Proc. Combust. Inst. 25 (1994) 1375-1381.

[42] Kee R.J., Rupley F.M., Miller J.A., Sandia Report SAND 89-8009, Sandia National Laboratories, 1989.

[43] Kee R.J., Warnatz J., Miller J.A., Sandia Report SAND83-8209, Sandia National Laboratories, 1983.

[44] Dong Y., Holley A.T., Andac M.G., Egolfopoulos F.N., Davis S.G., Middha P., Wang H., Combust. Flame 142 (2005) 374-387.

[45] Egolfopoulos F.N., Dimotakis P.E., Proc. Combust. Inst. 27 (1998) 641-648.

[46] Nishioka M., Law C.K., Takeno T., Combust. Flame 104 (1996) 328-342.

[47] Westbrook C.K., Pitz W.J., Herbinet O., Curran H.J., Sillke E.J., Combust. Flame 156 (2009) 181–199.

[48] Wang H., Dames E., Sirjean B., Sheen D.A., Tangko R., Violi A., Lai J.Y.W., Egolfopoulos F.N., Davidson D.F., Hanson R.K., Bowman C.T., Law C.K., Tsang W., Cernansky N.P., Miller D.L., Lindstedt R.P., A high-temperature chemical kinetic model of *n*-alkane (up to *n*-dodecane), cyclohexane, and methyl-, ethyl-, *n*-propyl and *n*-butyl-cyclohexane oxidation at high temperatures, JetSurF version 2.0, September 19, 2010 (http://melchior.usc.edu/JetSurF/JetSurF2.0).

[49] Law C.K., Proc. Combust. Inst. 22 (1988) 1381-1402.

[50] Law C.K., Sung C.J., Prog, Energy Combust. Sci. 26 (2000) 459-505.

[51] Li B., Liu N., Zhao R., Zhang H., Egolfopoulos F.N., "Flame propagation of mixtures of air with high molecular weight neat hydrocarbons and practical jet and diesel fuels", Proc. Combust. Inst. 34, doi:10.1016/j.proci.2012.05.063.

[52] Won S.H., Dooley S., Dryer F.L., Ju Y., Proc. Combust. Inst. 33 (2011) 1163-1170.

[53] Won S.H., Ju Y., Combust. Flame 157 (2010) 411-420.

Chapter 6: An Experimental and Modeling Study of the Propagation and Extinction of Cyclopentadiene

6.1 Introduction

Aromatics are present in significant quantities in all petroleum-derived practical fuels (e.g., [1,2]), and the understanding of their fundamental combustion properties is essential to the development of reliable combustion models. In past studies (e.g., [3-7]), it has been shown that the cyclopentadienyl (CPDyl, C_5H_5) radical is an important transition species between cyclic and acyclic combustion. For example, in the oxidation of benzene (C_6H_6), CPDyl forms via

$$C_6H_5 + O_2 \Leftrightarrow C_6H_5O + O \qquad \text{(R1)}$$

$$C_6H_5O + M \Leftrightarrow C_5H_5 + CO + M \qquad \text{(R2)}$$

in which C_6H_5 corresponds to the phenyl radical and C_6H_5O to phenoxy. Thus, in order to describe the aromatics oxidation accurately, the details of CPDyl combustion need to be well characterized.

Few experimental studies of cyclopentadiene (CPD, C_5H_6) have been performed in order to understand the CPDyl combustion, compared to other compounds such as, for example, benzene and toluene. Previous studies on the pyrolysis of CPD in a flow reactor [8] and a shock tube [9-11], showed that the CPDyl radical decomposes mainly to propargyl (C_3H_3) and acetylene (C_2H_2) via

$C_5H_5 \Leftrightarrow C_3H_3 + C_2H_2$. (R3)

Oxidation studies of CPD have attracted more interest recently due to its importance in aromatics combustion. Burcat et al. [12] proposed a kinetic model of CPD using shock tube data, and the importance of cyclopentadienone (CPDone, C_5H_4O) during the oxidation of CPDyl was emphasized based on the study of the thermal decomposition of CPDone by Wang and Brezinsky [13]. However, another shock tube study performed by Murakami et al. [14] suggested that cyclopentadienoxy (CPDoxy, C_5H_5O) should be the major intermediate from the oxidation of CPDyl via

$C_5H_5 + O_2 \Leftrightarrow C_5H_5O + O$, (R4)

but no further discussion about the decomposition of CPDoxy was provided due to limited information. Recently, Butler and Glassman [15] studied the CPD oxidation in a plug flow reactor, and reported the lack of observable quantities of CPDone and indicated that the CPDoxy radical should be the main intermediate. In the same study [15], the CPDoxy radicals were determined to form either *n*-butadienyl (*n*-C_4H_5) and CO via

$C_5H_5O \Leftrightarrow n\text{-}C_4H_5 + CO$, (R5)

or 2,4-pentadienal-5-yl via the β-scission reaction

$C_5H_5O \Leftrightarrow CH{=}CH{-}CH{=}CH{-}CHO$ (R6)

to transfer from cyclic to acyclic molecular structures. The most recent kinetics study of CPD oxidation was done by Robinson and Lindstedt [16], in which it was shown that in

Butler and Glassman's experiments [15], the dominant CPDyl removal paths are oxidative via HO_2 attack, i.e.,

$$C_5H_5 + HO_2 \Leftrightarrow C_5H_5O + OH. \qquad \text{(R7)}$$

Although many efforts have focused on the development of reliable kinetic models for CPD/CPDyl, challenging problems are still remaining due to the inherent complexity of the kinetics and the lack of a sufficient experimental database, especially in flames. The present study thus aims to provide archival experimental data for the propagation and extinction of CPD flames for the first time, as to the authors' knowledge such data do not exist in the literature. Laminar flame speeds, S_u^o, and extinction strain rates, K_{ext}, were determined in the counterflow configuration for a wide range of equivalence ratios, ϕ. The experiments were carried out at atmospheric pressure and elevated unburned mixture temperatures. Further insight was provided into the physical and chemical processes that control the burning characteristics of CPD/air mixtures through detailed numerical simulations.

6.2 Experimental Approach

Similarly to previous studies (e.g., [17-19]), the experiments were performed in the counterflow configuration, under ambient pressure, and $0.7 \leqslant \phi \leqslant 1.5$ for both flame propagation and extinction. The burners include several internal and external heating capabilities as well as aerodynamically designed nozzles and N_2 co-flow channels surrounding the main nozzles. The shape of the nozzle results in top-hat exit velocity

profile, while the shape of the co-flow channel assures isolation of the main jet from the ambient. The single-flame configuration was used to determine both S_u^o's and extinction resulting from counterflowing an ambient temperature N_2 jet against an opposing fuel/air jet (e.g., [20]). Burner nozzle diameters, D = 14 mm, and nozzle separation distances, L = 14 mm, were used.

A major challenge with CPD experiments is that it is not a stable species, and dimerizes easily to dicyclopentadiene (DCPD, $(C_5H_6)_2$) at room temperature. As a result, in the present study DCPD (TCI America, 97%) was chosen as the fuel source. DCPD can quickly decompose into CPD at temperatures above 150 ℃. DCPD is a white crystalline solid at room temperature with a melting point 32.5 ℃ and boiling point 170 ℃. In order to perform the experiments with DCPD, modifications of the experimental configuration had to be made and are shown schematically in Fig. 2.2. DCPD was first melted within a heated oil bath and then injected into a nebulizer by a high-precision syringe pump. The high-precision syringe pump was heated at temperatures about 35 ℃ to keep DCPD in the liquid phase. Uniform size fuel droplets, ranging from 0.5 μm to 5 μm, were produced by a nebulizer that were mixed and vaporized instantly with portion of the test air instantly in a glass vaporization chamber heated at 200 ℃. The gaseous mixture was sent then through a heated coil with wall temperature at 250 ℃, which allows for a total residence time around 5-6 seconds ensuring thus full monomerization of DCPD. Such conditions allow for the conversion

of more than 97% DCPD to CPD, with isoprene being the main impurity. The balance of the test air was added after the heated coil in order to cool down the mixture and achieve the desired ϕ. All measurements were made at an unburned mixture temperature T_u = 353 K.

The axial flow velocities were measured along the stagnation streamline using digital particle image velocimetry (DPIV). The flow was seeded with submicron size droplets of silicon oil that was previously mixed with the fuel at small concentrations, i.e. 0.2~0.5%. A dual laser head, Solo Nd:YAG laser system (New Wave Research, type Solo-III-15) and a PIV imager intense system (LaVision) were used in this work. To determine S_u^o, the minimum point of the velocity profile upstream of the flame was measured and defined as a reference flame speed, Su,ref. The absolute value of the maximum velocity gradient in the hydrodynamic zone is defined as the imposed strain rate, K. Monitoring the variation of Su,ref with K, S_u^o could be determined by performing a non-linear extrapolation of $S_{u,ref}$ to $K = 0$, using a recently developed computationally-assisted technique [20-22]. Similar to S_u^o, K_{ext} cannot be measured directly. Its determination requires a near-extinction flame being established first, followed by measurement of the prevailing K just upstream of the flame. Subsequently, the fuel flow rate in the fuel/air jet is varied slightly to achieve extinction [20]. For fuel-lean mixtures this is done by reducing the fuel flow rate, while for fuel-rich mixtures,

extinction is achieved by increasing the fuel flow rate. The modification to K due to the slight change in the fuel flow rate has been determined to be insignificant.

6.3 Numerical Approach

S_u^o's and K_{ext}'s were computed using the PREMIX code [23,24] and an opposed-jet code [25,26] respectively. Both are modified to account for thermal radiation of CH_4, CO, CO_2, and H_2O in the optically thin limit and are coupled with the Sandia CHEMKIN [27] and Transport [28] subroutine libraries. The H and H_2 diffusion coefficients of several key pairs are based on the recently updated set of Lennard–Jones parameters [29,30],

The experimental results were mainly simulated using two kinetic models. USC Mech II [31], hereafter referred to as Model I, was developed by Wang and co-workers to describe the high-temperature oxidation of hydrogen, carbon monoxide, and C_1-C_4 hydrocarbons, but it contains also benzene and toluene kinetics, which however require further validation. Dooley et al. [32] developed a detailed kinetic model for jet fuel surrogates that include oxidation kinetics of toluene, hereafter referred to as Model II. Both models include oxidation kinetics of CPD as a sub-model for aromatics flame. The consumption of CPD and CPDyl radicals via O_2, HO_2, O, OH, and H are similar in both models, as determined in the study by Zhong and Bozzelli [33]. Regarding the oxidation kinetics of CPDone and CPDoxy, Model I includes reaction rates that are mostly estimated, while in Model II the rates recommended by Alzueta et al. [34] have

been adopted. The laminar flame speeds of CPD/air mixtures computed by Lindstedt and Park [35] using their recent developed kinetic model [16] were also plotted in order to compare with Models I and II.

6.4 Results and Discussion

Figure 6.1 depicts the experimental and computed S_u^o's of CPD/air mixture along with the predictions using Models I and II. The experimentally determined peak S_u^o value is 50 cm/s at ϕ = 1.05. Using Model I, the experimental S_u^o's are predicted closely for all 's. The largest discrepancy is about 2 cm/s, but still within the experimental uncertainty. Model II results in good agreements with the data for ϕ < 1.0, however the data are over-predicted for ϕ > 1.0. Simulation results using kinetic model from Ref. 16 under-predict the data for ϕ < 1.0, but show a general good agreement for ϕ > 1.0. Lindstedt and coworkers [16, 35] argued that the reaction pathways of CPD flames under fuel rich conditions result in substantial formation of propargyl and acetylene with the C_3H_3 + OH and HCCO + O_2 reactions exerting a strong influence on computed burning velocities. The determination by Klippenstein et al. [36] was used for the latter reaction with the estimated rates and product channels of Hansen et al. [37] applied for the C_3H_3 + OH reaction [16]. The latter channel is absent in JetSurf 2.0 and related work [38] suggests that the earlier estimate [37] provides an upper limit. Though Lindstedt and coworkers [16, 35] suggested new reaction pathways in CPD flames, due to the wide verification of C_0-C_4 sub-models of Models I and II in predicting

high-temperature global flame phenomena such as laminar flame speeds and extinction limits, Models I and II were used to perform the analysis in the following discussion.

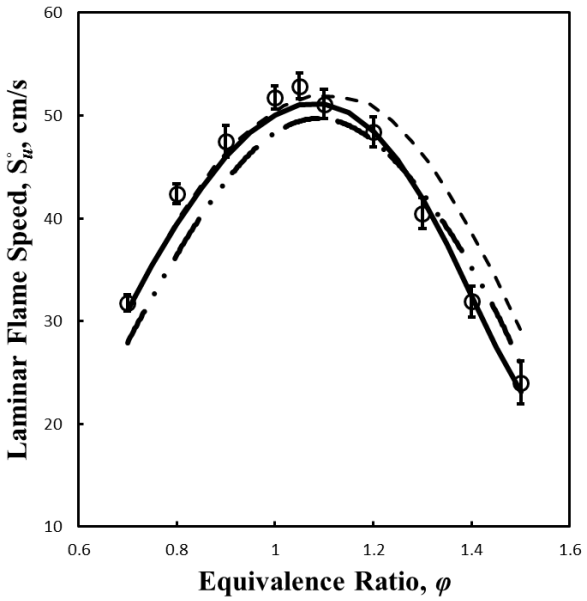

Figure 6.1. Experimental and computed laminar flame speeds of cyclopentadiene/air flames at T_u = 353 K and p = 1 atm. Symbols: present experimental data. Solid lines: simulations using Model I. Dashed Lines: simulations using Model II. Dashed-dot Lines: simulations provided by Lindstedt and Park [35] using kinetic model in Ref. 16. The error bars shown in the present experimental data are based on the 2-σ standard deviations.

Figure 6.2 depicts the logarithmic sensitivity coefficients of S_u^o with respect to kinetics for a ϕ = 0.7 CPD/air flame. Unlike *n*-alkane [20] and cycloalkane [39] flames whose propagation is sensitive only to the small hydrocarbon chemistry, S_u^o's of CPD/air flames are sensitive also on the kinetics of the fuel and the subsequent intermediates such as CPDyl and CPDoxy. The recombination of CPDyl with the H

radical to form CPD retards S_u^o. The H-abstraction reaction of CPD to form CPDyl is shown to be slow and retards propagation. The production of CPDoxy via R7, favors S_u^o by consuming HO_2 and producing OH.

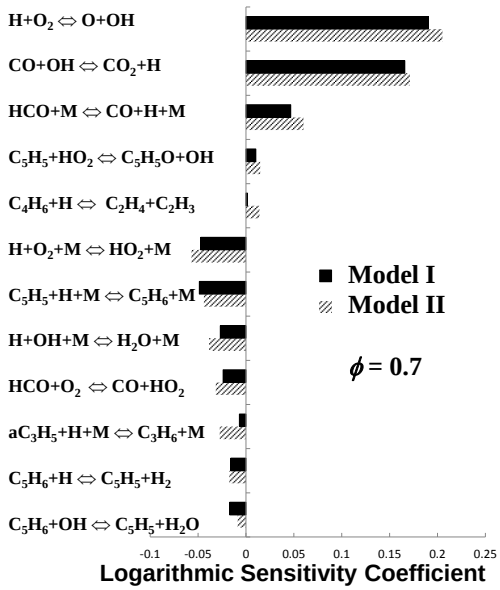

Figure 6.2. Ranked logarithmic sensitivity coefficients of laminar flame speeds with respect to kinetics, computed using Models I and II for a $\phi = 0.7$ cyclopentadiene/air flame at T_u = 353 K and p = 1 atm.

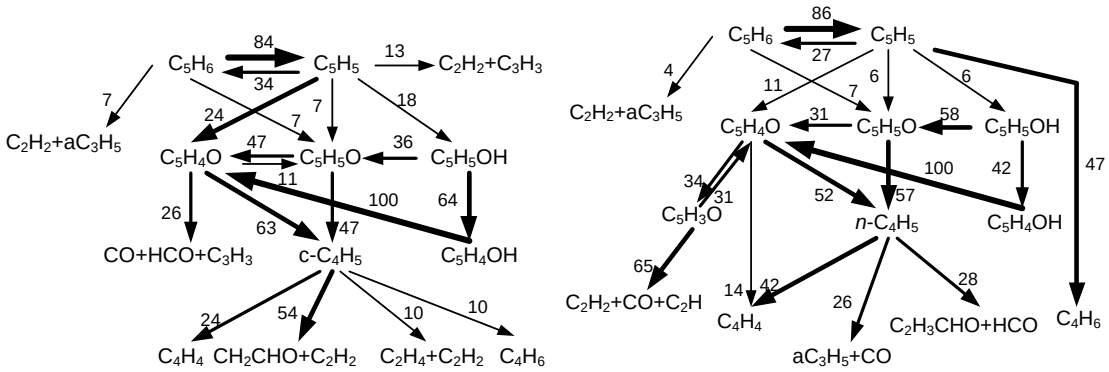

(a) (b)

Figure 6.3. Reaction path analysis of a $\phi = 0.7$ cyclopentadiene/air flame at $T_u = 353$ K, and $p = 1$ atm using (a) Model I, and (b) Model II. The numbers indicate the conversion percentages.

Figures 6.3 depict the reaction path analysis of a $\phi = 0.7$ CPD/air flame performed using Model I and Model II. As both models adopt the H-abstraction reactions of CPD from Zhong and Bozzelli [33], they exhibit a similar initial CPD consumption which approximately 85% of CPD producing CPDyl radicals. The rest of CPD produces either acetylene and allyl or CPDoxy. In both models, 30% of CPDyl recombines with H to form CPD. In Model I, 13% of CPDyl radicals decompose to acetylene and propargyl (C_3H_3) via reaction R3. In Model II, however, nearly half of the CPDyl radicals form 1,3-butadiene (C_4H_6) via reaction [33]

$$C_5H_5 + OH \Leftrightarrow C_4H_6 + CO. \qquad \text{(R8)}$$

In both Model I and Model II, the rest of the CPDyl radicals react to yield CPDoxy, CPDone, and cyclopentadienol (CPDol, C_5H_5OH). The ring opening process takes place via CPDone and CPDoxy. The CPDol radical either result in CPDoxy or CPDone via cyclopentadienol-yl (C_5H_4OH). Both CPDoxy and CPDone react to yield either cyclobutenyl (c-C_4H_5) in Model I or *n*-butadienyl in Model II. Cyclobutenyl is not a stable radical and thus is not considered as rate limiting in Model I. Figure 6.4 depicts the spatial mole fraction profiles of computed C_2H_2 and C_4H_6 concentration profiles for a $\phi = 0.7$ CPD/air flame using Models I and II. As expected, Model I results in about 2 times more C_2H_2 but about 10 times less C_4H_6 compared to Model II due to the different reaction pathways of CPDyl radicals. As reported in a previous study on cyclo-alkane flames [39], the reaction involving C_4H_6 can have a notable positive influence on flame propagation via reaction

$$C_4H_6 + H \Leftrightarrow C_2H_4 + C_2H_3. \qquad \text{(R9)}$$

Thus, the higher computed S_u^o values using Model II could be attributed to the excess production of C_4H_6 in Model II compared to Model I. S_u^o exhibits a finite positive sensitivity on R9 as shown also in Fig. 6.2.

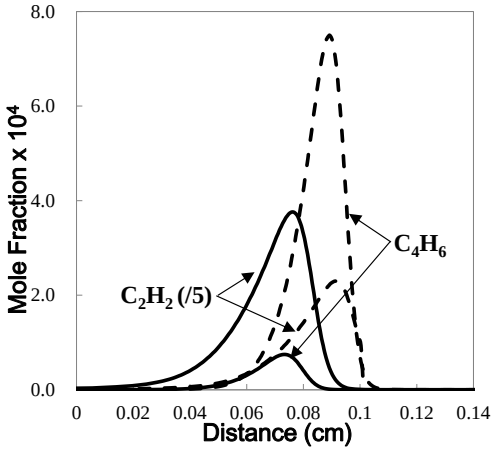

Figure 6.4. Computed intermediate species profiles for a $\phi = 0.7$ cyclopentadiene/air flame at $T_u = 353$ K and $p = 1$ atm, using Model I (solid lines) and Model II (dashed lines).

Given that flame propagation and extinction are both high temperature phenomena, extinction strain rates provide additional constraints for the flame kinetics of the fuels studied, especially considering the fact that K_{ext} is more sensitive to the reaction kinetics compared to S_u^o (e.g., [40, 41]). Thus, predicting flame extinction limits is an additional important validation test for a kinetic model.

Figure 6.5 depicts the experimental and computed K_{ext}'s of CPD/air mixtures along with the predictions using Model I and Model II. The experimentally determined peak K_{ext} value is around 900 s^{-1} at $\phi = 1.15$. Unlike the predictions obtained for flame propagation, using Model II better agreements are obtained with the K_{ext} data for all ϕ's. On the other hand, using Model I the K_{ext} data are under-predicted for all ϕ's.

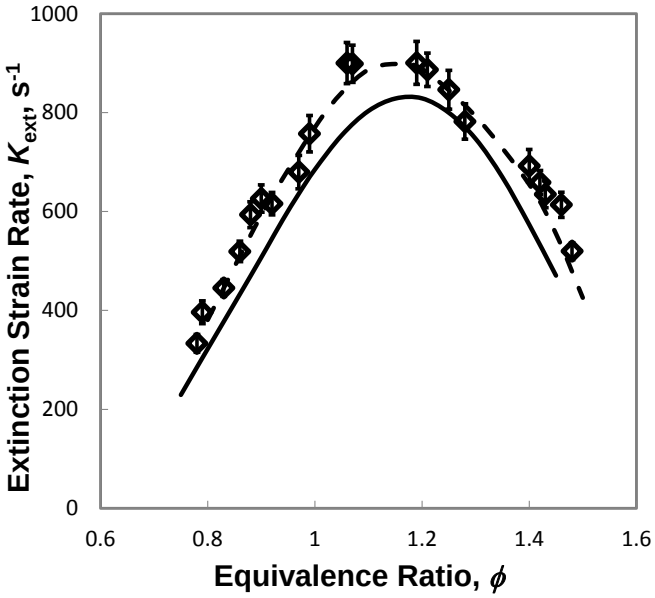

Figure 6.5. Experimental and computed extinction strain rates of cyclopentadiene/air flames at T_u = 353 K and p = 1 atm. Symbols: present experimental data. Solid lines: simulations using Model I. Dashed Lines: simulations using Model II. The error bars shown in the present experimental data are based on the 2-σ standard deviations.

The ranked logarithmic sensitivity coefficients of K_{ext} on kinetics are shown in Fig. 6.6 for a ϕ = 1.05 CPD/air flame. Similar to the results shown in Fig. 6.2, K_{ext}'s of CPD/air flames are sensitive not only to small hydrocarbon reactions but also to the fuel and related intermediates' chemistry. In addition, due to the different reaction pathways of CPDyl decomposition between Model I and Model II, the distribution of the resulting small intermediates could affect the prediction of K_{ext}.

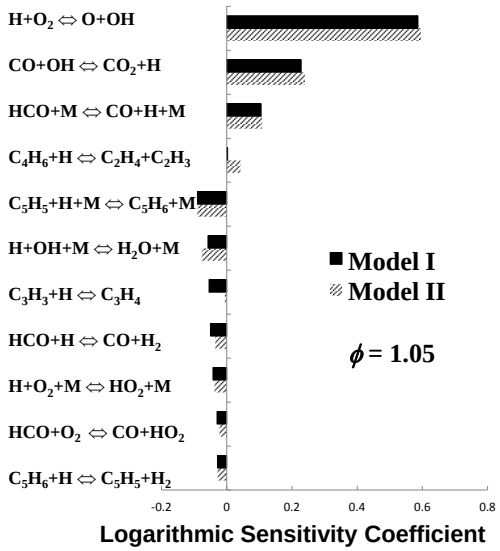

Figure 6.6. Ranked logarithmic sensitivity coefficients of extinction strain rates with respect to kinetics, computed using Models I and II for a $\phi = 1.05$ cyclopentadiene/air flame at $T_u = 353$ K and $p = 1$ atm.

Figure 6.7 depicts the computed species concentration profiles of C_3H_3 and C_4H_6 for a near-extinction $\phi = 1.05$ flame, using Models I and II. It is apparent that Model I results in notably higher production of C_3H_3, and notably less C_4H_6 compared to Model II similarly to the results shown in Fig. 6.4. C_3H_3 radicals are produced largely by R3, and can react with H to yield propyne (C_3H_4) via

$$C_3H_3 + H \Leftrightarrow C_3H_4, \qquad \text{(R10)}$$

a reaction that based on Model I, has a negative effect on extinction as shown in Fig. 6.6. On the other hand there is no measurable sensitivity of K_{ext} on R10 based on Model II

given that it results in significantly lower C_3H_3 concentrations. For similar reasons while K_{ext} is sensitive to R9 based on Model II, this is not the case for Model I.

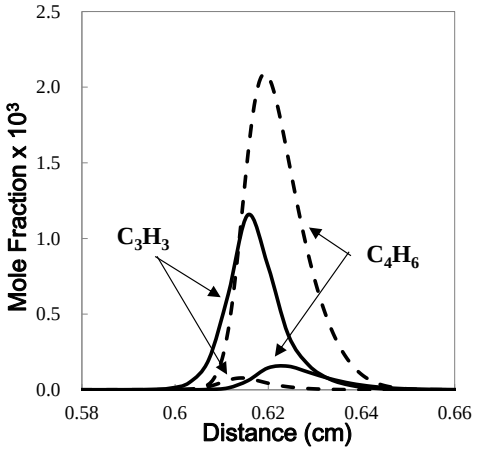

Figure 6.7. Computed intermediate species profiles for a near-extinction $\phi = 1.05$ cyclopentadiene/air flame at $T_u = 353$ K and $p = 1$ atm, using Model I (solid lines) and Model II (dashed lines).

Selected concentration profiles from the CPD oxidation in a plug flow reactor reported by Butler and Glassman [15] were modeled also in order to provide further insight into the oxidation of CPDyl radicals and the results are shown in Fig. 6.8. The experiments were conducted at initial temperature of 1198 K, initial fuel concentration of 2243 ppm, and $\phi = 1.03$. The computed results of Models I and II were time-shifted by -20 ms and -28 ms respectively to best fit the data. In general, both Models I and II exhibit good agreement with the experimental data for CPD consumption and CO production. Model I predicts closely the C_2H_2 profile but underpredicts the C_4H_6

concentrations by a factor of about 12. Model II predicts closely the C_4H_6 data, but it underpredicts the C_2H_2 data by a factor of 2.

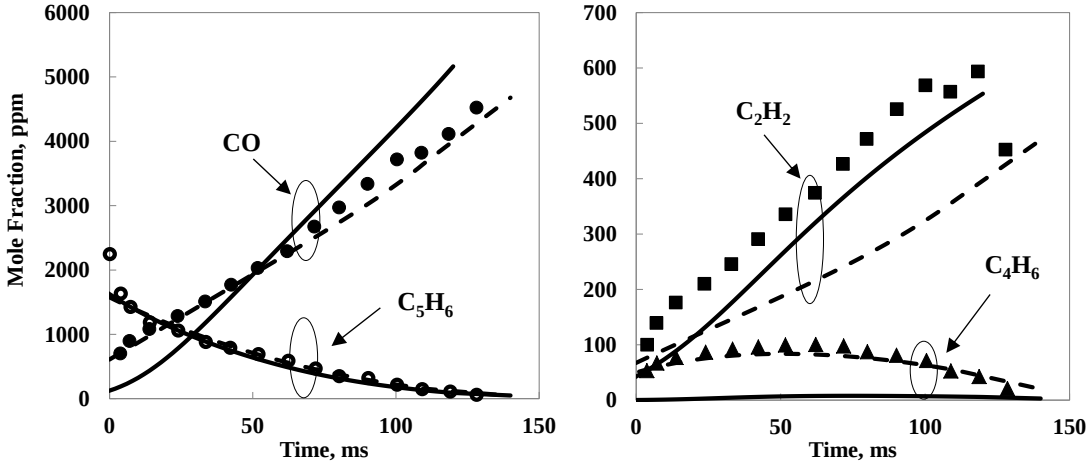

Figure 6.8. Concentration profiles during CPD oxidation in a plug flow reactor with initial temperature of 1198 K, initial fuel concentration of 2243 ppm, and $\phi = 1.03$. Symbols: experimental data from Butler and Glassman [15]; (○) C_5H_6, (●) CO, (■) C_2H_2, and (▲) C_4H_6; Lines: simulation with (a) Model I (solid lines) time-shifted by -20 ms and (b) Model II (dashed lines) time-shifted by -28 ms.

Based the results obtained from flame propagation, flame extinction, and the flow reactor, it is apparent that the production pathways of C_3H_3 via R3 and C_4H_6 via R8 constitute a source of uncertainty between Model I and Model II. To illustrate the attendant effects, Model I was modified by adding the rate constant of R8 by those of Model II. Figure 6.9 depicts the computed S_u^o's and K_{ext}'s using both the original and modified Model I. It can be seen that the modified Model I results in much improved predictions of the data for both flame propagation and extinction of CPD/air mixtures.

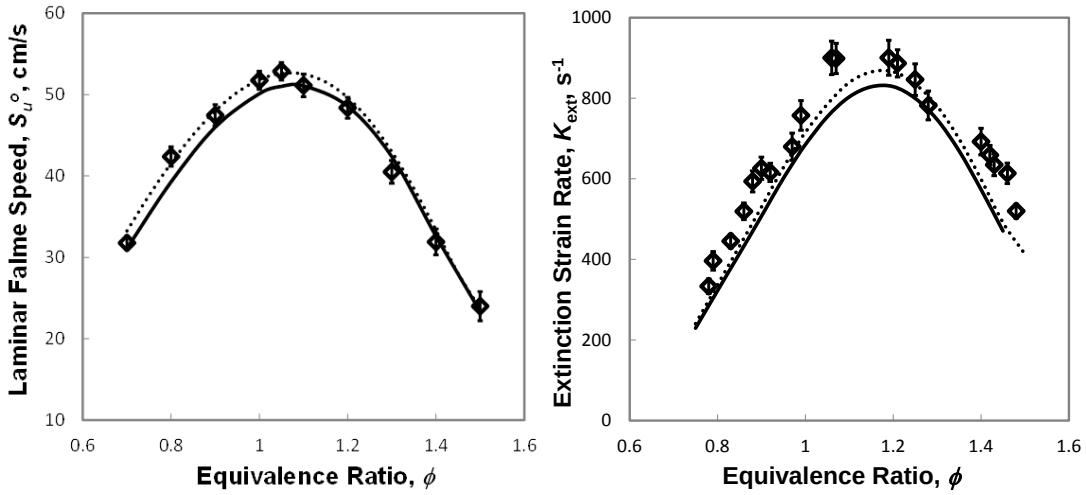

Figure 6.9. Experimental and computed laminar flame speeds and extinction strain rates of cyclopentadiene/air flames at $T_u = 353$ K and $p = 1$ atm. Symbols: present experimental data. Solid lines: simulations using Model I. Dotted lines: simulations using modified Model I by adding R8 from Model II. The error bars shown in the present experimental data are based on the 2-σ standard deviations.

6.5 Concluding Remarks

Laminar flame speeds and extinction strain rates of cyclopentadiene/air flames were determined experimentally over an extended range of equivalence ratios in the counterflow configuration under atmospheric pressure and at an elevated unburned mixture temperature. The experimental data are the first ones to be reported and were modeled using several detailed kinetic models. Overall satisfactory agreements were found. Sensitivity analyses revealed that the oxidation of cyclopentadiene/air mixtures depends notably on the chemistry of fuel itself and subsequent intermediates such as cyclopentadienone and cyclopentadienoxy radicals. The analysis further revealed that

reactions of small hydrocarbon intermediates resulting from the consumption of cyclopentadienyl have a significant effect on both flame propagation and extinction. Comparing the simulation results, it was concluded that among others, there are uncertainties associated with the consumption pathways of cyclopentadienyl, including $C_5H_5 \Leftrightarrow C_3H_3 + C_2H_2$ and $C_5H_5 + OH \Leftrightarrow C_4H_6 + CO$ that can have a rather significant effect on the prediction of various combustion properties both in homogeneous reactors and flames.

6.6 References

[1] A. Roubaud, R. Minetti, L.R. Sochet, Combust. Flame 121 (2000) 535–541.

[2] N. Grumman, Northrop Grumman Petroleum Product Survey Reports, Updated Annually, http://pps.ms.northropgrumman.com/.

[3] T. Edwards, L.Q. Maurice, J. Propul. Power 17 (2001) 461–466.

[4] A.S. Violi, S. Yan, E.G. Eddings, A.F. Sarofim, S. Granata, T. Faravelli, E. Ranzi, Combust. Sci. Technol. 174 (2002) 399-417.

[5] E.G. Eddings, S. Yan, W. Ciro, A.F. Sarofim, Combust. Sci. Technol. 117 (2005) 715-739.

[6] J.A. Cooke, M. Bellucci, M.D. Smooke, A. Gomez, A. Violi, T. Favarelli, E. Ranzi, Proc. Combust. Inst. 30 (2005) 439-446.

[7] S. Humer, A. Frassoldati, S. Granata, T. Faravelli, E. Ranzi, R. Seiser, K. Seshadri, Proc. Combust. Inst. 31 (2007) 393–400.

[8] O.S.L. Bruinsma, P.J.J. Tromp, H.J.J. de Sauvage Nolting, J. A. Moulijn, Fuel 67 (3) (1988) 334-340.

[9] A. Burcat, M. Dvinyaninov, Int. J. Chem. Kinet. 29 (7) (1997) 505-514.

[10] K. Roy, C. Horn, P. Frank, V.G. Slutsky, T. Just, Proc. Combust. Inst. 27 (1) (1998) 329-336.

[11] R.D. Kern, Q. Zhang, J. Yao, B.S. Jursic, R.S. Tranter, M.A. Greybill, J.H. Kiefer, Proceedings of Combustion Institute 27 (1) (1998) 143-150.

[12] A. Burcat, M. Dvinyaninov, E. Olchanski, Int. J. Chem. Kinet. 33 (9) (2001) 491-508.

[13] H. Wang, K. Brezinsky, J. Phys. Chem. A 102 (1998) 1530-1541.

[14] Y. Murakami, K. Mitsui, K. Naito, T. Itoh, T. Kobayashim, N. Fuji, Shock Waves 13 (2003) 149-154.

[15] R.G. Butler, I. Glassman, Proc. Combust. Inst. 32 (2009) 395-402.

[16] R.K. Robinson, R.P. Lindstedt, Combust. Flame 158 (4) (2011) 666-686.

[17] C. K. Wu, C.K. Law, Proc. Combust. Inst. 20 (1984) 1941-1949.

[18] G. Yu, C.K. Law, C.K. Wu, Combust. Flame 63 (1986) 339-347.

[19] D. L. Zhu, F.N. Egolfopoulos, C.K. Law, Proc. Combust. Inst. 22 (1988) 1537-1545.

[20] C. Ji, E. Dames, Y.L. Wang, H. Wang, F.N. Egolfopoulos, Combust. Flame 157 (2) (2010) 277-287.

[21] Y.L. Wang, A.T. Holley, C. Ji, F.N. Egolfopoulos, T.T. Tsotsis, H.J. Curran, Proc. Combust. Inst. 32 (2009) 1035-1042.

[22] P.S. Veloo, Y.L. Wang, F.N. Egolfopoulos, C.K. Westbrook, Combust. Flame 157 (10) (2010) 1989-2004.

[23] R.J. Kee, J.F. Grcar, M.D. Smooke, J.A. Miller, A FORTRAN Program for Modeling Steady Laminar One-Dimensional Premixed Flames, Sandia Report.SAND85-8240, Sandia National Laboratories, 1985.

[24] J.F. Grcar, R.J. Kee, M.D. Smooke, J.A. Miller, Proc. Combust. Inst. 21 (1986) 1773-1782.

[25] R.J. Kee, J.A. Miller, G.H. Evans, G. Dixon-Lewis, Proc. Combust. Inst. 22 (1988) 1479 – 1494.

[26] F.N. Egolfopoulos, C.S. Campbell, J. Fluid Mech. 318 (1996) 1-29.

[27] R.J. Kee, F.M. Rupley, J.A. Miller, Chemkin-II: A FORTRAN Chemical Kinetics Package for the Analysis of Gas-Phase Chemical Kinetics, Sandia Report SAND89-8009, Sandia National Laboratories, 1989.

[28] R.J. Kee, J. Warnatz, J.A. Miller, A FORTRAN Computer Code Package for the Evaluation of Gas-Phase Viscosities, Conductivities, and Diffusion Coefficients, Sandia Report SAND83-8209, Sandia National Laboratories, 1983.

[29] Y. Dong, A.T. Holley, M.G. Andac, F.N. Egolfopoulos, S.G. Davis, P. Middha, H. Wang, Combust. Flame 142 (2005) 374-387.

[30] P. Middha, H. Wang, Combust. Theor. Model. 9 (2005) 353-363.

[31] H. Wang, X. You, A.V. Joshi, S.G. Davis, A. Laskin, F.N. Egolfopoulos, C.K. Law, USC Mech Version II. High-Temperature Combustion Reaction Model of H_2/CO/C_1-C_4 Compounds. http://ignis.usc.edu/USC_Mech_II.htm, May 2007.

[32] S. Dooley, S.H. Won, M. Chaos, J. Heyne, Y. Ju, F.L. Dryer, K. Kumar, C-J. Sung, H Wang, M. Oehlschlaeger, R.J. Santoro, T.A. Litzinger, Combust. Flame 157 (12) (2010) 2333-2339.

[33] X. Zhong, J.W. Bozzelli, J. Phys. Chem. A 102 (1998) 3537-3555.

[34] M.U. Alzueta, P. Glarborg, K. Dam-Johansen, Int. J. Chem. Kinet. 32 (8) (2000) 498-522

[35] R.P. Lindstedt, S.W. Park, personal communication (2012).

[36] S.J. Klippenstein, J.A. Miller, L.B. Harding, Proc. Combust. Inst. 29 (2002) 1209-1217.

[37] N. Hansen, J.A. Miller, T. Kasper, K. Kohse-Höinghaus, P.R. Westmoreland, J. Wang, T.A. Cool, Proc. Combust. Inst. 32 (2009) 623–630.

[38] E. Meeks, C.V. Naik, K.V. Puduppakkam, A. Modak, C.K. Westbrook, F. Egolfopoulos, T. Tsotsis, Experimental and Modeling Studies of Combustion Characteristics of Conventional and Alternative Jet Fuels, NASA/CR NNC07CB45C-Final Report 1 (2009).

[39] C. Ji, E. Dames, B. Sirjean, H. Wang, F.N. Egolfopoulos, Proc. Combust. Inst. 33 (2011) 971-978.

[40] C.K. Law, Combustion Physics, first ed., Cambridge University Press, New York, USA, 2006, p. 410 (Chapter 10).

[41] C. Ji, E. Dames, H. Wang, F.N. Egolfopoulos, Combust. Flame (2011) doi:10.1016/j.combustflame.2011.10.01.

Chapter 7: Determination of Extinction Strain Rate: Molecular Transport Effects

7.1 Introduction

Flame properties involving diffusion-kinetic coupling are critical to a basic understanding of combustion properties of hydrocarbon fuels [1]. The extinction state of laminar, non-premixed counterflow flames represents one such key property. A large number of studies have been conducted to date especially in light of the recent interest in the combustion kinetics of real fuels and their single or multi-component surrogates (see, e.g., [2-11]). Holley et al. [8] carried out a detailed sensitivity analysis of non-premixed extinction strain rate with respect to kinetic and transport model parameters. It was found that the flame extinction responses could be particularly sensitive to the mass diffusivity of the fuel, especially for heavy fuel molecules. The cause is quite clear, as in these flames fuel diffusion is typically slow due to the fuel size and weight but diffusion is critical to supplying the fuel to the thermal mixing layer, allowing it react with the oxidizer flowing from the opposite direction. Won et al. [3] developed a radical index method for determining the chemical kinetic contribution to non-premixed flame extinction of large hydrocarbons. It was shown that the mass diffusivity of the fuel plays a role critical to the flame extinction; and it becomes possible to isolate the fuel kinetic effects only when the transport effects are properly accounted for.

A class of compounds of particular interest to a range of real liquid fuels is normal paraffin. Previously, Ji et al. [10] made measurements for the extinction strain rates, K_{ext}, of counterflow, non-premixed *n*-decane (*n*-$C_{10}H_{22}$) and *n*-dodecane (*n*-$C_{12}H_{26}$) flames. They found that JetSurF 1.0 [12] overpredicts the K_{ext} data notably. Interestingly, the model predicts the laminar flame speeds and shock tube ignition delay time rather well. Sensitivity analyses suggest that the uncertainty in the kinetic parameters alone could not explain the observed discrepancies between the experimental and computed K_{ext} or the kinetic uncertainty alone is not enough to reconcile K_{ext} with flame propagation and shock tube ignition data. Rather, the sensitivity tests suggest that the uncertainties of the transport properties could be the cause for the discrepancy.

In the JetSurF effort [12], the diffusion coefficients of long-chain *n*-alkanes were calculated via the Lennard-Jones 12-6 potential parameters for the self-interaction of the hydrocarbon molecules. These potential parameters were only rough estimates as they are based on the equations of the law of corresponding states [13] using more basic phase-change properties including the critical pressure and temperature and boiling points. The method was used earlier for estimating the Lennard-Jones 12-6 parameters of polycyclic aromatic hydrocarbons [14]. Since the equations used to estimate the LJ parameters are empirical and their use for large *n*-alkanes represents an extrapolation of data from which these equations were developed, the accuracy of the potential parameters are obviously highly uncertain. Aside from this concern, there is very little theoretical

evidence that the mixing rule for the potential parameters is valid or the spherical, isotropic potential interactions are adequate to describe chain-like *n*-alkane molecules.

Jasper and coworkers [15, 16] carried out classical trajectory studies of several *n*-alkanes in some typical diluent gases to determine diffusion collision cross sections. They showed that diffusion coefficients of *n*-alkanes estimated from the use of the law of corresponding states deviate quite notably from the classical trajectory results. Unfortunately, their work had included *n*-alkane molecules only up to *n*-heptane, which is somewhat short of allowing us to test the plausible cause for the experiment and model discrepancy observed for non-premixed flame extinction of *n*-$C_{10}H_{22}$ and *n*-$C_{12}H_{26}$ of Ji et al. [10] just discussed.

The main objectives of current study is to extend a recently developed transport theory of cylindrical molecular structure in dilute gases [17] to model the binary diffusion coefficients of long-chain *n*-alkanes up to *n*-dodecane in N_2 and He. Next, we show that the non-premixed flame K_{ext} of *n*-$C_{10}H_{22}$ and *n*-$C_{12}H_{26}$ of Ji et al. [10] can be predicted accurately with the updated binary diffusion coefficients of *n*-$C_{10}H_{22}$ and *n*-$C_{12}H_{26}$ in N_2 with either the multicomponent or mixture averaged transport formulation, provided that the Soret effect on the transport of large fuel molecules is accounted for.

7.2 Experimental Approach

To supplement the data from a previous study [10], additional measurements were made for non-premixed flame extinction of *n*-dodecane. The experiments were carried

out at atmospheric pressure in the counterflow configuration (see, [9, 29-31]). Details of the measurement have been discussed in Chapter 2 [10]. Briefly, non-premixed flames were established by impinging a fuel/N_2 stream on to an opposing ambient temperature O_2 stream. The burner nozzle diameter and the burner separation distance were 1.4 cm. Screens were placed in the burner to assure top-hat burner velocity profile at the nozzle exit. The gaseous flow rates were metered using sonic nozzles, which were calibrated using a dry-test meter with a reported accuracy of ±0.21%. The upstream pressure of each sonic nozzle was monitored by a pressure gauge with ±0.25% precision. The vaporization system included a precision syringe pump of ±0.35% accuracy and a glass nebulizer (Meinhard TR-50-A1), through which the liquid fuel was injected as fine droplets into a crossflow of heated nitrogen. All gas lines were heated to prevent fuel vapor condensation. The temperature of the gas lines was measured with K-type inline thermocouples. The temperature of the unburned fuel/N_2 stream, T_u, was measured at the center of the burner exit. The variation of this temperature is within ±5 K. Flow composition uncertainty has been determined to be less than 0.5% [10]. Flow velocity measurements were made by seeding the flow with submicron size silicon oil droplets and by using particle image velocimetry (PIV). The uncertainty associated with the PIV measurements is within 0.8 to 1.0% [10]. The maximum absolute axial velocity gradient on the fuel side of the hydrodynamic zone was defined as the strain rate, K, and K_{ext} was determined for a near extinction flame. The uncertainty of K_{ext} to be quoted here is the $\pm 2\sigma$ standard deviation of repeated measurements.

7.3 Numerical Approach

K_{ext} was computed using an opposed-jet flow code [32] developed originally by Kee et al. [33]. This code was modified to allow the use of a wider range of boundary conditions than the initial version and to account for thermal radiation of CH_4, H_2O, CO and CO_2 at the optically thin limit [34]. The JetSurF 1.0 kinetic model [12] was used to describe the high-temperature pyrolysis and oxidation of *n*-$C_{10}H_{22}$ and *n*-$C_{12}H_{26}$.

For K_{ext} computations, a two-point continuation approach solves for K at the state of extinction [35, 36]. The experimental values of the axial velocity gradients at the burner exits were considered as the respective boundary conditions in the simulation [31]. The code was integrated with the Sandia Transport subroutine libraries [37] with the diffusion coefficients of H and H_2 in several key diluent gases updated from Ref [38] and those of *n*-$C_{10}H_{22}$ and *n*-$C_{12}H_{26}$ in N_2 from the current diffusion coefficient model. Molecular transport was treated comparing both mixture-averaged formulation and multicomponent formulation.

We note that the mixture-averaged transport formulation of the original Sandia PREMIX and OPPDIF codes does not consider the Soret effect of large/heavy molecules even if the thermal diffusion (TDIF) keyword is turned on. To account for thermal diffusion of heavy fuel molecules, the approximation of Rosner et al. [39] for the thermal diffusion factor α_T was implemented into the mixture-averaged formulation. The thermal diffusion factor of species B in A takes the form of

$$\alpha_T = [0.454 \cdot d(\Lambda + 0.261) + 0.116(\Lambda - 1)][1 - C/T], \quad (6)$$

where Λ is related to molecular size disparity, which may be evaluated by $\Lambda \cong 1.31\,\mathrm{Sc}\,(1 + \mathrm{d})^{-1/2}$, Sc is the Schmidt number, $d = (M_B\text{-}M_A)/(M_B\text{+}M_A)$ is the normalized molecular mass disparity, and

$$C = 1.45[\varepsilon_{BA}/k_B - 85], \quad (7)$$

For the cases considered here, $C/T \ll 1$ and thus the temperature correction is unimportant. Four computational cases were used to examine the impact of updated binary diffusion coefficients on non-premixed flame extinction of *n*-$C_{10}H_{22}$ and *n*-$C_{12}H_{26}$. They are summarized in Table 7.1. While Cases I and II test the predictions of K_{ext} using the old diffusion coefficient estimates [12] from the law of corresponding state with the purpose of comparing the impact of the Soret effect, Cases III and IV test the updated diffusion coefficients.

Table 7.1. Summary of computational cases.

Case	Source of parameters	Formulation	Soret effect
I	JetSurF [12][a]	Multicomponent	Yes
II	JetSurF [12][a]	Multicomponent	No
III	This work	Mixture averaged	Yes[b]
IV	This work	Multicomponent	Yes

[a] Estimated using the law of corresponding state [13, 14].

[b] Using the thermal diffusion ratio of Rosner et al. (eq. 6) [39].

7.4 Results and Discussion

Figure 7.1 shows the computed K_{ext} compared to the experimental data collected in the current work from counterflow non-premixed flames of *n*-$C_{12}H_{26}$ in N_2 at 473 K against O_2 at 300 K over a range of fuel to N_2 mass ratio. The effective potential parameters are summarized in Table 7.2. Cases I and II both use the diffusion coefficient estimates from the law of corresponding state. These estimates are shown to grossly overpredict K_{ext}. Comparing the Cases I and II, we see that K_{ext} becomes lower with the Soret effect considered. As the fuel is transported to the mixing zone by molecular diffusion, it encounters an upward temperature, which by thermal diffusion pushes it back towards the colder fuel/N_2 jet. Thus, the Soret effect reduces the rate at which the fuel

can be transported into the mixing zone and makes the flame more readily to undergo extinction.

Table 7.2. Effective LJ-12-6 potential parameters of n-alkane-N2 interactions for calculating the binary diffusion coefficients of n-alkane in N2.

Species	σ (Å)	ε/k_B (K)[a]
n-butane	4.749	101.6
n-pentane	5.086	107.2
n-hexane	5.437	106.8
n-heptane	5.744	111.7
n-octane	6.106	104.2
n-nonane	6.415	103.6
n-decane	6.683	107.8
n-undecane	6.994	103.4
n-dodecane	7.222	109.8

[a] An average value of 106 K may be used for all species considered.

The updated diffusion coefficients of *n*-$C_{12}H_{26}$ in N_2 lead to significantly better predictions for K_{ext} (Cases III and IV), as seen in Fig. 7.1. As Table 7.1 shows, there are

two differences between the two cases. Case III uses the mixture-averaged transport formula with Rosner's approximate thermal diffusion ratio; Case IV employs multicomponent transport formulation with a more exact thermal diffusion ratio [20]. Interestingly, the computed K_{ext} values do not differ significantly, suggesting that the mixture-averaged formation is adequate at least for the conditions of the present study. Similar comparisons may be made using the K_{ext} data of Ji et al. [10] for both *n*-$C_{12}H_{26}$ and *n*-$C_{10}H_{22}$. As Fig. 7.2 shows the updated diffusion coefficients yield predicted K_{ext} values much closer to the experimental data, whether one uses the mixture-averaged or multicomponent transport. These results indicate that accurate diffusion coefficients of large fuel molecules and the Soret effect are both important elements towards a satisfactory prediction of flame properties that are governed by diffusion-kinetic coupling.

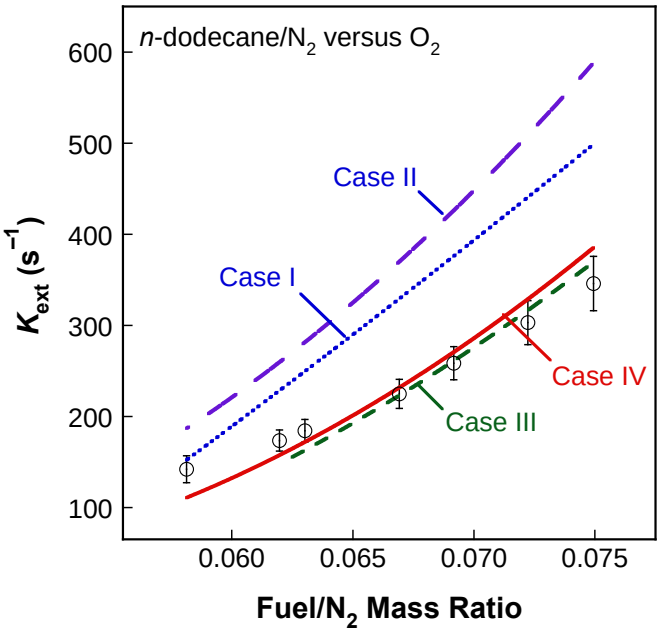

Figure 7.1. Extinction strain rate of non-premixed n-$C_{12}H_{26}/N_2$-O_2 flames (T_u = 473 K for the fuel jet and 300 K for the oxygen jet) with p = 1 atm. Symbols: experimental data (this work); lines are simulations (see Table 7.1).

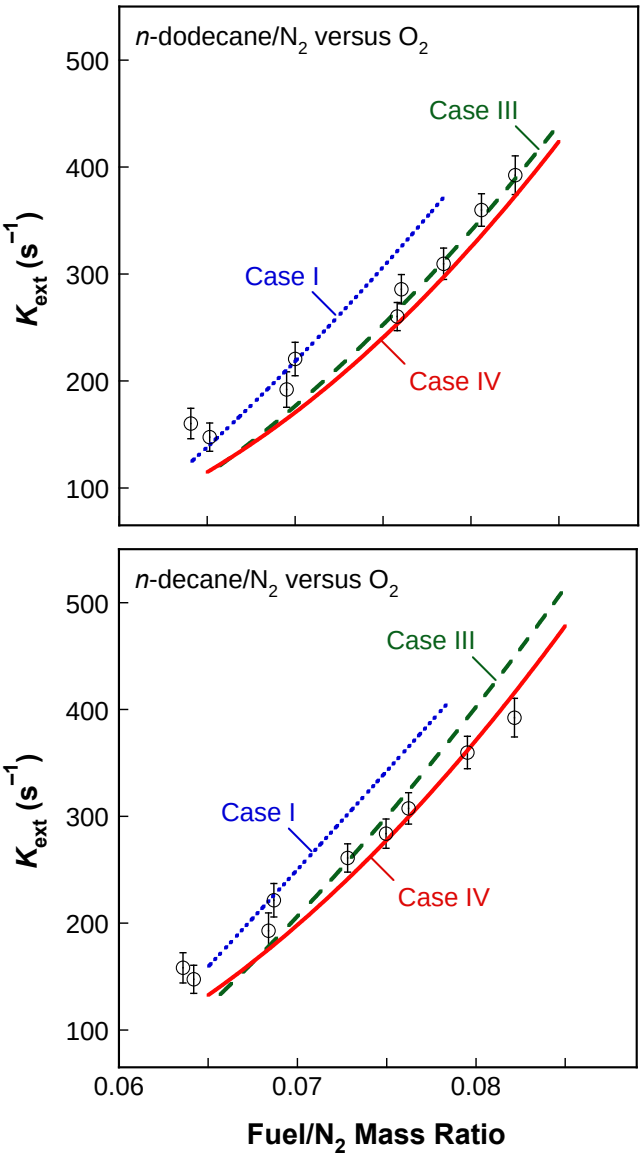

Figure 7.2. Extinction strain rate of non-premixed n-$C_{12}H_{26}/N_2$-O_2 flames and n-$C_{10}H_{22}/N_2$-O_2 flames all at T_u = 403 K for the fuel jet and 300 K for the oxygen jet, with p = 1 atm. Experimental data (symbols) were taken from Ref. [10]; lines are simulations (see Table 7.1).

To amplify the above point, we plot in Fig. 7.3 the structures of the near extinction flames of *n*-dodecane/N_2 (473 K) versus O_2 (300 K), computed for Case III and IV. Except for the shift in the stagnation surface marked by the vertical dashed-dotted-dashed lines, the two structures are nearly the same. The fuel is transported to the mixing layer by diffusion and is decomposed to a small number of key intermediates, including ethylene, methane, propene, 1,3-butadiene, and hydrogen. The concentrations of these intermediates reach their respective peaks when the concentration of *n*-$C_{12}H_{26}$ drops to a negligible level. The oxidation of the intermediates follows and the concentrations of the intermediates drop rapidly as they enter into the region where the H atom peaks in its concentration. The molecular diffusion process of the fuel enables the delivery of the fuel into the thermal mixing layer, allowing it to undergo pyrolytic reactions, replacing the fuel by the key intermediates just discussed.

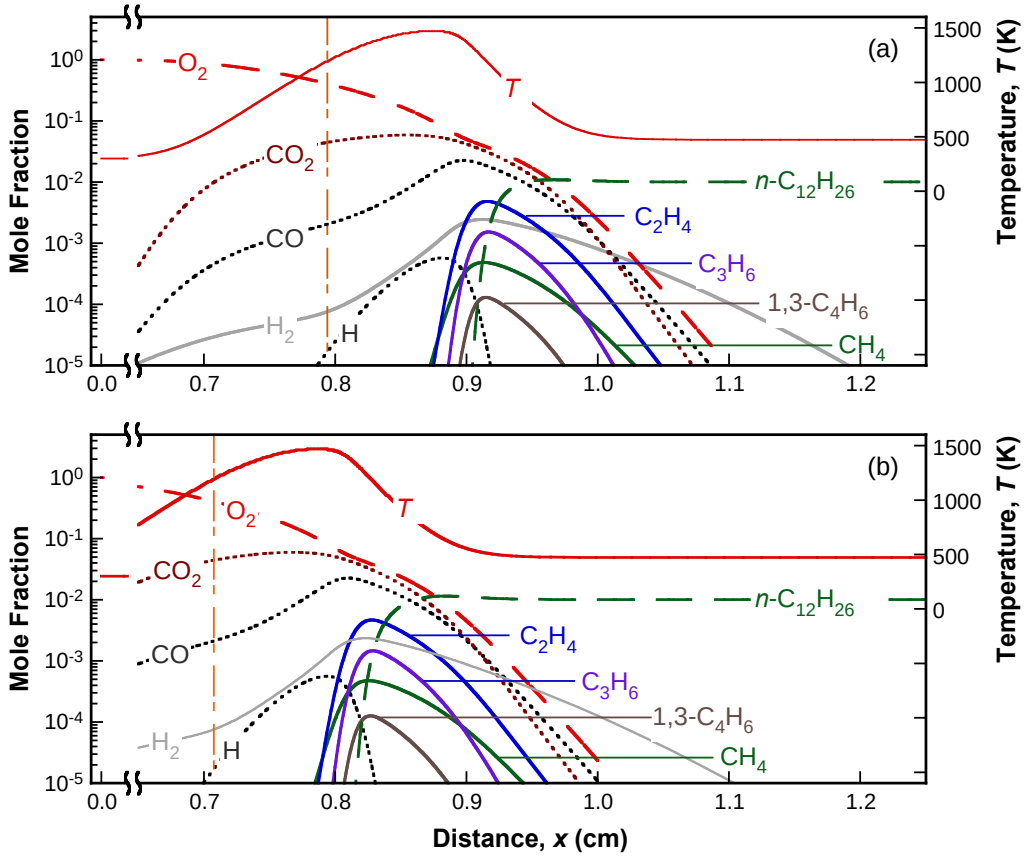

Figure 7.3. Structures of *n*-dodecane/N_2 (473 K) versus O_2 (300 K) near extinction flames computed for (a) Case IV (full multicomponent and thermal diffusion transport with updated diffusion coefficients) and (b) Case III (mixture averaged transport with the thermal diffusion ratio of Rosner et al. [39]). The vertical dashed-dotted-dashed line indicates the position of the stagnation surface.

7.5 Concluding Remarks

The gas-phase binary diffusion coefficient of *n*-alkane in nitrogen is studied using gas-kinetic theory analysis. Effective Lennard-Jones 12-6 potential parameters are

proposed for *n*-butane through *n*-dodecane in nitrogen. It is shown that the updated diffusion coefficients resolve the earlier difficulty of predicting the extinction strain rate of non-premixed counterflow flames of *n*-dodecane/N_2 and *n*-decane/N_2 against O_2. The ability of the generalized transport theory for cylindrical structures in dilute gases to reconcile a wide range of binary diffusion coefficient data and to predict the flame extinction data suggests that the theory is valid for the diffusion coefficients of long-chain molecules. It is also shown that the mixture-average transport formulation is adequate for predictions of the extinction strain rate, provided that the Soret effect is taken into consideration.

7.6 References

1. C. K. Law, Combustion physics, Cambridge university press, 2006.
2. M. Colket, T. Edwards, S. Williams, N. P. Cernansky, D. L. Miller, F. Egolfopoulos, P. Lindstedt, K. Seshadri, F. L. Dryer, C. K. Law, *Development of an experimental database and kinetic models for surrogate jet fuels*, 45th AIAA Aerospace Sciences Meeting and Exhibit, 2007; Reno, Nevada, 2007; paper no. AIAA-2007-0770.
3. S. H. Won, S. Dooley, F. L. Dryer, Y. Ju, Combust. Flame 159 (2012) 541-551.
4. S. Dooley, S. H. Won, M. Chaos, J. Heyne, Y. Ju, F. L. Dryer, K. Kumar, C.-J. Sung, H. Wang, M. A. Oehlschlaeger, Combust. Flame 157 (2010) 2333-2339.
5. S. H. Won, W. Sun, Y. Ju, Combust. Flame 157 (2010) 411-420.

6. K. Seshadri, T. Lu, O. Herbinet, S. Humer, U. Niemann, W. J. Pitz, R. Seiser, C. K. Law, Proc. Combust. Inst. 32 (2009) 1067-1074.

7. S. Honnet, K. Seshadri, U. Niemann, N. Peters, Proc. Combust. Inst. 32 (2009) 485-492.

8. A. Holley, X. You, E. Dames, H. Wang, F. Egolfopoulos, Proc. Combust. Inst. 32 (2009) 1157-1163.

9. A. Holley, Y. Dong, M. Andac, F. Egolfopoulos, T. Edwards, Proc. Combust. Inst. 31 (2007) 1205-1213.

10. C. Ji, Y. L. Wang, F. N. Egolfopoulos, J. Propul. Power 27 (2011) 856-863.

11. B. Li, Y. Zhang, H. Zhang, F. N. Egolfopoulos, Proc. Combust. Inst. 35 (2015) 965-972.

12. B. Sirjean, E. Dames, D. Sheen, X. You, C. Sung, A. Holley, F. Egolfopoulos, H. Wang, S. Vasu, D. Davidson A high-temperature chemical kinetic model of n-alkane oxidation. 2009, http://web.stanford.edu/group/haiwanglab/JetSurF/JetSurF1.0/index.html

13. L. S. Tee, S. Gotoh, W. E. Stewart, Ind. Eng. Chem. Fundmen. 5 (1966) 356-363.

14. H. Wang, M. Frenklach, Combust. Flame 96 (1994) 163-170.

15. A. W. Jasper, E. Kamarchik, J. A. Miller, S. J. Klippenstein, J. Chem. Phys. 141 (2014) 124313.

16. A. W. Jasper, J. A. Miller, Combust. Flame 161 (2014) 101-110.

17. C. Liu, Z. G. Li, H. Wang, Phys. Rev. E submitted (2015).

18. W. S. McGivern, J. A. Manion, Combust. Flame 159 (2012) 3021-3026.

19. J. A. Manion, W. S. McGivern, *Direct measurements of binary gas phase diffusion coefficients for Combustion Applications*, Argonne National Laboratory, Darien, IL, 2011,

20. J. O. Hirschfelder, C. F. Curtiss, R. B. Bird, M. G. Mayer, Molecular theory of gases and liquids, Wiley, New York, 1954.

21. R. C. Reid, J. M. Prausnitz, B. E. Poling, The properties of gases and liquids, McGraw-Hill, New York, 1987.

22. R. Trengove, H. Robjohns, P. J. Dunlop, Ber. Bunsen. Phys. Chem. 86 (1982) 951-955.

23. K. Chae, P. Elvati, A. Violi, J. Phys. Chem. B 115 (2010) 500-506.

24. A. Einstein, Ann. Phys. 17 (1905) 549.

25. Z. Li, H. Wang, Phys. Rev. E 68 (2003) 061206.

26. Z. Li, H. Wang, Phys. Rev. E 68 (2003) 061207.

27. C. Liu, H. Wang, J. Chem. Phys. Manuscript in preparation (2015).

28. A. Boushehri, J. Bzowski, J. Kestin, E. Mason, J. Phys. Chem. Ref. Data 16 (1987) 445-466.

29. C. Wu, C. Law, Symp. Int. Combust. 20 (1985) 1941-1949.

30. D. Zhu, F. Egolfopoulos, C. Law, Symp. Int. Combust. 22 (1989) 1537-1545.

31. C. Ji, E. Dames, Y. L. Wang, H. Wang, F. N. Egolfopoulos, Combust. Flame 157 (2010) 277-287.

32. F. N. Egolfopoulos, C. S. Campbell, J. Fluid Mech. 318 (1996) 1-29.

33. R. J. Kee, J. A. Miller, G. H. Evans, G. Dixon-Lewis, Symp. Int. Combust. 22 (1989) 1479-1494.

34. F. Egolfopoulos, Symp. Int. Combust. 25 (1994) 1375-1381.

35. M. Nishioka, C. Law, T. Takeno, Combust. Flame 104 (1996) 328-342.

36. F. N. Egolfopoulos, P. E. Dimotakis, Symp. Int. Combust. 27 (1998) 641-648.

37. R. J. Kee, G. Dixon-Lewis, J. Warnatz, M. E. Coltrin, J. A. Miller, A Fortran computer code package for the evaluation of gas-phase, multicomponent transport properties, Livermore, CA, 1986.

38. Y. Dong, A. T. Holley, M. G. Andac, F. N. Egolfopoulos, S. G. Davis, P. Middha, H. Wang, Combust. Flame 142 (2005) 374-387.

39. D. Rosner, R. Israel, B. La Mantia, Combust. Flame 123 (2000) 547-560.

Chapter 8: Determination of Laminar Flame Speeds Using Axisymmetric Bunsen Flames: Intricacies and Accuracy

8.1 Introduction

Combustion of fossil fuels has been a significant driver in accelerating industrial and economic development for more than a century [1,2]. This was accompanied by an attendant increase in fundamental understanding of the combustion processes through identification of parameters controlling the combustion phenomena and formulating a basic combustion theory [3-8]. From the early treatment of combustion problems [9-11], laminar flames were recognized as an important ingredient in developing combustion theories and models for a wide range of practical applications.

The significance of determining the laminar flame combustion parameters for the design and optimization of energy production systems has lead to the development of a series of experimental flame configurations such as the Bunsen flame [12-16], the counter-flow flames [17-19], the stagnation flame [20-22], and the spherically expanding flame [19,23-26]. The exploitation of these experimental tools primarily offers a viable means of estimating fundamental combustion properties such as ignition characteristics, laminar flame speeds, strain sensitivity and extinction strain rates [26,27].

The laminar flame speed (S_u^o) is the one of the most important, observable, traditional target parameter. Data acquired for laminar flame speed plays a significant role in developing kinetic models and is used in the prediction of critical combustor design parameters such as flashback and blow-off [26-29]. It also serves as a scaling parameter in turbulent combustion [2,30,31].

Amongst the various laminar flame configurations, the Bunsen flame is historically the oldest [12,32-34], the simplest, and the most popular one, exploited from the very early days of combustion analyses. Since then this configuration has been widely accepted as a suitable test bed for the investigation and testing of a range of combustion theories and characteristics [2,3,11,13,32,33,35-61]. Since its initial introduction, the Bunsen flame technique has significantly evolved to current day maturity benefitting from continuous developments in flame measuring techniques [14,16,25,27,44,47,49,56,61-67], burner operation control and regulation methodologies [6,22,26,27,43,49,51,62,63,65,66,68] and impressive advances in laminar flame simulation techniques [29,64,69,70-72]. Nevertheless, uncertainties still remain regarding the control of its operating parameters, the optimum experimental methodologies and the interpretation of the experimental results [22,27,38,40,41,46,48,53,59]. The difficulty in interpretation of the experimental results stems primarily from the uncertainties involved in estimation of flame speed using the flame surface area or the flame angle methods.

Recently, renewed interest has emerged in the technique due to its amenability and suitability in quantifying, in a straightforward manner, S_u^o's of a multiplicity of fuel blends, over a wide range of conditions [16,27,55-58,60,61], as mandated by the urgent need for advanced low emission new combustor concepts. As a consequence, the exploitation of a simplified experimental methodology, whereby the reliability of the results could be verified or systematically adjusted by accompanying direct numerical simulations (DNS), would be an attractive and cost effective procedure under conditions of routine S_u^o evaluations in laboratory and industrial level. This particular approach of

utilizing DNS to correct for non-idealities in combustion measurements has found success in cases such as improving the quality of extrapolation techniques to obtain flame speed using counter-flow flames [73], and elucidating probe effects in sampling low-pressure flames [74].

In the present work, a parametric study was carried out on the effect of a series of parameters on the S_u^o acquisition uncertainty for methane (CH_4) and propane (C_3H_8) flames. With the advent of DNS the experimental results from the Bunsen cone technique can now be more systematically verified/validated by concomitant computational results. The aim here is to measure the Bunsen cone laminar flame characteristics with a low cost/minimal involvement methodology and then correlate their departure from the "target" values with the help of the DNS results. This could allow the deduction of suitable correction factors, which would systematically incorporate the uncertainties involved in the described routine experimental campaign. This procedure could lead to an easy-to-validate method for measuring S_u^o using the Bunsen flame method.

8.2 Experimental Approach

Experiments were completed by collaborators from University of Patras, Laoratory of Applied Thermodynamics, the detail description of the experimental setup can be found elsewhere [76]. In short, flames with low and high Re were measured to allow for an evaluation of the effect of Re on the flame speed measurement methods. To vary Re, the inlet mixture velocity of the measured Bunsen flames was a set as a multiple of the expected unburned laminar flame speed at each equivalence ratio. For CH_4, reactant

velocities investigated at different equivalence ratios were $3.5*S_u^o$, $4*S_u^o$, $4.5*S_u^o$. Bunsen flames were also stabilized and measurable at inlet mixture reactant velocities as low as $3*S_u^o$. The investigated ϕ's for CH_4 ranged from about Φ=0.8 (the blow off limit for all air inlet conditions) up to 1.5. Stable and measurable flames were stabilized between Φ=0.85 and 1.2 which had well defined and symmetric cone characteristics. Tip flickering was observed but not as significant as that observed in propane flames. At lower reactant velocities (e.g. below $3*S_u^o$) intense curvature and low cone height were the main characteristics of the flames especially due to the nozzle exit boundary layer. Above Φ=1 a diffusion flame envelope was seen to develop. Above 1.2 intense flickering and curvature of the flame tip but no tip opening was identified up to Φ=1.5, as also observed in [75]. A lean CH_4/air flame is also expected to exhibit tip opening, but this phenomenon could not be observed in the present experimental configuration, presumably because the range of equivalence ratios were limited to 0.85 for successful flame stabilization (e.g. [76]).

For C_3H_8, reactant velocities investigated at different ϕ's were $3*S_u^o$, $3.5*S_u^o$, $4*S_u^o$. Bunsen flames were also stabilized and measurable at $2.5*S_u^o$. The investigated ϕ's range from about Φ=0.82 (the blow off limit for all air inlet conditions) up to 1.5. Stable and measurable flames were stabilized between Φ=0.85 and 1.2. The selected flames had well defined and symmetric cone characteristics, although an imperceptible tip flickering was also observed more than that for the CH_4 flames. At lower reactant velocities (below

2.5*S_u^o) intense curvature and low flame cone heights were the main characteristics of the flames mainly due to the thickness of the boundary layer at the nozzle exit. Also above Φ=1 the diffusion envelope was formed and its intensity increased in proportion to the equivalence ratio. Above Φ=1.2 intense flickering and curvature of the flame tip were observed and at Φ between 1.4 and 1.45 the flame tip opened and was rather insensitive to any further variation of the velocity of the reactants, as also reported in literature (e.g. [75], [77]), rendering these flames rather inappropriate for laminar flame speed estimation.

Two well-established techniques were employed to determine the flame speed (S_u) from the images; the term S_u^o is reserved for the true laminar flame speed. The first one is using the angle of the flame image and the velocity of the reactants and the second involves the flame front area and the volumetric flow rate of the reactants. Once the targeted flame is stabilized on the nozzle rim, digital camera images (Shutter speed: 1/25, Aperture: F5.6 ISO 800) were taken to determine the flame front angle and cone surface area. The velocity of the reactants was determined from the mass flow rate of the used mixture and the nozzle diameter. Flame speeds were then calculated from direct flame photographs using the cone angle method. S_u is then determined from the knowledge of the fuel-air mixture nozzle exit velocity (U_e) and the angle (α) of the flame front with respect to the vertical axis (Both the bulk value, U_b, i.e. mass-weighted average velocity and the value corresponding to the flat portion of the exit profile, U_p, were used in place of U_e). The flame speed is then given as:

$$S_u = U_e * \sin(\alpha) \quad (1)$$

Flames with low and high Re were evaluated using the cone surface area and the flame front angle techniques to establish accuracy of each method as a function of Re. As Cadwell et al. [78] have shown, the uniform velocity across the nozzle tends to revert to a parabolic velocity distribution over a comparatively short distance downstream of the exit plane. Also Johnston [79] found that the measured burning velocity decreased as the flow rate increased introducing yet another uncertainty in the cone angle method for tall Bunsen flames. Thus it was concluded that the use of high flow rates with their associated taller cones should better be avoided when the cone angle method is employed. At higher reactant velocities (High Re) the cone area method is considered suitable in achieving a more sharply defined surface area at the rim and the apex and therefore is conducive to a more accurate estimation of the cone area. However in this technique the round vertex of the cone and the curvature near the burner rim are two effects with strongly changing curvature that introduce an additional source of inaccuracy as mentioned by Andrews and Bradley [80]. The inner edge was used in the cone area method and as Fristrom [81] has shown this inner region of the luminous zone represents the best location to measure gas velocities and areas for these curved flames. Taking into account the merits and drawbacks of each method both techniques were exploited to illustrate the limitations of each methodology.

The volumetric flow rates (Q) of the C_3H_8/air and CH_4/air mixtures were acquired by using calibrated sonic nozzles with Omega® pressure regulators with an accuracy of

±0.5%. S_u was then deduced from the division of the volumetric flow rate of the reactants by the area of the flame cone.

$$S_u = Q/A_b \quad (2)$$

8.3 Numerical Approach

Complementing the experiments, direct numerical simulations (DNS) are carried out which involve the solution of the full set of conservation equations of mass, momentum, species, and energy along with reaction chemistry as specified by a chemical mechanism for the fuel-air mixture [82]. Radiation heat loss is incorporated using an optically thin radiation model with the significant radiating species considered being H_2O, CO, CO_2, and CH_4.

Two kinetic models were used in this work, one for CH_4/air and another for C_3H_8/air mixtures. They are both derived from the USC Mech II kinetic model [83], which consists of 111 species and 784 elementary reactions. The full model is reduced using DRG [84] to a 35 species, 226 reaction model for CH_4/air mixtures and a 44 species, 342 reaction model for C_3H_8/air mixtures. Both models incorporate chemistry for excited species: CH^* [85], OH^* [85], and CO_2^* [86]. The excited state species were used to track the flame surface consistent with experiments that use total luminescence to track the flame surface. Figure 8.1 shows comparisons between S_u^o's computed from the reduced models along with those predicted by the full USC Mech II model using the PREMIX code [87]. The results are in good agreement over the range of ϕ's studied in this work.

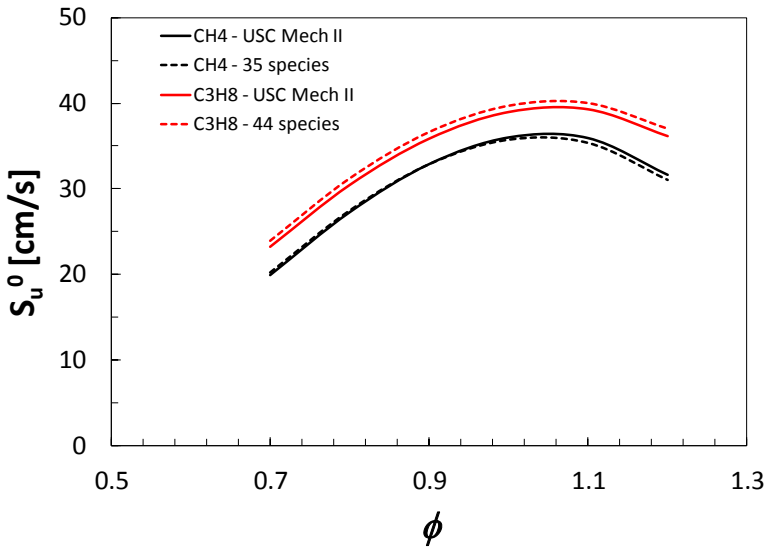

Figure 8.1. S_u^o's as a function of ϕ as obtained from the full USC Mech II kinetic model and the reduced models derived for CH_4 and C_3H_8.

The numerical simulations are carried out using laminarSMOKE [82], which is an open-source computational framework for modeling steady and unsteady reacting flow configurations. laminarSMOKE is built on the framework of OpenFOAM [88] which is an open-source finite-volume CFD code. A time-splitting technique is used in laminarSMOKE to handle the stiffly-coupled energy and species transport equations [82]. The continuity and momentum equations are handled in a segregated manner using a PISO algorithm [89]. The code is highly parallelized with inter-processor communication being handled by MPI protocols.

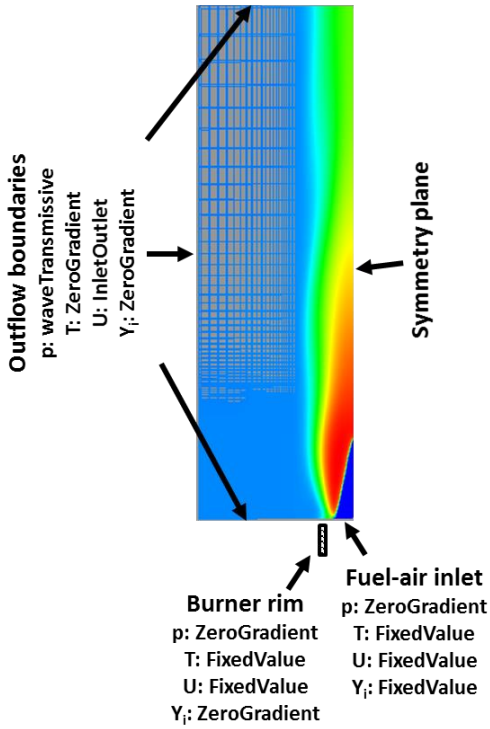

Figure 8.2. Computational grid used in the numerical simulations overlaid with boundary conditions applied for pressure, temperature, velocity, and chemical species.

An axisymmetric grid as shown in Fig. 8.2, with a radius of 6 cm and height of 20 cm is used in the numerical simulations. The approximate flame height and thickness are estimated using the 1-D calculations. The initial grid is constructed to be uniform in the area where the flame is expected to reside. The grid spacing in this region is set to be about 3 cells per flame thickness. A stretched non-uniform grid is utilized outside of this refined area. An initial non-reacting flow-field is established following which the mixture is ignited and the simulation is carried on until a steady-state solution for the flame is reached. Steady-state is established by ensuring that residuals for pressure, temperature, and velocity have reached a constant value. Further, the flame position and height are

observed to be constant. At this point, an adaptive mesh refinement is performed at the flame front to increase the grid resolution in that location. The location of the flame front is determined by computing the gradient and curvature of the temperature field. The simulation results from steady state are mapped on to the refined grid and computations are performed till a new steady state is achieved. This sequence of steps is carried out repeatedly till a highly refined flame region is established with an average of 70-80 cells through the flame thickness for each condition investigated. This level of refinement is considered adequate for the laminar conditions investigated in this work. Figure 8.3 shows a plot of temperature as a function of distance along a 1-D cut through the flame for a CH_4-air mixture with ϕ=0.80 at the high Re condition. The data points in Fig. 8.3 correspond to individual grid points illustrating the refinement achieved in the solution through the flame thickness.

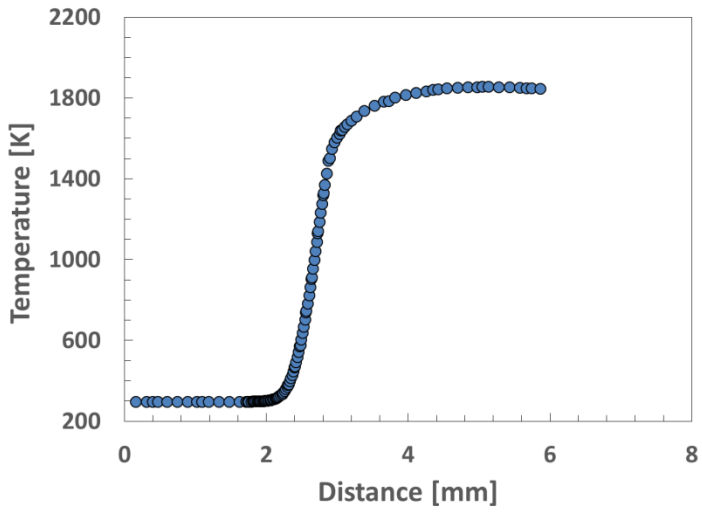

Figure 8.3. Temperature as a function of distance along a 1-D cut through the flame front for a CH_4/air mixture with ϕ=0.80 at the high Re condition.

Figure 8.2 also shows the boundary conditions used in the numerical simulations. The inlet velocity profile is specified according to the one measured in the experiments. A fixed temperature of 298 K is also specified at the inlet along with species mass fractions corresponding to the fuel-air equivalence ratio. The nozzle wall temperature is also set to 298 K following experimental observations. No species diffusion is allowed into the walls which are also assigned no-slip boundary conditions. Far-field boundary conditions are implemented at the outflow boundaries using the waveTransmissive and InletOutlet boundary conditions for pressure and velocity respectively.

Similarly to the experiments, numerical simulations were carried out to obtain highly resolved flame fronts for CH_4/air and C_3H_8/air mixtures at five different ϕ's (0.8, 0.9, 1.0, 1.1, and 1.2) for two different inlet Re. In estimating S_u, both the angle and area methods are utilized as in the experiments. For the angle method, the cone angle is estimated using the healthy region of the flame surface away from the tip and burner rim. For the area method, an iso-surface of total luminescence ($CH^*+OH^*+CO_2^*$) is estimated.
Similar to the experiments, the inner edge of the cone is utilized in the area method. A curve is fit to the iso-surface and utilized to extrude a 3-D conical surface using CAD software (SolidWorks). The area of the surface is estimated using the same software. Equations 1 and 2 were then utilized to obtain S_u.

8.4 Results and Discussion

Experimental and numerical results were obtained for CH_4/air and C_3H_8/air mixtures at 1 atm and 298 K for a variety of ϕ's at the medium and high Re inlet conditions. To eliminate any confusion, the different inlet Re cases will be referred to as low and high

Re inlet conditions. We analyze the results in three parts. First, non-idealities introduced into the measurement technique due to effects such as the inlet boundary layer, extinction at the burner rim, strain and curvature effects, etc. are studied using numerical simulations which allow for systematically isolating these effects. The effect of these non-idealities as they pertain to errors introduced in the interpretation methods, viz. the angle and area methods to estimate S_u are studied using experimental and simulation results. Next, the complete set of results from the parametric analysis for CH_4/air and C_3H_8/air mixtures from experiments and simulations with varying ϕ and inlet Re are presented. Finally, we try to estimate correction factors for the experimental and computed S_u based on known values of S_u^o.

8.4.1 Non-ideal effects in Bunsen flames

i) Effect of boundary layer

In the experiments, a contoured nozzle is used to minimize the effect of boundary layers and produce an almost top-hat velocity profile. However, a finite boundary layer always develops whose thickness decreases with increasing inlet velocity. The presence of a boundary layer has been known to affect measurements that utilize an angle method to estimate S_u[16]. Using the numerical simulations we attempt to understand the effect of the boundary layer.

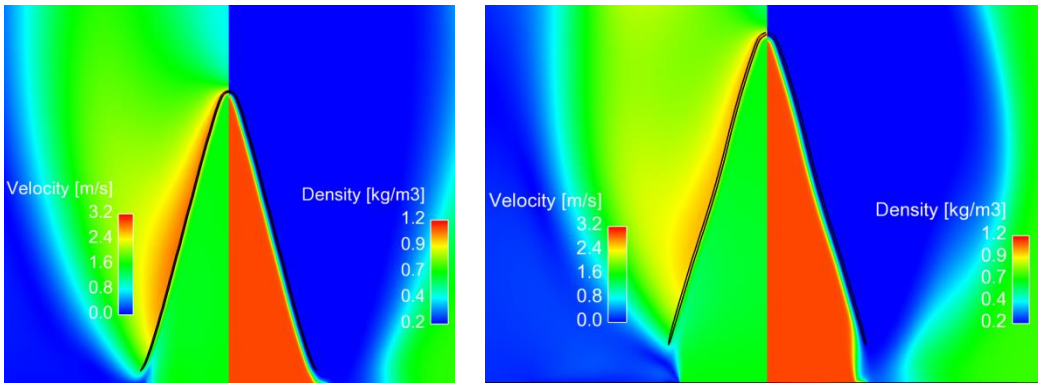

Figure 8.4. Iso-contours of velocity (*left*) and density (*right*) for a CH_4/air flame at ϕ=1.0 with a high Re at the inlet for a) case with an inlet boundary layer and b) case without an inlet boundary layer. The black iso-surface represents the location of the flame front.

Numerical simulations were carried out for CH_4/air and C_3H_8/air mixtures at ϕ=1 for the medium and high Re condition. In each case, the simulation is carried out using the experimentally measured velocity profile with the boundary layer and with a top-hat uniform velocity profile. The velocity used for the top-hat profile is equal to the velocity in the flat region for the profile with a boundary layer causing it to have a higher net flow rate. Figure 8.4 shows results for the CH4/air cases at ϕ=1.0 using the high Re inlet condition with and without an inlet boundary layer. Velocity iso-contours are plotted on the left and density iso-contours on the right. The flame location is indicated by a black line corresponding to an iso-surface of the total luminescence. One of the effects of removing the inlet boundary layer appears to be that the flame is lifted higher away from the burner rim. The flame is still stabilized by heat loss to the burner rim but is lifted up due to the finite velocity at the burner rim. A benefit of this is that the curvature in the flame surface near the rim as observed for the case with the boundary layer is absent for

the case without the boundary layer. The edges of the cone formed by the flame surface are hence almost exactly straight.

The simulations are carried out till steady state and the flame surface is identified. Next, S_u is estimated using the angle method and the flame surface in the "healthy" region, i.e., far from the tip and the extinguished region close to the burner rim. Table 8.1 shows the results of this analysis. In each case, S_u can be estimated using the velocity corresponding to the flat section (U_p) or the bulk velocity (U_b) as mentioned in Section 2. For the cases with no boundary layer, U_p and U_b are essentially the same. The percentages in brackets give the corresponding differences from S_u^o. At low and high Re, the cases without boundary layer have less difference from S_u^o as compared to the cases with boundary layer. However, at high Re, the differences are comparable to each other due to decrease in the thickness of the boundary layer. Using U_b to compute S_u under predicts the known values of S_u^o for the cases with a boundary layer. Overall, with or without boundary layers, the error in S_u computed using U_p or U_b seems to be significant (4-20%), with the error being generally higher in the presence of a boundary layer at the inlet. The lowest error is obtained for the case with high Re and no boundary layer at the inlet.

Table 8.1. S_u calculations using simulation results with and without the presence of boundary layer in the inlet velocity profile for a CH_4/air flame at ϕ=1.0. The values in the brackets indicate the percentage difference for each S_u from S_u^0.

		U_p (m/s)	U_b (m/s)	α (deg)	S_u (m/s)		S_u^0 (m/s)
					Using U_p	Using U_b	
Low Re	With BL	1.125	0.884	21.51	0.412 (+15%)	0.324 (-10%)	0.359
	No BL	1.125	1.125	21.75	0.416 (+16%)	0.416 (+16%)	0.359
High Re	With BL	1.58	1.27	14.79	0.403 (+12%)	0.324 (-10%)	0.359
	No BL	1.58	1.58	15.78	0.430 (+20%)	0.430 (+20%)	0.359

ii) Pressure induced velocity changes

Figure 8.5 shows simulation results for a CH4/air flame at ϕ=1.0 for the high and low Re cases. Iso-contours of pressure are plotted on the left while those for radial velocity are plotted on the right. The radial velocity is expressed as a percentage value of the inlet velocity. The black line corresponds to an iso-surface of the total luminescence and denotes the flame surface. The figure shows that a small but finite pressure jump exists across the flame. The radial velocity iso-contours shows a small region near the bottom of the flame close to the burner rim where its magnitude rises to about 10-20% of the inlet velocity. This is driven by the pressure jump across the flame and the region of local extinction near the burner rim which causes some flow of unburned gas from the core to flow out without passing through the flame surface.

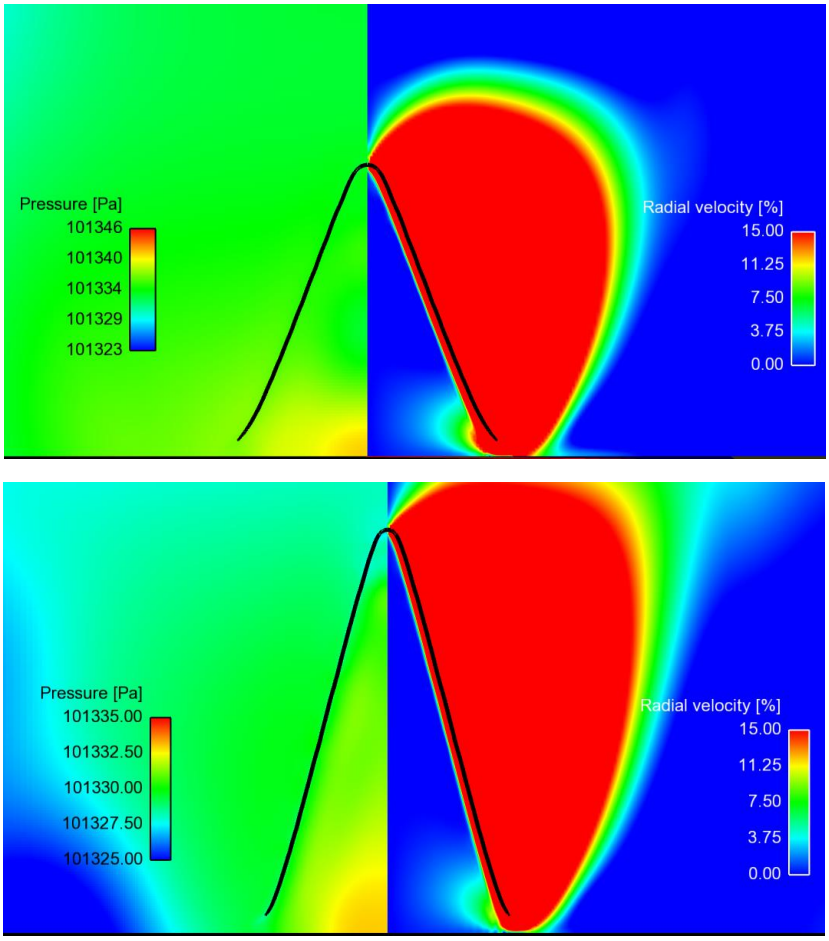

Figure 8.5. Iso-contours of pressure (*up*) and radial velocity (*down*) for a CH_4/air flame at ϕ=1.0 for a) high Re case and b) low Re case. Radial velocity is expressed as a percentage of the inlet velocity.

This has an implication on the region of the flame surface used in the angle method. Care must be taken to ensure that the "healthy" flame surface used to estimate the angle should not include any region where this pressure induced radial velocity exists. This further implies that while using the flame angle method, it is preferable to have a taller flame using a higher inlet Re so as to increase the length of the "healthy" surface that can be used to determine the flame angle.

iii) Tip curvature effects

The curved tip of the Bunsen flame has been the subject of research in several previous works [84, 90]. In utilizing the flame angle method for estimating S_u, the curvature at the tip can affect the "healthy" region of the flame used to determine the flame angle. In this respect, it is desired to avoid the flame tip region altogether in determining the flame angle. Figure 8.6 shows iso-surfaces of velocity overlaid on iso-contours of temperature a CH_4/air and a C_3H_8/air flame at ϕ=1.0 for the high inlet Re case. As long as the flame surface utilized for the angle calculation lies outside of the region where the velocity iso-surfaces start to bend towards each other and stop being parallel to one another, the angle method should remain unaffected by the flame tip.

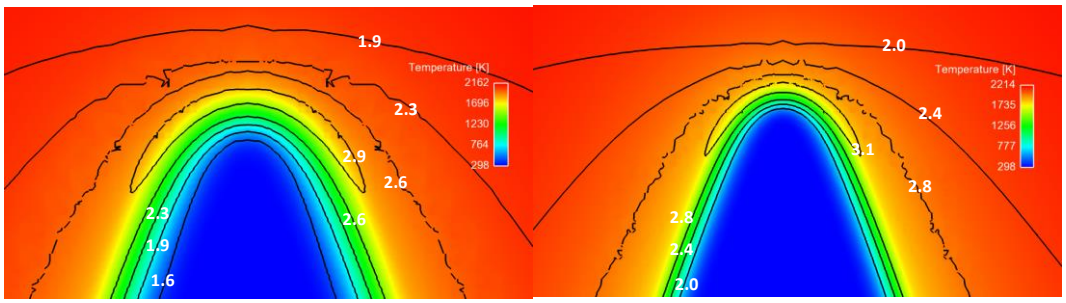

Figure 8.6. Iso-surfaces of velocity overlaid on iso-contours of temperature for a) CH_4/air flame at ϕ=1.0 for high Re case and b) C_3H_8/air flame at ϕ=1.0 for high Re case. Velocity values for iso-surfaces are in units of m/s.

iv) Flame surface identification

It is worthy to consider the location of the flame surface as determined from the luminescence with respect to temperature iso-surfaces as determined from the simulation.

This information is provided in Fig. 8.7 where iso-surfaces of temperature are overlaid on iso-contours of density for a CH_4/air flame at ϕ=1.0 for high Re case. The flame surface as determined by an iso-surface of total luminescence is shown by a black line. It can be noted from the figure that the flame surface determined by total luminescence corresponds to a temperature iso-surface of about 1800 K. The value of luminescence used to locate the flame surface is half the maximum value in the domain. Following the discussion presented by Bradley [80] and Santoro [16], the appropriate flame area to be deduced for use in Eq. 2 is that corresponding to the unburned gases just before reactant pre-heating. This area is unavailable in the experimental measurements but can be obtained using the numerical simulations. Estimates for S_u were obtained using different temperature iso-surfaces and compared to the one obtained using the total luminescence. These results are presented in Fig.8.8. S_u^o for this case is estimated as 35.97 cm/s using PREMIX calculations. As seen from Fig. 8.8, the temperature iso-surfaces tend to overestimate S_u^o.

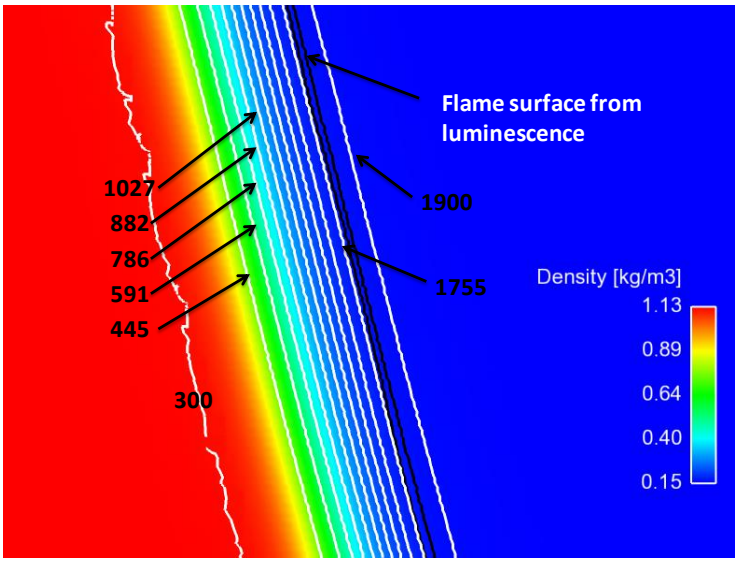

Figure 8.7. Iso-surfaces of temperature overlaid on iso-contours of density for a CH_4/air flame at ϕ=1.0 for high Re case.

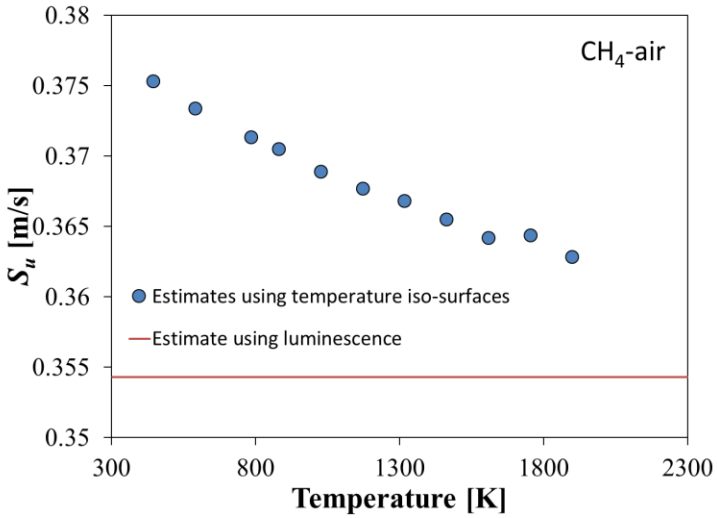

Figure 8.8. S_u estimates using different temperature iso-surfaces for a CH_4/air flame at ϕ=1.0 for high Re case. S_u estimated using the luminescence iso-surface is also presented for the same case.

v) Extinction at the burner rim

Figure 8.9 shows simulation results obtained for a CH_4/air flame at ϕ=1.0 for a high Re case. Fluid flow paths are highlighted by streamlines colored by velocity magnitude. The plot shows iso-contours of heat release rate. As can be seen from Fig. 8.9(a), the flame is extinguished near the burner rim due to heat loss to the constant temperature wall. A similar effect is observed in the experimental result for a CH_4/air flame presented in Fig. 8.9 (b). This poses a problem in utilizing the flame surface area method to determine flame speed.

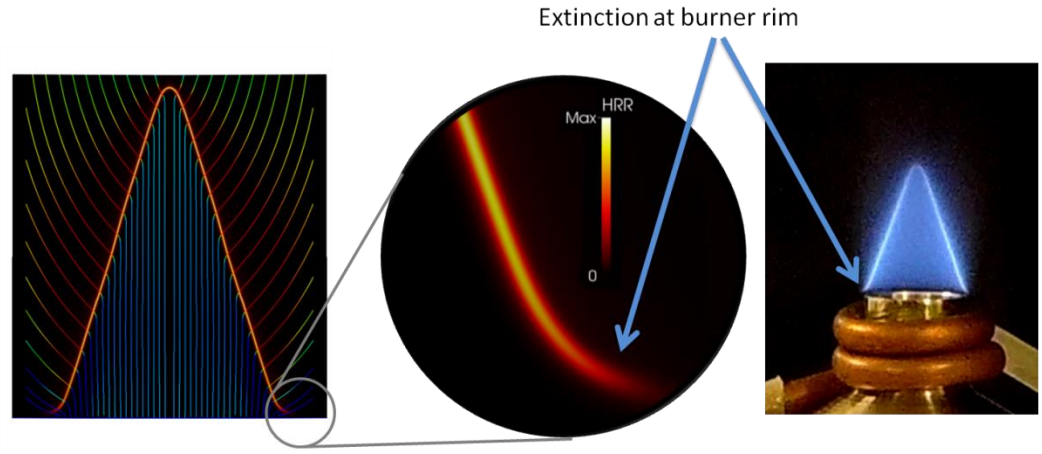

Figure 8.9. (a) Fluid flow path highlighted by streamlines overlaid on iso-contours of heat release rate for a CH_4/air flame at ϕ=1.0 for a high Re case. (b) Snapshot of experimental observation of a CH_4/air flame at ϕ=0.9 for a high Re case.

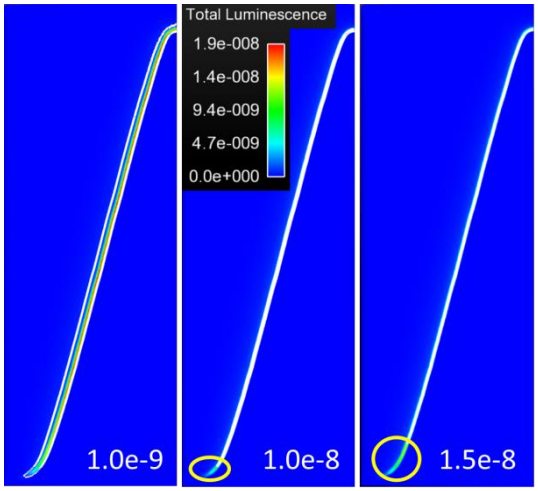

Figure 8.10. Iso-contours of total luminescence for a CH_4/air flame at ϕ=1.0 for high Re case overlaid with iso-surfaces of total luminescence having three different values; a)1e-9; b)1e-8; c)1.5e-8.

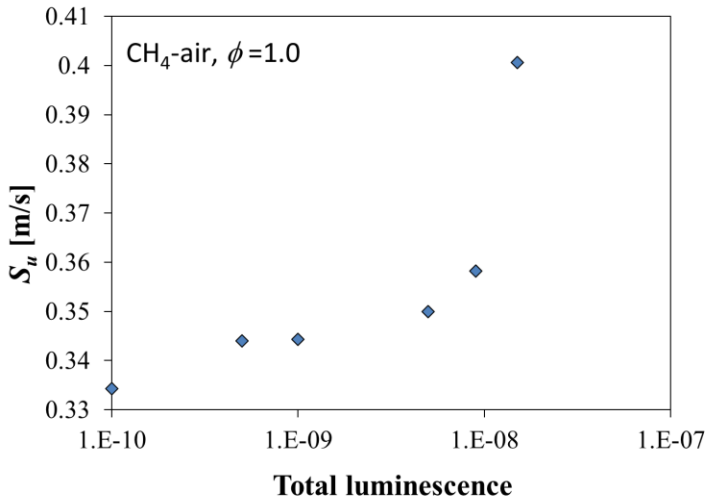

Figure 8.11. S_u estimates using different temperature iso-surfaces for a CH_4/air flame at ϕ=1.0 for high Re case. S_u estimated using the luminescence iso-surface is also presented for the same case.

Figure 8.10 shows iso-contours of total luminescence for a CH_4/air flame at ϕ=1.0 for high Re case overlaid with iso-surfaces of total luminescence corresponding to three different values: 1e-9, 1e-8, and 1.5e-8. The maximum value of total luminescence in the domain corresponds to 1.80e-8. Figure 8.11 shows S_u values estimated using different total luminescence iso-surfaces. Using the iso-surface corresponding to half the maximum value of total luminescence gives an S_u value of 35.43 cm/s which compares well to an S_u^o of 35.97 cm/s obtained using PREMIX calculations. As will also be seen in the results presented below for other ϕ's for CH4/air and C3H8/air flames, good agreement between S_u and S_u^o is obtained by using a total luminescence iso-surface corresponding to half the maximum value.

vi) Stretch effects

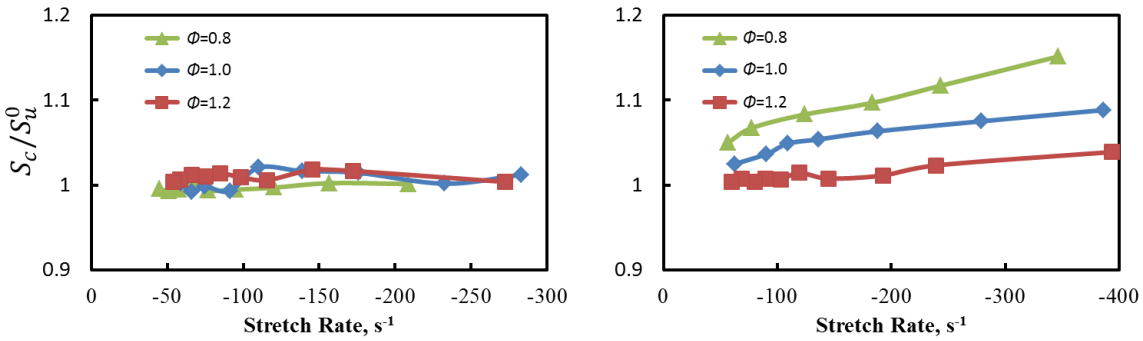

Figure 8.12. Ratio of consumption speed to S_u^o computed locally along the flame surface plotted as a function of local stretch rate for three different ϕ's for a) CH_4/air flames and b) C_3H_8/air flames.

The Bunsen flame method inherently incorporates stretch effects into the flame speed determination. However, the effect of local stretch on the flame surface can be evaluated by computing a local consumption speed and comparing it to S_u^o. The consumption speed (S_c) is computed using the following equation:

$$S_c \equiv \frac{\int_{-\infty}^{+\infty} \dot{\omega}_F (\mathbf{n} \cdot d\mathbf{x})}{\rho_u Y_{F,u}} \qquad (3)$$

Figure 8.12 shows results obtained for three different ϕ's for CH_4/air and C_3H_8/air flames. As can be seen from the results, for CH_4 flames whose Lewis number (*Le*) is close to unity, the ratio of S_c to S_u^o is close to 1. On the other hand, for C_3H_8 flames, whose Le is greater than unity, the ratio of S_c to S_u^o increases with increasing negative stretch values. Flame stretch increases towards the apex of the flame as seen in Fig. 8.12.

8.4.2 Results of the parametric analysis

Figure 8.13 depicts results obtained from experiments for CH_4/air and C_3H_8/air mixtures. S_u's computed using the angle and area techniques for different inlet Re and ϕ are compared with accurate S_u^o literature values [91]. Figure 8.14 shows similar results obtained from numerical simulations. In this case, the S_u's are compared with computed S_u^o's.

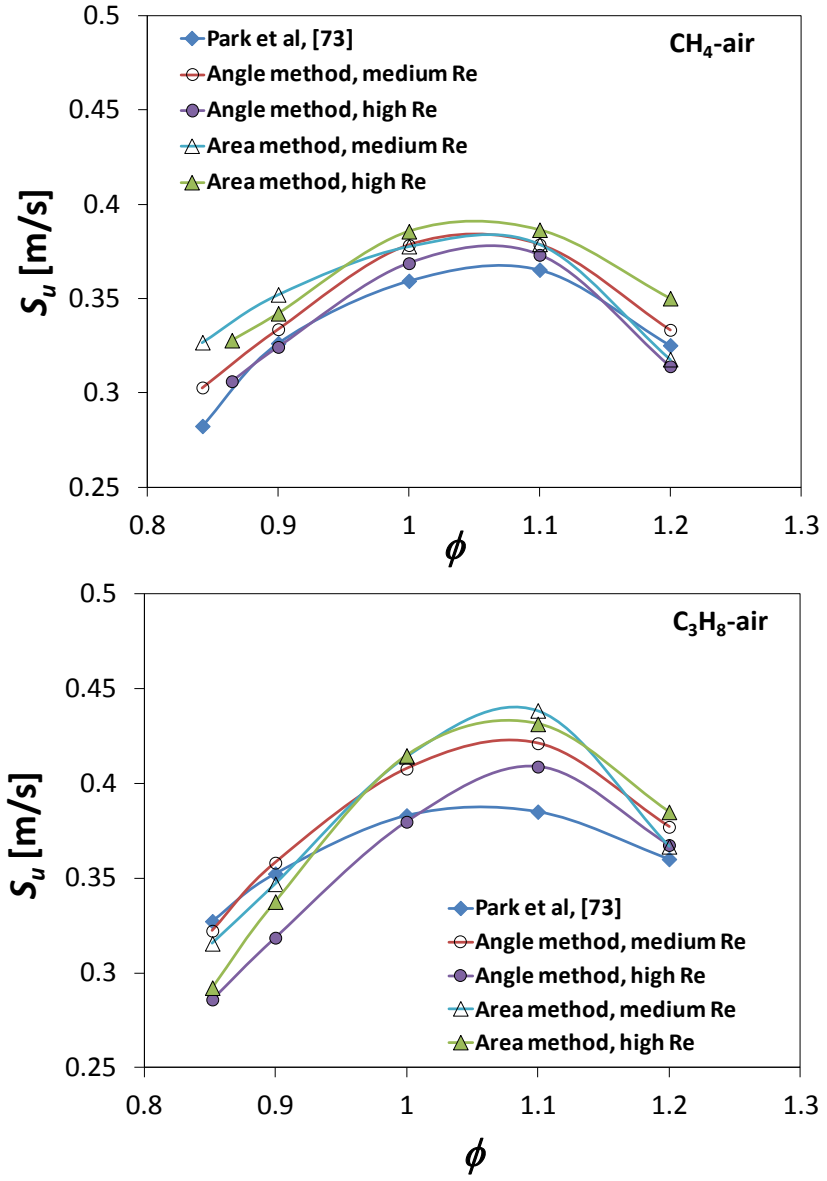

Figure 8.13. Experimental results for measured flame speeds using area and angle methods at different inlet Re for CH_4/air and C_3H_8/air mixtures.

Considering the results for CH_4/air mixtures in Fig. 8.13(a), it can be seen that all methods give results close to the reference value at stoichiometry and the spread away from the reference value increases as the mixture is made lean or rich. This is consistent with the flame being strongest near stoichiometry and extinction near the burner rim

which occurs more readily for weakly burning flames. It is also seen that all measured results overestimate the reference values of S_u^o. Next it is seen that the angle method performs better than the area method at both Re especially at lean and stoichiometric conditions. Further the area method at high Re appears to perform better than the area method at low Re at lean and stoichiometric conditions. This is consistent with the higher surface area produced at high Re resulting in a lower sensitivity to computed S_u. Considering the results for C_3H_8/air mixtures presented in Fig. 8.13(b), the agreement is not as good as that observed for CH_4 especially at stoichiometry and $\phi = 1.1$. The area methods and angle method at medium Re show results close to each other but the angle method at high Re shows considerable difference from the other methods. It is to be noted that the bulk velocity, U_b is used in the angle method for all cases presented in Fig. 8.13 and Fig. 8.14.

Figure 8.14(a) shows simulation results for the CH_4/air mixtures. The area method is seen to clearly perform better than the angle method at both Re. The angle method produces results consistently lower than the values predicted by the area method. It is to be noted that if U_p is used to estimate S_u using the angle method instead of U_b, the values are consistently higher than the reference values. Figure 8.14(b) shows simulation results for the C_3H_8/air mixtures. Similar to the results for CH_4/air flames, simulation results for C_3H_8/air flames show better agreement with S_u^o using the area method as compared to the angle method.

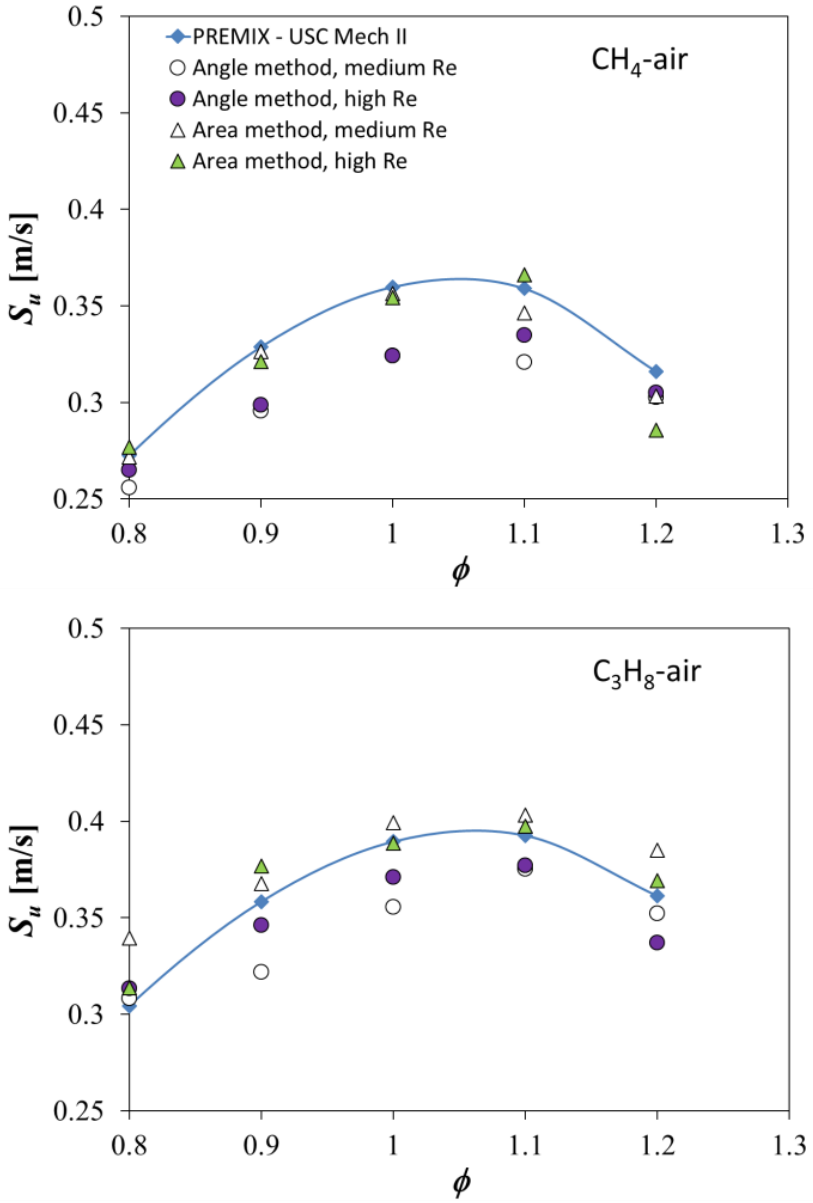

Figure 8.14. Simulation results for flame speeds estimated using area and angle methods at different inlet Re for CH_4/air and C_3H_8/air mixtures.

8.4.3 Correction factors

We now estimate simple correction factors for S_u based on experiments and simulations that can be multiplied to the estimated value of S_u using the angle or area methods to obtain the reference S_u^o values. The assumption is that the correction factor for experiments and simulations are almost the same, since they are processed in a similar manner. The correction factor is given by,

$$\text{CF} = \frac{S_{u\,num}}{S^0_{u\,num}} \cong \frac{S_{u\,exp}}{S^0_{u\,exp}} \qquad (4)$$

where the value of $S^o_{u\,num}$ are obtained from freely propagating flame speeds using PREMIX. The values of $S^o_{u\,exp}$ thus can be derived using the equation (4) and be compared with those values from literature [91]. The objective is to see the percentage difference of the S_u^o obtained from Bunsen flame experiments as compared to those obtained from literature. Figure 8.15(a) shows the ratio of S_u^o for CH_4/air mixtures and Fig. 8.15(b) shows the same for C_3H_8/air mixtures. It can be observed that the S_u^o for CH_4/air mixtures are consistently over predicted (close to 1.1) over the range of ϕ unlike for the C_3H_8-air mixtures that tend to be less than 1 for lean mixtures and increases close to stoichiometry. It is to be noted that these trend lines being estimated using all data points (angle and area methods, different Re) encapsulate a range of factors within them. The results seem to indicate that it may be possible to use simple algebraic scaling factors using such analyses to correct S_u measured using the Bunsen flame technique and evaluate S_u^o.

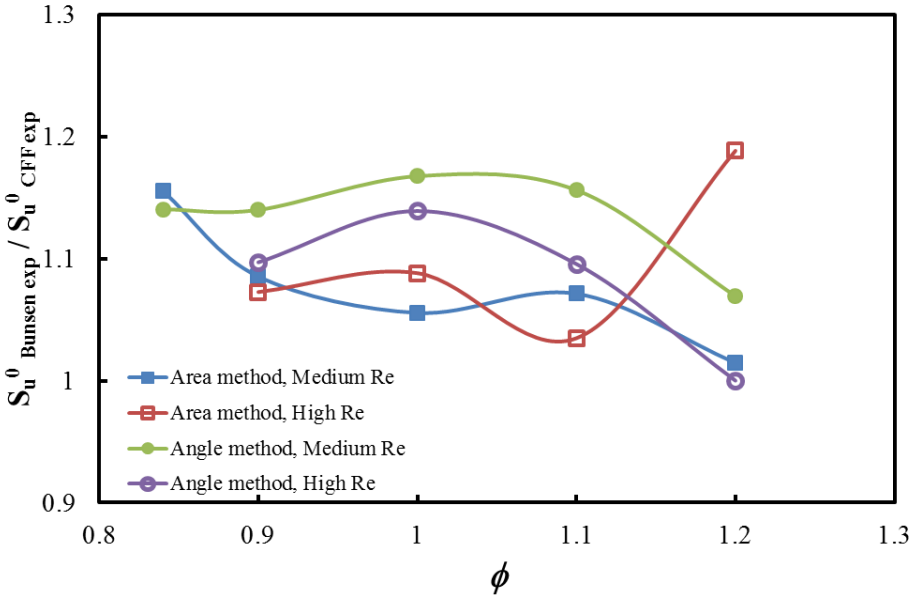

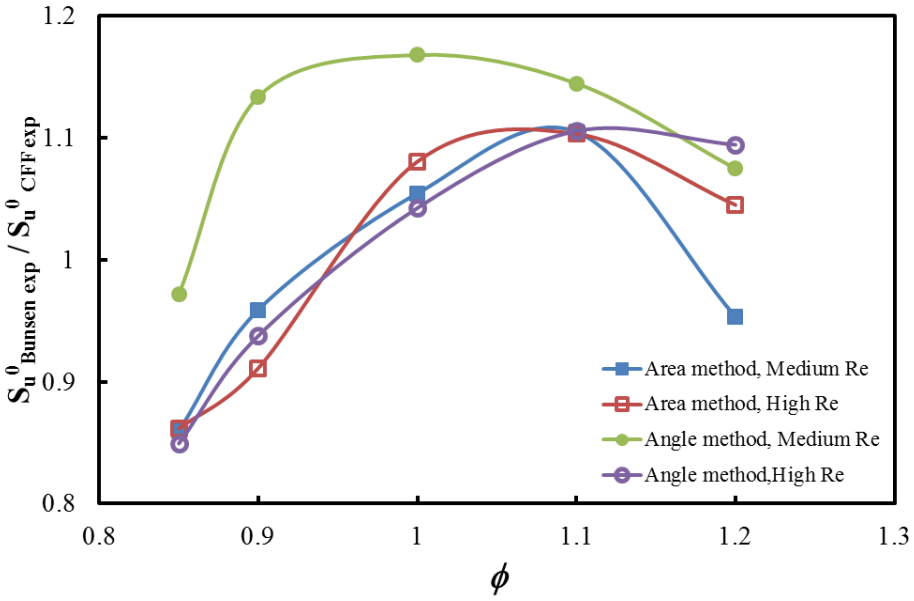

Figure 8.15. Ratio of S_u^o for CH_4/air and C_3H_8/air mixtures from experiments and literature.

8.5 Concluding Remarks

A parametric study of Bunsen flame techniques for measuring flame speeds of methane/air and propane/air mixtures was carried out using experiments and numerical simulations. Two common techniques, the angle method and the area method are utilized to extract the flame speed. The simulation results show a large effect of the boundary layer in the inlet to flame speed estimated using the angle method. In case of the area method, underestimation of flame surface area near the burner rim due to local extinction of the flame is seen to be one of the primary sources of measurement error. From the experimental data, the flame speed for methane/air mixtures is overestimated in general, and on average is within 6 % of the reference value. Trends are qualitatively similar to each other using different estimation techniques and inlet velocities. For propane-air mixtures, the average deviation from the reference value is also about 6 %. However, the trends are considerably different especially at rich mixture conditions. Simulation results for methane/air mixtures show the area method, which uses half the maximum intensity of OH^* to generate the flame surface gives good agreement with reference flame speeds. The angle method however under predicts the flame speed. For propane-air mixtures, the simulation results show more deviation from the reference value closer to stoichiometry than at lean conditions as in the experiments. Trends generated for simple correction factors from experiment and simulation results show similar behavior for both fuels. These correction factors in essence reflect the effect of measurement method (angle or area) and inlet velocity for different equivalence ratios and fuels. Future work will focus on extension of such correction factors to take into account inlet temperature and pressure variations.

8.6 References

[1] Letheby, J. Franklin Inst. 82 (1866) 331-338.

[2] D. Bradley, Proc. Comb. Inst., 24 (1992) 247-262.

[3] E. Mallard, H. Le Chatelier, Annales des Mines, 8 (1883) 274-618.

[4] M. E. Harris, J. Grumer, G. von Elbe, B. Lewis, Symp. on Combust. and Flame and Explosion Phenomena, 3 (1948) 80-89.

[5] G.E. Andrews, D. Bradley, Combust. Flame, 18 (1972) 133-153.

[6] C.K. Law, Combust. Flame, 53 (1983) 153.

[7] N. Peters, F.A. Williams, Combust. Flame, 68 (1987) 185-207.

[8] G. Dixon-Lewis, Proc. Comb. Inst. 23 (1991) 305-324.

[9] H. Le Chatelier, E. Mallard, Compte Rend. Acad. Sci., 93 (1881) 145-148.

[10] B. Lewis, G. von Elbe, J. Chem. Phys., 11 (1943) 75.

[11] F. W. Stevens, Nat. Advisory Comm. Aeronaut. Rep. 305, (1929).

[12] R. Bunsen, Poggendorffs Ann. der Physik und der Chemie, 131 (1866) 161.

[13] L. Ubbelohde, E. Koelliker, J. Gasbeleucht. 59 (1916) 49-57.

[14] F.A. Smith, S.F. Pickering, J. Research Nat. Bur. Std., 17 (1936) 7–43.

[15] C.K. Law, P. Cho, M. Mizomoto, H. Yoshida, Proc. Comb. Inst., 21 (1988) 1803-1809.

[16] N. Bouvet, C. Chauveau, I. Gökalp, S.-Y. Lee, R.J. Santoro, Int. J. of Hydrogen Energ., 36 (2011) 992-1005.

[17] H. Tsuji, I. Yamaoka, Proc. Comb. Inst., 11 (1967) 979-984.

[18] D.L. Zhu, F.N. Egolfopoulos, C.K. Law, Proc. Comb. Inst., 22 (1989) 1537-1545.

[19] J. Jayachandran, A. Lefebvre, R. Zhao, F. Halter, E. Varea, B. Renou, F. N. Egolfopoulos, Proc. Comb. Inst., In Press, Corrected Proof, (2014).

[20] C. K. Law, S. Ishizuka, M. Mizomoto, Proc. Comb. Inst., 18 (1981) 1791-1798.

[21] C.K. Wu, C.K. Law, Proc. Comb. Inst., 20 (1985) 1941-1949.

[22] C. M. Vagelopoulos, F. N. Egolfopoulos, Proc. Comb. Inst., 27 (1998) 513-519.

[23] F. W. Stevens, Nat. Advisory Comm. Aeronaut. Rep. 176, (1924).

[24] J. Manton, G. von Elbe, B. Lewis, Proc. Comb. Inst., 4 (1953) 358-363.

[25] C.J. Rallis, A.M. Garforth, Prog. Energy Combust. Sci., 6 (1980) 303–329.

[26] D. Bradley, R.A. Hicks, M. Lawes, C.G.W. Sheppard, R. Woolley, Combust. Flame, 115 (1998) 126-144.

[27] F.N. Egolfopoulos, N. Hansen, Y. Ju, K. Kohse-Höinghaus, C.K. Law, F. Qi, Prog. Energy Combust. Sci., 43 (2014) 36-67.

[28] R.J. Kee, J. A. Miller, G. H. Evans, G. Dixon-Lewis, Proc. Comb. Inst., 22 (1989) 1479–1494.

[29] G. Dixon-Lewis, T. David, P.H. Gaskell, J.A. Miller, R.J. Kee, M.D. Smooke, N. Peters, E. Effelsberg, J. Warrantz, F. Behrendt, Proc. Comb. Inst., 20 (1985) 1893–1904.

[30] L. M. Bollinger, D. T. Williams, Nat. Advisory Comm. Aeronaut., Rep. 932. (1949).

[31] D. Bradley, P.H. Gaskell, X.J. Gu, A. Sedaghat, Combust. Flame, 143 (2005) 227-245.

[32] F. A. Smith, S.F. Pickering, Bureau of St. Jour. of Research (1879).

[33] M. Gouy, Ann. chim. Phys . 18 (1879) 27.

[34] H. Schmidt, Ann. der Physik, 334 (1909) 971–1028.

[35] W. Michelson, Ann.der Physik, 37 (1889) 1-24.

[36] C.K Law, C.J Sung, Prog. Energy Combust. Sci., 26 (2000) 459-505.

[37] C.J. Sun, C.J. Sung, C.K. Law, Proc. Comb. Inst., 25 (1994) 1391-1398.

[38] H. Daneshyar, J.M.C. Mendes-Lopes, Int. J. of Mech. Sci., 24 (1982) 529-535.

[39] A.K. Gupta, H.A. Valeiras, Combust. Flame, 55 (1984) 245-2540.

[40] C.K. Law, P. Cho, M. Mizomoto, H. Yoshida, Proc. Comb. Inst., 21 (1988) 1803-1809.

[41] K. Müller-Dethlefs, A.F. Schlader, Combust. Flame, 27 (1976) 205-215.

[42] H. Edmondson, M. P. Heap, Combust. Flame, 15 (1970) 179-187.

[43] D.A. Senior, Combust. Flame, 5 (1961) 7-10.

[44] D.K. Kuehl, Proc. Comb. Inst., 8 (1961) 510-521.

[45] I. Kimura, H. Ukawa, Proc. Comb. Inst., 8 (1961) 521-523.

[46] J. Diederichsen, R.D. Gould, Combust. Flame, 9 (1965) 25-31.

[47] F. R. Caldwell, H. P. Broida, J. J. Dover, Nat. Bureau of St., (1951).

[48] M. Gerstein, Proc. Comb. Inst., 4 (1953) 35-43.

[49] C. Halpern, J. Research Nat. Inst. Standards Tech., 60 (1958).

[50] H.R. Poorman, Eng. Thesis, California Institute of Technology, (1953).

[51] J.W. Linnett, Proc. Comb. Inst., 4 (1953) 20-35.

[52] G. L., Dugger, S. Heimel, Nat. Advisory Comm. Aeronaut, TN2624, (1952).

[53] F. A. Smith, Proc. of the Symp. on Comb., 1–2 (1948) 206-219.

[54] W. Linnett, M.F. Hoare, Symp. on Combust. and Flame, and Explosion Phenomena, 3 (1948) 195-204.

[55] N. Bouvet, S.-Y. Lee, I. Gökalp, R. J. Santoro, Third European Combustion Meeting ECM (2007).

[56] J. Natarajan, T. Lieuwen, J. Seitzman, Combust. Flame, 151 (2007) 104-119.

[57] B. Bunkute, J.B. Moss, Third European Combustion Meeting ECM (2007).

[58] Y. Kochar, T. Lieuwen, J. Seitzman, Proc. of the 6th U.S. Nat. Comb.Meeting (2009).

[59] F.J. Higuera, Combust. Flame, 157 (2010) 1586-1593.

[60] Y. N. Kochar, S. N. Vaden, T. C. Lieuwen, J. M. Seitzman, 48th AIAA Aerospace Sciences Meeting Including the New Horizons Forum and Aerospace Exposition, Orlando, Florida (2010).

[61] C. Cohé, D. F. Kurtuluş, C. Chauveau, I. Gökalp, Third European Combustion Meeting ECM (2007).

[62] J. Oh, D. Noh, Energy, 45 (2012) 669-675.

[63] J. Fu, C. Tang, W. Jin, Z. Huang, Int. J. Hydrogen Energy, 39 (2014) 12187-12193.

[64] M. D. Smooke, Proc. Comb. Inst., 34 (2015) 65-98.

[65] J. Fu, C. Tang, W. Jin, L. D. Thi, Z. Huang, Y. Zhang, Int. J. Hydrogen Energy, 38 (2013) 1636–1643.

[66] G. Garcia-Soriano, F. J. Higuera, J. L. Castillo, P. L. Garcia-Ybarra, Proc. of the European Combustion Meeting (2009).

[67] J. Diederichsen, R.D. Gould, Combust. Flame, 9 (1965) 25-31.

[68] R. B. Morrison, R.A. Dunlap, Aeron. Research Center of Michigan, Project MX-794 (1948).

[69] J. Jayachandran, A. Lefebvre, R. Zhao, F. Halter, E. Varea, B. Renou, F. N. Egolfopoulos, Proc. Comb. Inst., in press, (2014).

[70] M.D. Smooke, V. Giovangigli, IMPACT of Comp. in Sci. and Eng., 4 (1992) 46-79.

[71] C. Duwig, L. Fuch, 47th AIAA Aerospace Sciences Meeting Including The New Horizons Forum and Aerospace Exposition Orlando, Florida (2009).

[72] G. Janiga, D. Theveni, Fifth European Combustion Meeting ECM (2009).

[73] Mittal, V., Pitsch, H., Egolfopoulos, F. N, Combust. Theory and Modell. 16 (2012) 419-433.

[74] Gururajan, V., Egolfopoulos F.N., Kohse-Höinghaus, K. Proc. Comb. Inst. 35 (2015) 821-829.

[75] C.K. Law , S. Ishizuka, P. Cho, Combust. Sci. Tech. 28 (1982) 3-4.

[76] M. Mizomoto, Y. Asaka, S. Ikai, C.K. Law, Proc. Combust. Inst. 20 (1985) 1933-1939.

[77] S. H. Chung, T. M. Vu , M. S. Cha, B. J. Lee, "Tip opening of premixed bunsen flames: Extinction with negative stretch and local Karlovitz number", Combust. Flame, In Press, (2014)

[78] F. R. Caldwell, H. P. Broida, J.J. Dover, Ind. And Chem., 43 (1951) 2731-2739.

[79] W.C. Johnston, Soc. Auto. Eng. J. 55 (1947) 62-65.

[80] G.E. Andrews, D. Bradley, Combust. Flame, 18 (1972) 133–153.

[81] R. M. Fristrom, Phys. of Fluids, 8 (1965) 273-280.

[82] A. Cuoci, A. Frassoldati, T. Faravelli, E. Ranzi, Combust. Flame 160 (2013) 870-886.

[83] H. Wang, X. You, A. V. Joshi, Scott G. Davis, A. Laskin, F.N. Egolfopoulos C. K. Law, USC-Mech Version II. High-Temperature Combustion Reaction Model of H2/CO/C1-C4 Compounds. http://ignis.usc.edu/USC_Mech_II.htm.

[84] T. Lu, C.K. Law, Proc. Combust. Inst. 30 (2005) 1333–1341.

[85] A. Hossain, Y. Nakamura, Combust. Flame 161 (2014) 162-172.

[86] M. Kopp, E.L. Petersen, F. Guthe, 51st AIAA aerospace sciences meeting, Grapevine, TX, 2013.

[87] R.J. Kee, J.F. Grcar, M.D. Smooke, J.A. Miller, A FORTRAN Program for Modeling Steady Laminar One-Dimensional Premixed Flames, Sandia Report. SAND85-8240, Sandia National Laboratories, 1985.

[88] http://www.openfoam.org/

[89] R.I. Issa, J. Comp. Phys. 62 (1986) 40-65.

[90] T. Poinsot, T. Echekki, M.G.Mungal, Combust. Sci. Tech. 81 (1992) 45-73.

[91] O. Park, P. S. Veloo, N. Liu, F. N. Egolfopoulos, Proc. Comb. Inst., 33 (2011) 887-894.

Chapter 9: Zimont Scale Vortex Interactions with Premixed Flames

9.1 Introduction

The vortex-flame interaction is a complicated yet fundamental problem in combustion theory [1-3]. Such topic requires extensive computation resources and experimental capabilities, and often provides only limited information. A study of the interaction of a vortex with a laminar flame can provide valuable insights into the dynamics of the coupling of fluid mechanics and chemistry with reasonable cost.

Previous work of vortex-laminar flame interaction has been conducted mostly on the scale vortex size, l_v, greater than the flame thickness, δ_f[4-8]. Under such condition, flame is stretched and wrinkled by the vortex. Three phenomenons have been observed in these vortex flame interaction, namely the dilatation and expansion of the vortex by the heat release in the flame; convection and stretching of the flame by the vortex and production of vorticity by flame curvature. While these studies are important towards the understanding of global flame vortex interaction, they provide little information about the fine scale flame dynamics response to vortex when large vortex cascades into size comparable to l_v, a scenario typically happened in turbulent environment.

Oran and co-workers [9,10] showed that the flame thickness increases by turbulent motions, which affects the flame structure in the preheat zone and their effect becomes less pronounced with increasing temperature toward the reaction zone. Their results shows that such flame broadening is determined by scales large or equal to the flame

thickness rather than small-scale motions, i.e. kolmogorov scale. The turbulent energy cascade fails to penetrate the internal structure of the flame, i.e. reaction zone, δ_r, a scale much smaller than δ_f.

Bilger and co-workers [11] showed similar results via experiments that considerable broadening of the flame front can occur at Re number conditions relevant to high-speed propulsion while there is no evidence of flame reaction zone thickening at Karlovitz numbers, Ka = 100, which suggests that flamelet model may be extend well beyond the regime as traditional classification of combustion regimes.

Recently, Bobbitt and Blanquart [12] studied the interaction of a single vortex with a premixed flame through sets of vortex size and strength. Their simulation results identified the existence of four regimes in the vortex laminar flame interaction and showed the final characteristics of the initial vortex. Their results also suggest that strong vortex of size much smaller than δ_f persist after passing through the flame.

In the current study, Zimont scale, $l_v \approx \delta_f$, [13,14] vortex-laminar flame interaction is investigated with simplified chemistry model to establish a foundation for the following investigation using realistic fuels i.e. JP-10 with detailed chemistry model, because very little work has been done on this topic utilizing aviation fuels. The implications of previous work [9-11] suggest that such flame front broadening can cause significant differences in the interaction between turbulent flow structures and flame fronts while considering small MW fuels vs. large MW fuels.

The objective of this study is to validate if the flame front broadening phenomenon occurs with Zimont scale vortex-flame interaction; the impact of flow field distortion on light and heavy hydrocarbon fuel decomposition. The results will be presented in the same manner following the objective steps.

9.2 Numerical Approach

Detail description of the 3D code can be found in Chapter 3. In short, a finite volume based CFD code package called laminarSMOKE is used [16-19]. A time-splitting technique is used in laminarSMOKE to handle the stiffy-coupled energy and species transport equation [20, 21], the continuity and momentum equations are handled using PISO algorithm [22].

A steady state acceleration field was introduced by introducing a source term explicitly in the momentum equation. A two-dimensional, Cartesian, 2.5 cm × 2.5 cm computation domain was used to represent a typical stagnation flow configuration, with impinging flow velocity 0.8 m/s, of a CH4/air mixture from the left boundary. A no-slip, no-penetration, adiabatic wall boundary condition was set at the right end of the domain and outlet boundary conditions were used in the vertical direction. The field can be visualized in Fig. 9.1, where vortex is imposed in the location adjacent to the flame front, with a vortex size $l_v/\delta_f = 0.2$ and vortex strength $u_v/s_u^o = 4$, where u_v is the characteristic velocity of the vortex and s_u^o is the laminar flame speed. All cases were performed on a uniform mesh of 40,000 cells until a steady state solution was reached.

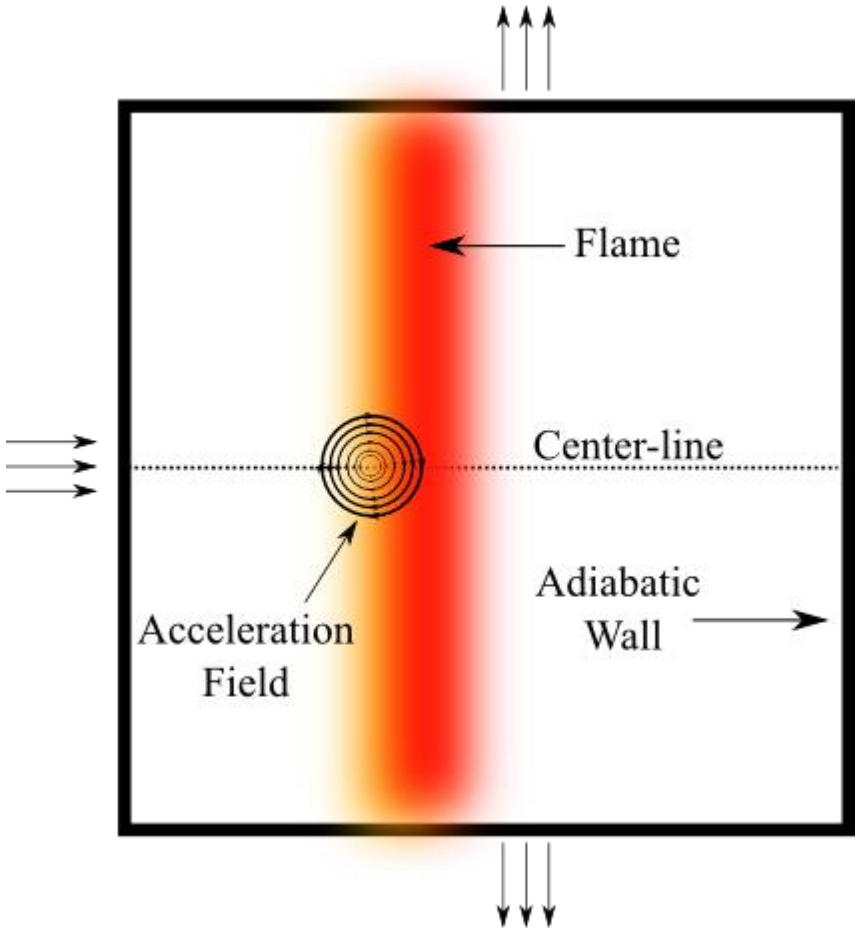

Figure 9.1. Schematic view of the computation domain.

All 2-D simulations were performed using a three-step kinetic model, hereafter referred as TSM. Lagrangian temperature histories, using particles injected at specific locations in the presence/absence of vortex, were imported to the SENKIN code [23], upon which a detailed chemistry model, JetSurF 1.0 [24], was used to investigate the fuel decomposition process.

9.3 Results and Discussion

9.3.1 Vortex-Flame Interaction

Figure 9.2 depicts the centerline velocity and temperature profile for a stoichiometric, 0.1 atm CH_4/Air flame using the TSM. The case without the presence of a vortex is referred to as the unperturbed case (UPC) and the one with the vortex is referred as the perturbed case (PC). The UPC shows the classic velocity distribution with a single peak due to thermal dilatation. In the PC, however, because of the presence of the vortex due to the acceleration field near the flame, the velocity profile consists of two peaks. The first velocity peak is caused by the fluid particle passing through the acceleration field and the second velocity peak is due to the combined effect of vortex and thermal expansion, causing a much higher peak than the unperturbed case. The result shows that a strong vortex, $u_v/s_u^o = 4$ in this case, affects the velocity distribution and readjusts the flame location due to the local velocity field distortion.

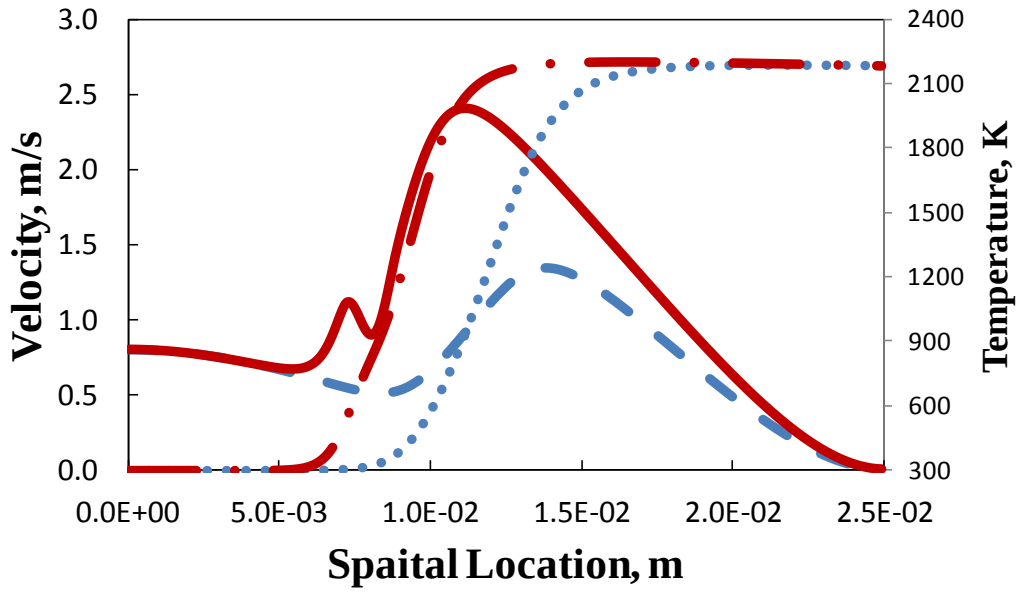

Figure 9.2. Velocity component in x-direction and Temperature as a function of spatial location. (---) V_{upc}; (–) V_{pc}; (···) T_{upc}; (-·-) T_{pc}

Figure 9.3 shows the temperature contour plot and streamline trajectory for the UPC ((a) and (b)) and the PC ((c) and (d)), respectively. The temperature and velocity fields in the UPC are symmetric about the center line. However, due to the presence of a clockwise rotational acceleration field near the flame front, the velocity below the centerline is lower than the corresponding location in the UPC, and the velocity above the centerline is likewise higher. This non-uniform distribution of velocities causes the flame to readjust to a new location. More interestingly, the vortex carries the relatively "cold" reactant mixture into the region above the centerline and circulates a "hot" reactant-product mixture, the overall effect amounts to a redistribution of the species and a broadening of the preheat zone near the vortex region, causing a milder temperature gradient near centerline as shown in Fig 9.3 (c).

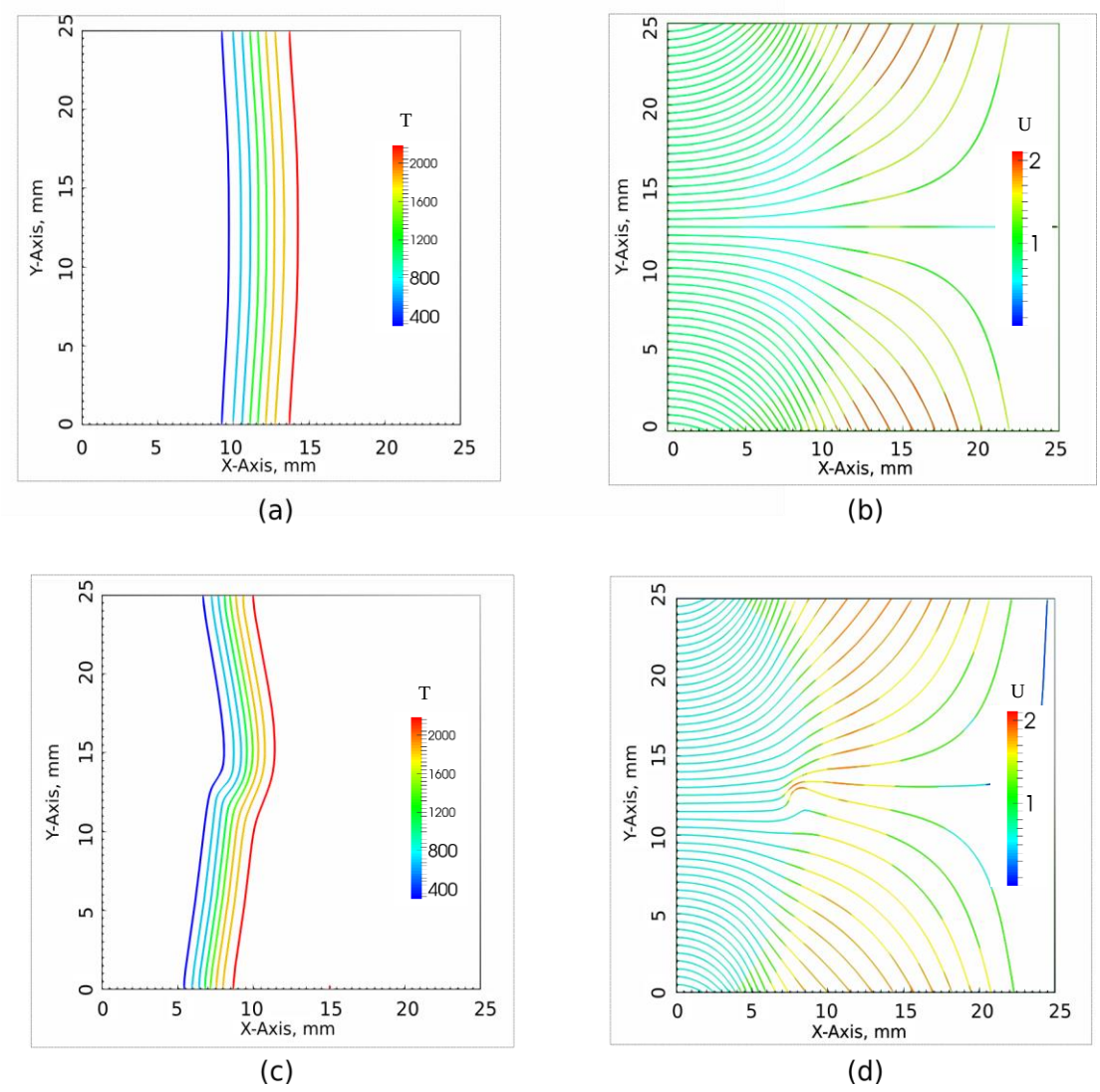

Figure 9.3. (a) Temperature contours for the UPC; (b) Streamlines for the UPC; (c) Temperature contours for the PC; (d) Streamlines for the PC.

Figure 9.4 (a) depicts the streamlines near the vortex region. As can be deduced from the density of streamlines, the velocities far from the vortex are high compared to those close to the vortex. The path lines far above the vortex cover a longer distance with high

velocity, while those far below the vortex experience a shorter path but at lower velocities. The velocities close to the vortex center however are much smaller in comparison, meaning the mixture inside the vortex is subject to a longer residence time. This phenomenon is illustrated in Fig. 9.4 (b), where particles are injected at a constant rate from the left boundary, thus the time histories for each particle can be traced in material/Lagrangian coordinates. The difference in path lengths for equal times is immediately apparent.

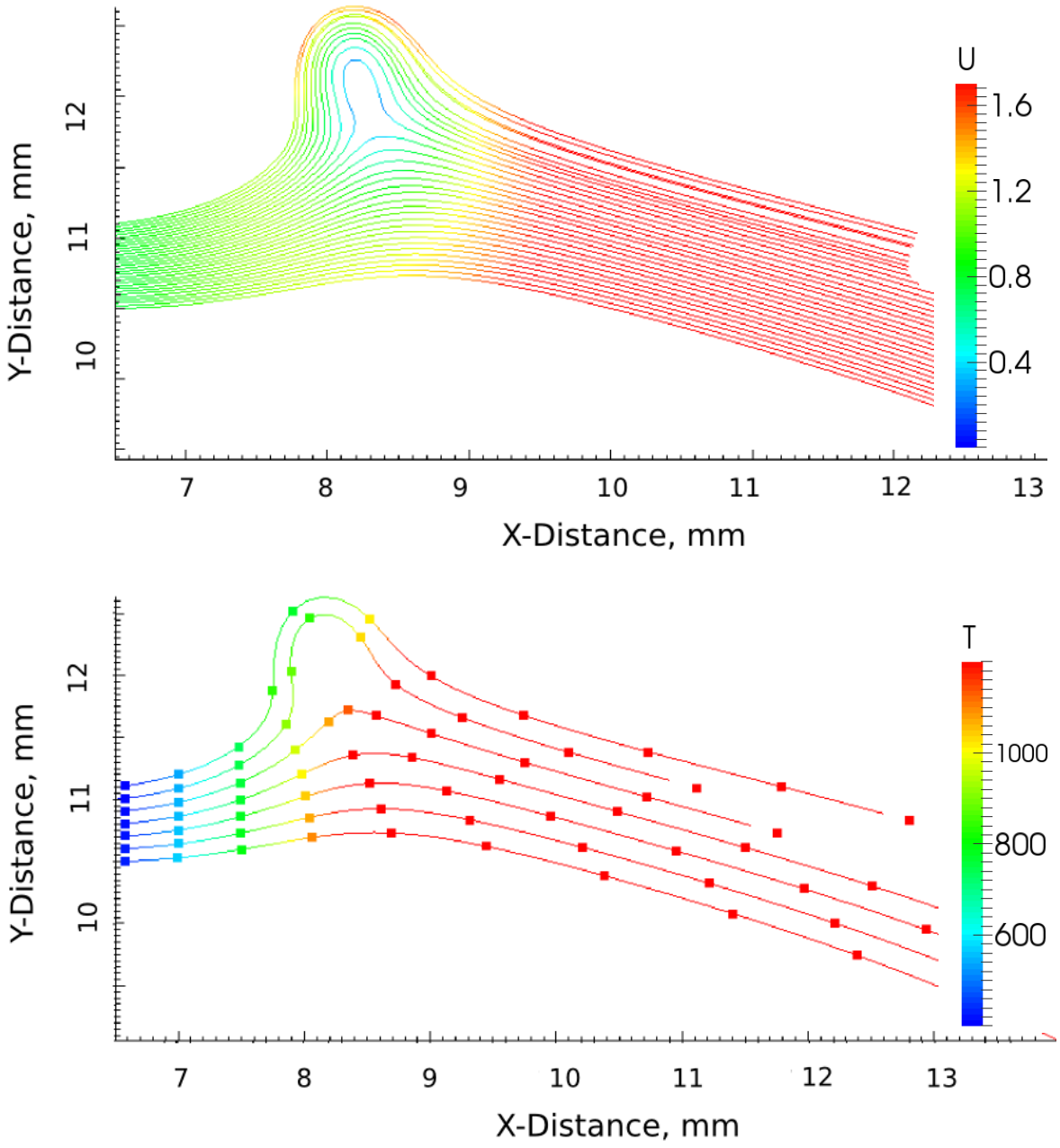

Figure 9.4. (a) Streamlines ; (b) Path lines carrying particles depicted at different times

9.3.2 Fuel Decomposition

The thermal structure of a flame is more or less determined by the local hydrodynamic conditions. It is thus reasonable to assume that the thermal structure brought about by the vortex-flame interaction described above is a good representation for any fuel subjected to the same velocity field. But while two flames corresponding to two different fuels may have the same thermal structures, they can vary remarkably in their chemical structures. It is of natural interest to study this difference and we can exploit the information in Fig. 9.4 (b), i.e. Temperature histories of fluid packets in the vicinity of the vortex.

If we further simplify the problem by ignoring differences in the flame thickness caused by different mass diffusivities, and idealize each fluid packet as a zero-dimensional batch reactor subject to a varying temperature field, we can model its chemical composition over time. This simplified approach allows us to use detailed chemistry at very little computational cost.

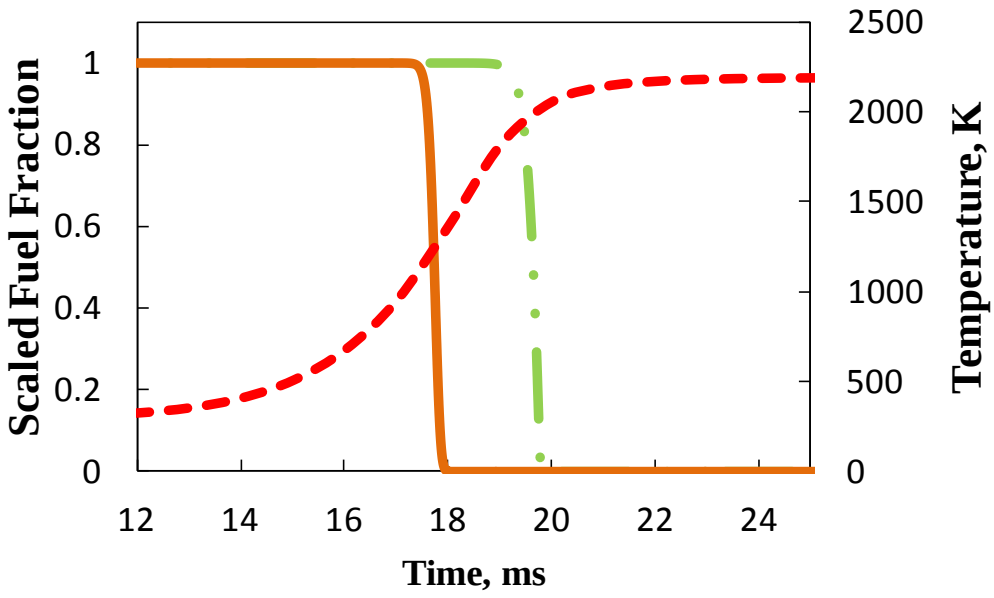

(a)

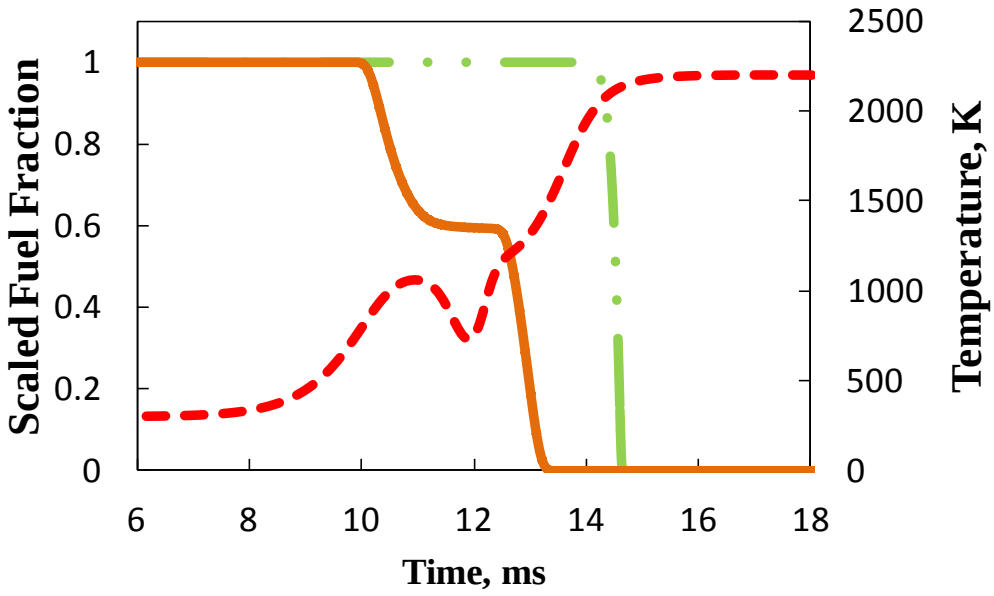

(b)

Figure 9.5. (a) The UPC Fuel Fraction and Temperature as functions of time; (b) The PC Fuel Fraction and Temperature as functions of time (–· –) CH_4/Air mixure at $\phi = 1.0$, T_u = 300 K and P = 0.1 atm; (—) n-$C_{12}H_{26}$/Air mixure at $\phi = 1.0$, T_u = 300 K and P = 0.1 atm; (---) Temperature.

Figure 9.5 depicts the temperature of a fluid packet originating from the center-line as it moves in space, i.e. in material/Lagrangian coordinates. Fig 9.5 (a) shows the UPC where *n*-$C_{12}H_{26}$ starts to decompose around 1050 K and is consumed almost entirely at 1500 K. CH_4 is not consumed until the temperature reaches about 1800 K. It confirms our long held understanding that long chain can be easily decomposed through β-session at moderately high temperatures. Fig 9.5 (b) is the corresponding plot for the PC. The temperature field is distorted due to the presence of vortex, as described in the previous section. While CH4 is not affected by the non-monotonic temperature profile, *n*-$C_{12}H_{26}$ exhibits some interesting behavior. When the temperature reaches its first peak around 1000 K, *n*-$C_{12}H_{26}$ starts to decompose. But right after the temperature exceeds 1200 K, it falls back to about 700 K in less than 2 ms. The residence time is not long enough to complete the decomposition process; 40% of the fuel is decomposed in this case. The fuel stops decomposition due to the temperature dip caused by the vortex and proceeds in a mixture containing C_1-C_4 hydrocarbon fragments from β-session. The fuel is entirely consumed once the temperature climbs back to 1000 K again.

The residence time for *n*-$C_{12}H_{26}$ is significantly different in these two cases. In the unperturbed case, the fuel is completely consumed in less than half a microsecond, while in the perturbed case, it lasts more than 3 ms. Such differences in fuel residence times also imply that the distribution of C_1-C_4 hydrocarbon fragments in both time and space is no

longer the same and the chemical structure inside the flame differs. The results presented here only represent one path line of the temperature-time history. Our preliminary results suggest that for each path line, the temperature-time history is different, meaning each profile could lead to different decomposition distribution in time and space.

These findings underline the importance of chemistry when heavy hydrocarbons are burnt in the turbulent conditions, an aspect that is usually overlooked in favor of modeling all complexities using simple fuels like methane and hydrogen. Figure 9.5 (b) shows that the strong bond energy in simple fuels may not be applicable to heavy hydrocarbons and could be misleading.

9.4 Concluding Remarks

Laminar vortex-flame interactions were studied numerically using a stagnation flow configuration in a two-dimensional Cartesian domain. The Lagrangian temperature histories were extracted from the simulation result and implemented in SENKIN, where detailed chemistry was employed. Results from the vortex-flame interaction were found to thicken the preheat zone by mixing the cold reactant with heated mixtures. The flame was seen to readjust its location based on local velocity changes. In the SENKIN simulations, the results for *n*-dodecane were found to be significantly different from methane. The difference in the consumption pathways between methane and *n*-dodecane emphasizes the importance of heavy hydrocarbon chemistry when dealing with turbulent combustion.

9.5 References

[1] P.-H. Renard, D. Thevenin, J.C. Rolon, and S.M. Candel, Prog. Energy Combust Sci. 26(2000) 225-282.

[2] J. F. Driscoll, Prog. Energy Combust. Sci. 34 (2008) 91-134.

[3] N. Peter, Proc. Combust. Inst. 32 (2009) 1-25.

[4] W.-H. Jou, and J.J. Riley, AIAA J. 27 (1989) 1543-1557.

[5] A. M. Laverdant, and S. M. Candel, Prop. Power. 5 (1989) 134-143.

[6] C. J. Rutland, and J.H. Ferziger, Combust. Flame. 84 (1991) 343-360.

[7] T. Poinsot, D. Veynante, and S. M. Candel, J. Fluid Mech. 228 (1991) 561-606.

[8] J. B. Bell, N.J. Brown, M. S. Day, M.Frenklach, J. F. Grcar, and S. R. Tonse, Proc. Comb. Inst, 28 (2000) 1933-1939.

[9] A. Y. Poludnenko, and E.S. Oran, Combust. Flame. 157 (2010) 995-1011.

[10] P. E. Hamlington, A.Y. Poludnenko, and E. S. Oran, Phys. Fluids. 23(2011) 125111.

[11] M. J. Dunn, A. R. Masri, and R. W. Bilger, Combust. Flame. 151 (2007) 46-60.

[12] B. Bobbit, and G. Blanquart, 8th US National Combustion Meeting

[13] V. L. Zimont, Combust. Expl Shock Waves. 15 (1979) 305-311.

[14] N. Peters, J. Fluid Mech. 384 (1999) 107-132.

[15] R.J. Kee, M.E. Coltrin, P. Glarborg, Chemically reacting flow: theory and practice, Wiley Interscience. (2005)

[16] J. H. Ferziger, M. Perić, Computational methods for fluid dynamics, Chapter 5, Berlin: Springer, 1996

[17] A. Cuoci, A. Frassoldati, T. Faravelli, E. Ranzi, Combust. Flame 160 (2013) 870-886

[18] OpenFOAM, www.openfoam.org, 2014

[19] A. Cuoci et al., OpenSMOKE: numerical modeling of reacting systems with detailed kinetic mechanisms, in: XXXIV Meeting of the Italian Section of the Combustion Institute, Rome, Italy, 2011.

[20] G. Strang, SIAM Journal on Numerical Analysis 5 (1968), 506-517

[21] P. N Brown, G. D. Byrne, A. C. Hindmarsh, SIAM journal on scientific and statistical computing 10(5) (1989), 1038-1051

[22] R.I Issa, Journal of Computational Physics, 62 (1986) 40-65

[23] A.E. Lutz, R.J. Kee, J.A. Miller, Report SAND-87-8248; Sandia National Laboratories: Albuquerque, NM, 1988.

[24] Sirjean, B., Dames, E., Sheen, D. A., You, X.-Q., Sung, C., Holley, A. T., Egolfopoulos, F. N.,Wang, H.,Vasu, S. S., Davidson, D. F., Hanson, R. K., Pitsch, H., Bowman, C. T., Kelley, A., Law, C. K., Tsang, W., Cernansky, N. P., Miller, D. L., Violi, A., and Lindstedt, R. P., "A High-Temperature Chemical Kinetic Model of n-Alkane Oxidation, JetSurF Version 1.0," http://melchior.usc.edu/JetSurF/JetSurF1.0/ Index.html [retrieved 15 Sept. 2009].

Chapter 10: Conclusions and Recommendations

10.1 Concluding Remarks

In this dissertation, a detailed experimental and numerical investigation into the fundamental flame properties of heavy hydrocarbons was conducted, with the main goal being the accurate determination of laminar flame speeds and extinction strain rates of a wide range of fuel surrogate candidates and realistic fuels in the counterflow configuration. The experimental data were modeled using a variety of chemical kinetic models. Rigorous sensitivity analyses on both chemical kinetics and molecular transport as well as reaction path analyses were performed to illustrate the chemical and physical mechanisms that control the combustion of these fuels.

To assess the uncertainties stemming from the current practices that are used to interpret experimental data and derive the laminar flame speed, direct numerical simulations of counterflow flames were carried out for *n*-dodecane/air flames. The effect of molecular transport was studied by varying the fuel diffusivity. The results showed that for fuel lean hydrocarbon/air mixtures, the preferential diffusion of heat or mass as manifested by the Lewis number dominates the flame response to stretch. For fuel rich mixtures, the controlling factor was determined to be the differential diffusion of the reactants into the reaction zone for heavy hydrocarbons. The conclusion is that using extrapolation equations derived based on asymptotics analysis and simplifying

assumptions to obtain the laminar flame speeds, could result in significant errors for rich flames of heavy hydrocarbons.

Compare to flame propagation, flame extinction is more sensitive on molecular transport, especially under non-premixed condition. It is shown that the updated diffusion coefficients resolve the earlier difficulty of predicting the extinction strain rate of non-premixed counterflow flames of *n*-dodecane/N_2 and *n*-decane/N_2 against O_2. It is also shown that the mixture-average transport formulation is adequate for predictions of the extinction strain rate, provided that the Soret effect is taken into consideration.

A parametric study of Bunsen flame techniques for measuring flame speeds of methane/air and propane/air mixtures was carried out using experiments and numerical simulations. Two common techniques, the angle method and the area method are utilized to extract the flame speed. The simulation results show a large effect of the boundary layer in the inlet to flame speed estimated using the angle method. In case of the area method, underestimation of flame surface area near the burner rim due to local extinction of the flame is seen to be one of the primary sources of measurement error. Simulation results for methane/air mixtures show the area method gives good agreement with reference flame speeds. The angle method however under predicts the flame speed. For propane-air mixtures, the simulation results show more deviation from the reference value closer to stoichiometry than at lean conditions as in the experiments. Thus, using

the Bunsen flame technique to measure propagation speeds of flames of heavy hydrocarbons can result in notable errors.

Laminar vortex-flame interactions were studied numerically using a stagnation flow configuration in a two-dimensional Cartesian domain. The Lagrangian temperature histories were extracted from the simulation result and implemented in SENKIN, where detailed chemistry was employed. Results from the vortex-flame interaction were found to thicken the preheat zone by mixing the cold reactant with heated mixtures. The flame was seen to readjust its location based on local velocity changes. In the SENKIN simulations, the results for *n*-dodecane were found to be significantly different from methane. The difference in the consumption pathways between methane and *n*-dodecane emphasizes the importance of heavy hydrocarbon chemistry when dealing with turbulent combustion.

10.2 Recommendations for Future Work

The direct numerical simulations of a variety of combustion phenomena constitute the core of the present study to investigate rigorously the fundamental combustion and emission characteristics of practical fuels and reexamine the conventional methods in determining such characteristics based on combustion theory. Simple configuration such as counterflow flames and Bunsen flames may nevertheless result in complex flow field phenomenon and complication which can only be solved via direct numerical simulation. Many problems of interest should be addressed further and recommendations for future work are listed below:

The experiments should be extended to higher pressures using novel approaches such as spherical expanding flames in order to validate the kinetic models at condition relevant to engines (~40 atm). The experiments should also be extended to sub-atmospheric pressure to validate the kinetics relevant to the condition from low-pressure flame sampling experiments (~0.1 atm) and would allow for the validation of pressure dependent rate constants.

Clear coupling phenomenon was already found for flame-vortex interaction at scale close to flame thickness, which is relevant in high intensity turbulent flame. Such phenomenon should be further investigated via both experiments and simulation especially for practical fuels towards a better understanding of flame behavior at condition relevant to engines.

With the advancements in direct numerical simulations, such powerful tool should not be limited to just mimic the experiments but to help in designing the experiments. The iteration time usually took several generations for perfecting the experimental design could be dramatically shortened via the assistance from full scale simulation.

Bibliography

A. Boushehri, J. Bzowski, J. Kestin, E. Mason, J. Phys. Chem. Ref. Data 16 (1987) 445-466.

A. Burcat, M. Dvinyaninov, E. Olchanski, Int. J. Chem. Kinet. 33 (9) (2001) 491-508.

A. Burcat, M. Dvinyaninov, Int. J. Chem. Kinet. 29 (7) (1997) 505-514.

A. Cuoci et al., OpenSMOKE: numerical modeling of reacting systems with detailed kinetic mechanisms, in: XXXIV Meeting of the Italian Section of the Combustion Institute, Rome, Italy, 2011.

A. Cuoci, A. Frassoldati, T. Faravelli, E. Ranzi, Combust. Flame 160 (2013) 870-886.

A. Einstein, Ann. Phys. 17 (1905) 549.

A. Einstein, Annalen der Physik 17 (1905) 549-560.

A. Holley, X. You, E. Dames, H. Wang, F. Egolfopoulos, Proc. Combust. Inst. 32 (2009) 1157-1163.

A. Holley, Y. Dong, M. Andac, F. Egolfopoulos, T. Edwards, Proc. Combust. Inst. 31 (2007) 1205-1213.

A. Hossain, Y. Nakamura, Combust. Flame 161 (2014) 162-172.

A. M. Laverdant, and S. M. Candel, Prop. Power. 5 (1989) 134-143.

A. Ristori, P. Dagaut, & M. Cathonnet, Combust. Flame 125 (2001) 1128-1137.

A. Roubaud, R. Minetti, L.R. Sochet, Combust. Flame 121 (2000) 535–541.

A. W. Jasper, E. Kamarchik, J. A. Miller, S. J. Klippenstein, J. Chem. Phys. 141 (2014) 124313.

A. W. Jasper, J. A. Miller, Combust. Flame 161 (2014) 101-110.

A. Y. Poludnenko, and E.S. Oran, Combust. Flame. 157 (2010) 995-1011.

A.E. Lutz, R.J. Kee, J.A. Miller, Report SAND-87-8248; Sandia National Laboratories: Albuquerque, NM, 1988.

A.J. Smallbone, W. Liu, C. Law, X. You, H. Wang, Proc. Combust. Inst. 32 (2009) 1245-1252.

A.K. Gupta, H.A. Valeiras, Combust. Flame, 55 (1984) 245-2540.

A.P. Kelley, A.J. Smallbone, D.L. Zhu, C.K. Law, Proc. Combust. Inst. 33 (2011) 963-970.

A.P. Kelley, C.K. Law, Combust. Flame 156 (2009) 1844-1851.

A.P. Kelley, J.K. Bechtold, C.K. Law, J. Fluid Mech. 691 (2012) 26-51.

A.S. Violi, S. Yan, E.G. Eddings, A.F. Sarofim, S. Granata, T. Faravelli, E. Ranzi, Combust. Sci. Technol. 174 (2002) 399-417.

A.T. Holley, X.Q. You, E. Dames, H. Wang, F.N. Egolfopoulos, Proc. Combust. Inst. 32 (2009) 1157-1163.

A.T. Holley, Y. Dong, M.G. Andac, & F.N. Egolfopoulos, Combust. Flame 144 (2006) 448–460.

A.T. Holley, Y. Dong, M.G.Andac, F.N. Egolfopoulos, & T. Edwards, Proc. Combust. Inst. 31 (2007) 1205–1213

B. Bobbit, and G. Blanquart, 8th US National Combustion Meeting

B. Bunkute, J.B. Moss, Third European Combustion Meeting ECM (2007).

B. Lecordier. Etude de l'interaction de la propagation d'une flamme de prémélange avec le champ aérodynamique par association de la tomographie laser et de la PIV. PhD Thesis Report, Université de Rouen, France, 1997.

B. Lewis, G. von Elbe, J. Chem. Phys., 11 (1943) 75.

B. Li, N. Liu, R. Zhao, H. Zhang, & F.N. Egolfopoulos, Proc. Combust. Inst. 34 (2013) 727-733

B. Li, Y. Zhang, H. Zhang, F. N. Egolfopoulos, Proc. Combust. Inst. 35 (2015) 965-972.

B. Sirjean, E. Dames, D. A. Sheen, X. You, C. Sung, A. T. Holley, F. N. Egolfopoulos, H. Wang, S. S. Vasu, D. F. Davidson, R. K. Hanson, H. Pitsch, C. T. Bowman, A. Kelley, C. K. Law, W. Tsang, N. P. Cernansky, D. L. Miller, A. Violi, R. P. Lindstedt, http://melchior.usc.edu/JetSurF/JetSurF1.0/Index.html.

B.G. Sarnacki, G. Esposito, R.H. Krauss, & H.K. Chelliah, Combust. Flame, 159 (2012) 1026–1043.

B.H. Chao, F.N. Egolfopoulos, C.K. Law, Combust. Flame 109 (1997) 620-638.

C. Cohé, D. F. Kurtuluş, C. Chauveau, I. Gökalp, Third European Combustion Meeting ECM (2007).

C. Duwig, L. Fuch, 47th AIAA Aerospace Sciences Meeting Including The New Horizons Forum and Aerospace Exposition Orlando, Florida (2009).

C. Halpern, J. Research Nat. Inst. Standards Tech., 60 (1958).

C.J. Rutland, and J.H. Ferziger, Combust. Flame. 84 (1991) 343-360.

C. Ji, E. Dames, B. Sirjean, H. Wang, F.N. Egolfopoulos, Proc. Combust. Inst. 33 (2011) 971-978.

C. Ji, E. Dames, H. Wang, F.N. Egolfopoulos, Combust. Flame 159 (2011) 1070-1081.

C. Ji, E. Dames, Y.L. Wang, H. Wang, F.N. Egolfopoulos, Combust. Flame 157 (2) (2010) 277-287.

C. Ji, Y. L. Wang, F. N. Egolfopoulos, J. Propul. Power 27 (2011) 856-863.

C. K. Law, Combustion physics, Cambridge university press, 2006.

C. K. Law, S. Ishizuka, M. Mizomoto, Proc. Comb. Inst., 18 (1981) 1791-1798.

C. K. Wu, C.K. Law, Proc. Combust. Inst. 20 (1984) 1941-1949.

C. Liu, H. Wang, J. Chem. Phys. Manuscript in preparation (2015).

C. Liu, Z. G. Li, H. Wang, Phys. Rev. E submitted (2015).

C. M. Vagelopoulos, F. N. Egolfopoulos, Proc. Comb. Inst., 27 (1998) 513-519.

C. Wu, C. Law, Symp. Int. Combust. 20 (1985) 1941-1949.

C.F. Curtiss, & J.O. Hirschfelder, The Journal of Chemical Physics, 17 (1949) 550.

C.J. Rallis, A.M. Garforth, Prog. Energy Combust. Sci., 6 (1980) 303–329.

C.J. Sun, C.J. Sung, C.K. Law, Proc. Comb. Inst., 25 (1994) 1391-1398.

C.K. Law, C.J Sung, Prog. Energy Combust. Sci., 26 (2000) 459-505.

C.K. Law , S. Ishizuka, P. Cho, Combust. Sci. Tech. 28 (1982) 3-4.

C.K. Law Symposium (International) on Combustion, (1989) 1381–1402.

C.K. Law, C.J. Sung, H. Wang, & T.F. Lu, AIAA Journal 41(9) (2003) 1629–1646.

C.K. Law, C.J. Sung, Prog, Energy Combust. Sci. 26 (2000) 459-505.

C.K. Law, Combust. Flame, 53 (1983) 153.

C.K. Law, Combustion Physics, Cambridge University Press, 2008.

C.K. Law, D.L. Zhu, & G. Yu, Proc. Combust. Inst. 21 (1986) 1419–1426.

C.K. Law, F. Wu, F.N. Egolfopoulos, and H. Wang, "A Note on Rational Interpretation of Data on Laminar Flame Speeds," submitted to Combust. Flame

C.K. Law, F.N. Egolfopoulos, Proc. Combust. Inst. 24 (1992) 137-144.

C.K. Law, P. Cho, M. Mizomoto, H. Yoshida, Proc. Comb. Inst., 21 (1988) 1803-1809.

C.K. Law, Proc. Combust. Inst. 22 (1988) 1381-1402.

C.K. Law, Symposium (International) on Combustion (1989) 1381–1402.

C.K. Westbrook, W.J. Pitz, O. Herbinet, H.J. Curran, & E.J. Silke, Combust. Flame, 156 (2009) 181–199.

C.K. Wu, C.K. Law, Proc. Combust. Inst. 20 (1984) 1941–1949.

C.M. Vagelopoulos, F.N. Egolfopoulos, & C.K. Law, Symposium (International) on Combustion, 25 (1994) 1341–1347.

C.M. Vagelopoulos, F.N. Egolfopoulos, C.K. Law, Combust. Inst. 25 (1994) 1341-1347.

C.M. Vagelopoulos, F.N. Egolfopoulos, Combust. Inst. 25 (1994) 1317-1323.

C.T. Chong, S. Hochgreb, Proc. Combust. Inst. 33 (2011) 979–986.

D. Bradley, P.H. Gaskell, X.J. Gu, A. Sedaghat, Combust. Flame, 143 (2005) 227-245.

D. Bradley, P.H. Gaskell, X.J. Gu, Combust. Flame 104 (1996) 176-198.

D. Bradley, Proc. Comb. Inst., 24 (1992) 247-262.

D. Bradley, R.A. Hicks, M. Lawes, C.G.W. Sheppard, R. Woolley, Combust. Flame, 115 (1998) 126-144.

D. L. Zhu, F.N. Egolfopoulos, C.K. Law, Proc. Combust. Inst. 22 (1988) 1537-1545.

D. Rosner, R. Israel, & B. La Mantia, Combust. Flame, 123 (2000) 547–560.

D. Sheen, & H. Wang, Combust. Flame 158 (2011) 2358–2374.

D. Zhu, F. Egolfopoulos, C. Law, Symp. Int. Combust. 22 (1989) 1537-1545.

D.A. Senior, Combust. Flame, 5 (1961) 7-10.

D.A. Sheen, H. Wang, Combust. Flame 158 (2011) 2358-2374.

D.K. Kuehl, Proc. Comb. Inst., 8 (1961) 510-521.

D.L. Zhu, F.N. Egolfopoulos, C.K. Law, Proc.Combust. Inst. 22 (1988) 1537–1545.

D.R. Haylett, D.F. Davidson & R.K. Hanson, Combust. Flame 159 (2012) 552–561.

E. Mallard, H. Le Chatelier, Annales des Mines, 8 (1883) 274-618.

E. Meeks, C.V. Naik, K.V. Puduppakkam, A. Modak, C.K. Westbrook, F. Egolfopoulos, T. Tsotsis, Experimental and Modeling Studies of Combustion Characteristics of

Conventional and Alternative Jet Fuels, NASA/CR NNC07CB45C-Final Report 1 (2009).

E. Ranzi, A. Frassoldati, S. Granata, T. Faravelli, Ind. Eng, Chem, Res, 44(2005) 5170-5183.

E. Varea, V. Modica, A. Vandel, B. Renou, Combust. Flame 159 (2012) 577-590.

E.G. Eddings, S. Yan, W. Ciro, A.F. Sarofim, Combust. Sci. Technol. 117 (2005) 715-739.

F. A. Smith, Proc. of the Symp. on Comb., 1–2 (1948) 206-219.

F. A. Smith, S.F. Pickering, Bureau of St. Jour. of Research (1879).

F. Williams, Combustion Theory (2nd Editio) (1985).

F.A. Smith, S.F. Pickering, J. Research Nat. Bur. Std., 17 (1936) 7–43.

F.A. Williams, Combustion Theory, Benjamin Cummins, Palo Alto, CA, 1985.

F.J. Higuera, Combust. Flame, 157 (2010) 1586-1593.

F.N. Egolfopoulos, & C. Campbell, Combust. Flame, 117 (1999) 206–226.

F.N. Egolfopoulos, & P.E. Dimotakis, Symposium (International) on Combustion, 27 (1998) 641–648.

F.N. Egolfopoulos, C.S. Campbell, J. Fluid Mech. 318 (1996) 1-29.

F.N. Egolfopoulos, D.L. Zhu, C.K. Law, Proc. Combust. Inst. 23 (1991) 471-478.

F.N. Egolfopoulos, N. Hansen, Y. Ju, K. Kohse-Höinghaus, C.K. Law, F. Qi, Prog. Energy Combust. Sci., 43 (2014) 36-67.

F.N. Egolfopoulos, P. Cho, C.K. Law, Combust. Flame 76 (1989) 375-391.

F.N. Egolfopoulos, P. E. Dimotakis, Symp. Int. Combust. 27 (1998) 641-648.

F.N. Egolfopoulos, Proc. Combust. Inst. 25 (1994) 1375–1381.

F.R. Caldwell, H. P. Broida, J.J. Dover, Ind. And Chem., 43 (1951) 2731-2739.

F.W. Stevens, J. Am. Chem. Soc. 48 (1926) 1896-1906.

F.W. Stevens, J. Am. Chem. Soc. 50 (1928) 3244-3258.

F.W. Stevens, Nat. Advisory Comm. Aeronaut. Rep. 176, (1924).

F.W. Stevens, Nat. Advisory Comm. Aeronaut. Rep. 305, (1929).

F.Wu, A.P. Kelley, C.K. Law, Combust. Flame 159 (2012) 1417-1425.

G. Dixon-Lewis, Proc. Comb. Inst. 23 (1991) 305-324.

G. Dixon-Lewis, Proceedings of the Royal Society of London A: Mathematical, Physical and Engineering Sciences, 307 (1968) 111–135.

G. Dixon-Lewis, S.M. Islam, Proc. Combust. Inst. 19 (1982) 283–291.

G. Dixon-Lewis, T. David, P.H. Gaskell, J.A. Miller, R.J. Kee, M.D. Smooke, N. Peters, E. Effelsberg, J. Warrantz, F. Behrendt, Proc. Comb. Inst., 20 (1985) 1893–1904.

G. Garcia-Soriano, F. J. Higuera, J. L. Castillo, P. L. Garcia-Ybarra, Proc. of the European Combustion Meeting (2009).

G. Janiga, D. Theveni, Fifth European Combustion Meeting ECM (2009).

G. L., Dugger, S. Heimel, Nat. Advisory Comm. Aeronaut, TN2624, (1952).

G. Strang, SIAM Journal on Numerical Analysis 5 (1968), 506-517

G. Yu, C.K. Law, C.K. Wu, Combust. Flame 63 (1986) 339-347.

G.E. Andrews, D. Bradley, Combust. Flame, 18 (1972) 133–153.

G.L. Hubbard, C.L. Tien, ASME J. Heat Transfer 100 (1978) 235-239.

G.P. Smith, D.M. Golden, M. Frenklach, N.W. Moriarty, B. Eiteneer, M. Goldenberg, W.C. Gardiner Jr, (1999). GRI-Mech 3.0.

H. Daneshyar, J.M.C. Mendes-Lopes, Int. J. of Mech. Sci., 24 (1982) 529-535.

H. Edmondson, M. P. Heap, Combust. Flame, 15 (1970) 179-187.

H. Le Chatelier, E. Mallard, Compte Rend. Acad. Sci., 93 (1881) 145-148.

H. Schmidt, Ann. der Physik, 334 (1909) 971–1028.

H. Tsuji, I. Yamaoka, Proc. Comb. Inst., 11 (1967) 979-984.

H. Wang, E. Dames, B. Sirjean, D.A. Sheen, R. Tangko, A. Violi, J.Y.W. Lai, F.N. Egolfopoulos, D.F. Davidson, R.K. Hanson, C.T. Bowman, C.K. Law, W. Tsang, N.P. Cernansky, D.L. Miller, and R.P. Lindstedt, (2010) (http://melchior.usc.edu/JetSurF/JetSurF2.0)

H. Wang, K. Brezinsky, J. Phys. Chem. A 102 (1998) 1530-1541.

H. Wang, M. Frenklach, Combust. Flame 96 (1994) 163-170.

H. Wang, X. You, A. V. Joshi, Scott G. Davis, A. Laskin, F.N. Egolfopoulos C. K. Law, USC-Mech Version II. High-Temperature Combustion Reaction Model of H2/CO/C1-C4 Compounds. http://ignis.usc.edu/USC_Mech_II.htm.

H. Zhang, F.N. Egolfopoulos, Proc. Combust. Inst. 28 (2000) 1875-1882.

H.P.R. Ramirez, K. Hadj-Ali, P. Dievart, G. Moreac, & P. Dagaut, Energy Fuels, 24(2010), 1668-1676

H.R. Poorman, Eng. Thesis, California Institute of Technology, (1953).

H.S. Shen, J. Steinberg, J. Vanderover, Oehlschlaeger M.A., Energy Fuels, 23(2009) 2482-2489.

I. Kimura, H. Ukawa, Proc. Comb. Inst., 8 (1961) 521-523.

I.C. Mclean, D.B. Smith, S.C. Taylor, Proc. Combust. Inst. 25 (1994) 749-757.

J. A. Manion, W. S. McGivern, Direct measurements of binary gas phase diffusion coefficients for Combustion Applications, Argonne National Laboratory, Darien, IL, 2011,

J. B. Bell, N.J. Brown, M. S. Day, M.Frenklach, J. F. Grcar, and S. R. Tonse, Proc. Comb. Inst, 28 (2000) 1933-1939.

J. Biet, M.H. Hakka, V. Warth , P. Glaude , F. Battin-Leclerc, Energy Fuels, 22(2008), 2258-2269

J. Diederichsen, R.D. Gould, Combust. Flame, 9 (1965) 25-31.

J. F. Driscoll, Prog. Energy Combust. Sci. 34 (2008) 91-134.

J. Fu, C. Tang, W. Jin, L. D. Thi, Z. Huang, Y. Zhang, Int. J. Hydrogen Energy, 38 (2013) 1636–1643.

J. Fu, C. Tang, W. Jin, Z. Huang, Int. J. Hydrogen Energy, 39 (2014) 12187-12193.

J. H. Ferziger, M. Perić, Computational methods for fluid dynamics, Chapter 5, Berlin: Springer, 1996

J. Jayachandran, A. Lefebvre, R. Zhao, F. Halter, E. Varea, B.Renou, & F.N. Egolfopoulos, Proc. Comb. Inst, 35 (2015) 695–702.

J. Jayachandran, R. Zhao, & F.N. Egolfopoulos, Combust. Flame, 161 (2014) 2305–2316.

J. K. Bechtold, & M. Matalon, Combust. Flame, 127 (2001) 1906–1913.

J. Letheby, Franklin Inst. 82 (1866) 331-338.

J. Manton, G. von Elbe, B. Lewis, Proc. Comb. Inst., 4 (1953) 358-363.

J. Natarajan, T. Lieuwen, J. Seitzman, Combust. Flame, 151 (2007) 104-119.

J. O. Hirschfelder, C. F. Curtiss, R. B. Bird, M. G. Mayer, Molecular theory of gases and liquids, Wiley, New York, 1954.

J. Oh, D. Noh, Energy, 45 (2012) 669-675.

J. Ruan, H. Kobayashi, T. Niioka, Y. Ju, Combust. Flame (2001) 225-230.

J. Santer, F.M. Haas, Y. Ju, F.L. Dryer, Combust. Flame 161 (2014) 147-153.

J. Tien, M. Matalon, Combust. Flame, 84 (1991) 238-248.

J.A. Cooke, M. Bellucci, M.D. Smooke, A. Gomez, A. Violi, T. Favarelli, E. Ranzi, Proc. Combust. Inst. 30 (2005) 439-446.

J.D. Buckmaster, Acta Astronaut. 6 (1979) 741-769.

J.F. Grcar, R.J. Kee, M.D. Smooke, & J.A. Miller, Symposium (International) on Combustion, 21 (1988) 1773–1782.

J.H. Tien, M. Matalon, Combust. Flame 84 (1991) 238-248.

J.W. Linnett, Proc. Comb. Inst., 4 (1953) 20-35.

Ji C., Dames E., Wang H., F.N. Egolfopoulos, Combust. Flame 159 (2012) 1070-1081.

Ji C., Dames E., Wang Y. L., Wang H., & Egolfopoulos F. N. Combust. Flame, 157 (2010) 277–287.

Ji C., Egolfopoulos F.N., Proc. Combust. Inst. 33 (2011) 955-961.

Ji C., Sarathy S.M., Veloo P.S., Westbrook C.K., Egolfopoulos F.N., Combust. Flame 159 (2012) 1426-1436.

Ji C., Wang Y.L., Egolfopoulos F.N., J. Propul. Power 27 (2011) 856–863.

K. Chae, P. Elvati, A. Violi, J. Phys. Chem. B 115 (2010) 500-506.

K. Kumar, C.J. Sung, Combust. Flame 151 (2007) 209–224.

K. Kumar, G. Mittal, & C.J. Sung, Combust. Flame 156 (2009) 1278-1288.

K. Kumar, J.E. Freeh, C.J. Sung, Y. Huang, J. Propuls. Power 23 (2007) 428-436.

K. Mati, A. Ristori, S. Gail, G. Pengloan, P. Dagaut, Proc. Combust. Inst. 31 (2007) 2939–2946

K. Müller-Dethlefs, A.F. Schlader, Combust. Flame, 27 (1976) 205-215.

K. Roy, C. Horn, P. Frank, V.G. Slutsky, T. Just, Proc. Combust. Inst. 27 (1) (1998) 329-336.

K. Seshadri, S. Humer, & R. Seiser, Combust. Theory Model. 12(2008) 831-855.

K. Seshadri, T. Lu, O. Herbinet, S. Humer, U. Niemann, W. J. Pitz, R. Seiser, C. K. Law, Proc. Combust. Inst. 32 (2009) 1067-1074.

L. M. Bollinger, D. T. Williams, Nat. Advisory Comm. Aeronaut., Rep. 932. (1949).

L. S. Tee, S. Gotoh, W. E. Stewart, Ind. Eng. Chem. Fundmen. 5 (1966) 356-363.

L. Ubbelohde, E. Koelliker, J. Gasbeleucht. 59 (1916) 49-57.

L.K. Tseng, M.A. Ismail, G.M. Faeth, Combust. Flame 95 (1993) 410-426.

M. Colket, T. Edwards, S. Williams, N. P. Cernansky, D. L. Miller, F. Egolfopoulos, P. Lindstedt, K. Seshadri, F. L. Dryer, C. K. Law, 45th AIAA Aerospace Sciences Meeting and Exhibit, 2007; Reno, Nevada, 2007; paper no. AIAA-2007-0770.

M. D. Smooke, Proc. Comb. Inst., 34 (2015) 65-98.

M. E. Harris, J. Grumer, G. von Elbe, B. Lewis, Symp. on Combust. and Flame and Explosion Phenomena, 3 (1948) 80-89.

M. Gerstein, Proc. Comb. Inst., 4 (1953) 35-43.

M. Gouy, Ann. chim. Phys . 18 (1879) 27.

M. J. Dunn, A. R. Masri, and R. W. Bilger, Combust. Flame. 151 (2007) 46-60.

M. Kopp, E.L. Petersen, F. Guthe, 51st AIAA aerospace sciences meeting, Grapevine, TX, 2013.

M. Matalon, Combust. Sci. Technol. 31 (1983) 169-181.

M. Mehl, W.J. Pitz, C.K. Westbrook, & H.J. Curran, Proc. Comb. Inst, 33 (2011) 193–200.

M. Metghalchi, J.C. Keck, Combust. Flame 38 (1980) 143-154.

M. Mizomoto, Y. Asaka, S. Ikai, C.K. Law, Proc. Combust. Inst. 20 (1985) 1933-1939.

M. Nishioka, C.K. Law, T. Takeno, Combust. Flame 104 (1996) 328-342.

M. Peric, (1996). Computational methods for fluid dynamics. Heidelberg: Springer—Verlag.

M.D. Smooke, V. Giovangigli, IMPACT of Comp. in Sci. and Eng., 4 (1992) 46-79.

M.P. Burke, Z. Chen, Y. Ju, F.L. Dryer, Combust. Flame 156 (2009) 771-779.

M.U. Alzueta, P. Glarborg, K. Dam-Johansen, Int. J. Chem. Kinet. 32 (8) (2000) 498-522

N. Bouvet, C. Chauveau, I. Gökalp, S.-Y. Lee, R.J. Santoro, Int. J. of Hydrogen Energ., 36 (2011) 992-1005.

N. Bouvet, S.-Y. Lee, I. Gökalp, R. J. Santoro, Third European Combustion Meeting ECM (2007).

N. Grumman, Northrop Grumman Petroleum Product Survey Reports,

N. Hansen, J.A. Miller, T. Kasper, K. Kohse-Höinghaus, P.R. Westmoreland, J. Wang, T.A. Cool, Proc. Combust. Inst. 32 (2009) 623–630.

N. Liu, C. Ji, & F.N. Egolfopoulos, Combust. Flame 159 (2012) 465–475.

N. Peter, Proc. Combust. Inst. 32 (2009) 1-25.

N. Peters, F.A. Williams, Combust. Flame, 68 (1987) 185-207.

N. Peters, J. Fluid Mech. 384 (1999) 107-132.

N. Peters, Twenty-First Symposium (International) on Combustion (1986) 1231-1250.

O. Park, P. S. Veloo, N. Liu, F. N. Egolfopoulos, Proc. Comb. Inst., 33 (2011) 887-894.

O.S.L. Bruinsma, P.J.J. Tromp, H.J.J. de Sauvage Nolting, J. A. Moulijn, Fuel 67 (3) (1988) 334-340.

OpenFOAM, www.openfoam.org, 2014

P. Dagaut, M. Reuillon, M. Cathonnet, Combust. Sci. Technol. 103 (1994) 349-359.

P. E. Hamlington, A.Y. Poludnenko, and E. S. Oran, Phys. Fluids. 23(2011) 125111.

P. Glarborg, J.A. Miller, & R.J. Kee, Combust. Flame, 65 (1986) 177–202.

P. Middha, & H. Wang, Combustion Theory and Modelling, 9 (2005) 353–363.

P.A. Libby, F.A. Williams, Combust. Flame 44 (1982) 287-303.

P.D. Ronney, G.I. Sivashinksy, SIAM J. Appl. Math. 49 (1989) 1029-1046.

P.-H. Renard, D. Thevenin, J.C. Rolon, and S.M. Candel, Prog. Energy Combust Sci. 26(2000) 225-282.

P.N Brown, G. D. Byrne, A. C. Hindmarsh, SIAM journal on scientific and statistical computing 10(5) (1989), 1038-1051

P.S. Veloo, Y.L. Wang, F.N. Egolfopoulos, & C.K. Westbrook, Combust. Flame, 157 (2010) 1989–2004.

R. Bunsen, Poggendorffs Ann. der Physik und der Chemie, 131 (1866) 161.

R. Burrel , R. Zhao, D.J. Lee, H. Burbano , & F.N. Egolfopoulos, Proc. Comb. Inst, (2016) under review.

R. Grana, K. Seshadri, A. Cuoci, U. Niemann, T. Faravelli, E. Ranzi, Combust. Flame 159 (2012) 130–141.

R. M. Fristrom, Phys. of Fluids, 8 (1965) 273-280.

R. Trengove, H. Robjohns, P. J. Dunlop, Ber. Bunsen. Phys. Chem. 86 (1982) 951-955.

R.B. Morrison, R.A. Dunlap, Aeron. Research Center of Michigan, Project MX-794 (1948).

R.C. Reid, J. M. Prausnitz, B. E. Poling, The properties of gases and liquids, McGraw-Hill, New York, 1987.

R.D. Kern, Q. Zhang, J. Yao, B.S. Jursic, R.S. Tranter, M.A. Greybill, J.H. Kiefer, Proceedings of Combustion Institute 27 (1) (1998) 143-150.

R.G. Butler, I. Glassman, Proc. Combust. Inst. 32 (2009) 395-402.

R.H. Natelson, M.S. Kurman, N.P. Cernansky, & D.L. Miller, Fuel, 87(2008) 2339-2342.

R.I Issa, Journal of Computational Physics, 62 (1986) 40-65

R.J. Kee, & J.A Miller Sandia Report SAND86-8841, Sandia National Laboratories. (1986).

R.J. Kee, F. M. Rupley, J. A. Miller, M. E. Coltrin, J. F. Grcar, E. Meeks, H. K. Moffat, A. E. Lutz, G. DixonLewis, M. D. Smooke, J. Warnatz, G. H. Evans, R. S. Larson, R. E. Mitchell, L. R. Petzold, W. C. Reynolds, M. Caracotsios, W. E. Stewart, P. Glarborg, C. Wang, O. Adigun, CHEMKIN Collection, Release 3.6, Reaction Design, Inc., San Diego, CA (2000).

R.J. Kee, F.M. Rupley, J.A. Miller, Chemkin-II: A Fortran Chemical Kinetics Package for the Analysis of Gas-Phase Chemical Kinetics, Sandia Report, SAND89-8009, Sandia National Laboratories, 1989.

R.J. Kee, G. Dixon-Lewis, J. Warnatz, M. E. Coltrin, J. A. Miller, A Fortran computer code package for the evaluation of gas-phase, multicomponent transport properties, Livermore, CA, 1986.

R.J. Kee, J. A. Miller, G. H. Evans, G. Dixon-Lewis, Symp. Int. Combust. 22 (1989) 1479-1494.

R.J. Kee, J. Warnatz, J.A. Miller, A FORTRAN Computer Code Package for the Evaluation of Gas-phase Viscosities, Conductivities, and Diffusion Coefficients, Sandia Report, SAND83-8209, Sandia National Laboratories, 1983.

R.J. Kee, J.A. Miller, G.H. Evans, G.D. Lewis, Proc. Combust. Inst. 22 (1988) 1479–1494.

R.J. Kee, J.F. Grcar, M.D. Smooke, J.A. Miller, Premix: A FORTRAN Program for Modeling Steady Laminar One-dimensional Premixed Flames, Sandia Report, SAND85- 8240, Sandia National Laboratories, 1985.

R.J. Kee, M.E. Coltrin, & P. Glarborg, P Chemically reacting flow: theory and practice. John Wiley & Sons (2005).

R.K. Robinson, R.P. Lindstedt, Combust. Flame 158 (4) (2011) 666-686.

R.P. Lindstedt, S.W. Park, personal communication (2012).

S. Balusamy, A. Cessou, B. Lecordier, Exp. Fluids 50 (2011) 1109-1121.

S. Dooley, S.H. Won, M. Chaos, J. Heyne, Y. Ju, F.L. Dryer, K. Kumar, C-J. Sung, H Wang, M. Oehlschlaeger, R.J. Santoro, T.A. Litzinger, Combust. Flame 157 (12) (2010) 2333-2339.

S. H. Chung, T. M. Vu , M. S. Cha, B. J. Lee, Combust. Flame, 162 (2014) 1614-1621

S. H. Won, S. Dooley, F. L. Dryer, Y. Ju, Combust. Flame 159 (2012) 541-551.

S. H. Won, W. Sun, Y. Ju, Combust. Flame 157 (2010) 411-420.

S. Honnet, K. Seshadri, U. Niemann, & N. Peters, Proc. Combust. Inst. 32 (2009) 485-492.

S. Humer, A. Frassoldati, S. Granata, T. Faravelli, E. Ranzi, R. Seiser, & K. Seshadri, Proc. Combust. Inst. 31 (2007) 393–400.

S.C. Taylor, Burning Velocity and Influence of Flame Stretch, Ph.D. Thesis, University of Leeds, 1991.

S.D. Tse, D.L. Zhu, C.K. Law, Proc. Combust. Inst. 28 (2000) 1793-1800.

S.G. Davis, & C.K. Law, Combustion Science and Technology, 140 (1998) 427–449

S.H. Chung, C.K. Law, Combust. Flame 55 (1984) 123-125.

S.H. Won, S. Dooley, F.L. Dryer, & Y. Ju, Proc. Combust. Inst. 33 (2011) 1163-1170.

S.H. Won, Y. Ju, Combust. Flame 157 (2010) 411-420.

S.J. Klippenstein, J.A. Miller, L.B. Harding, Proc. Combust. Inst. 29 (2002) 1209-1217.

S.S. Vasu, D.F. Davidson, & R.K. Hanson, Combust. Flame 152 (2008) 125–143

T. Coffee , & J. Heimerl, Combust. Flame, 43 (1981) 273–289.

T. Edwards, L.Q. Maurice, J. Propul. Power 17 (2001) 461–466.

T. Lu, & C.K. Law, Combust. Flame, 144 (2006) 24–36.

T. Lu, C.K. Law, Proc. Combust. Inst. 30 (2005) 1333–1341.

T. Poinsot, D. Veynante, and S. M. Candel, J. Fluid Mech. 228 (1991) 561-606.

T. Poinsot, T. Echekki, M.G.Mungal, Combust. Sci. Tech. 81 (1992) 45-73.

U. Niemann, K. Seshadri, & F.A. Williams, Combust. Flame, 162 (2015) 1540-1549.

V. Gururajan, F.N. Egolfopoulos & K. Kohse-Höinghaus, Proc. Comb. Inst. 35 (2015) 821-829.

V. L. Zimont, Combust. Expl Shock Waves. 15 (1979) 305-311.

V. Mittal, H. Pitsch, F.N. Egolfopoulos, Combust. Theory and Modell. 16 (2012) 419-433.

W. Linnett, M.F. Hoare, Symp. on Combust. and Flame, and Explosion Phenomena, 3 (1948) 195-204.

W. Michelson, Ann.der Physik, 37 (1889) 1-24.

W. S. McGivern, J. A. Manion, Combust. Flame 159 (2012) 3021-3026.

W.C. Johnston, Soc. Auto. Eng. J. 55 (1947) 62-65.

W.-H. Jou, and J.J. Riley, AIAA J. 27 (1989) 1543-1557.

W.J. Pitz, C.J. Mueller, Prog. Energy Combust. Sci. 37 (2011) 330-350.

X. Qin, Y. Ju, Proc. Combust. Inst. 30 (2005) 233-240.

X. Zhong, J.W. Bozzelli, J. Phys. Chem. A 102 (1998) 3537-3555.

Y. Dong, A.T. Holley, M.G. Andac, F.N. Egolfopoulos, S.G. Davis, P. Middha, H. Wang, Combust. Flame 142 (2005) 374–387.

Y. Huang, C.J. Sung & J.A. Eng, Combust. Flame 139 (2004) 239–251.

Y. Kochar, T. Lieuwen, J. Seitzman, Proc. of the 6th U.S. Nat. Comb.Meeting (2009).

Y. Murakami, K. Mitsui, K. Naito, T. Itoh, T. Kobayashim, N. Fuji, Shock Waves 13 (2003) 149-154.

Y. N. Kochar, S. N. Vaden, T. C. Lieuwen, J. M. Seitzman, 48th AIAA Aerospace Sciences Meeting Including the New Horizons Forum and Aerospace Exposition, Orlando, Florida (2010).

Y.L. Wang, A.T. Holley, C. Ji, F.N. Egolfopoulos, T.T. Tsotsis, H. Curran, Proc. Combust. Inst. 32 (2009) 1035–1042.

Y.L. Wang, P.S. Veloo, F.N. Egolfopoulos, & T.T. Tsotsis, Proc. Combust. Inst. 33 (2011) 1003-1010.

Y.L. Wang, Q. Feng, F.N. Egolfopoulos, & T.T. Tsotsis, Combust. Flame, 158 (2011) 1507–1519.

Z. Chen, Combust. Flame 157 (2010) 2267-2276.

Z. Chen, Combust. Flame 158 (2011) 291-300.

Z. Chen, M.P. Burke, Y. Ju, Proc. Combust. Inst. 32 (2009) 1253-1260.

Z. Chen, X. Qin, B. Xu, Y. Ju, F. Liu, Proc. Combust. Inst. 31 (2007) 2693-2700.

Z. Li, H. Wang, Phys. Rev. E 68 (2003) 061207.